



UNIVERSITY OF THESSALY
SCHOOL OF ENGINEERING
DEPARTMENT OF MECHANICAL ENGINEERING

Master Thesis

**EXPERIMENTAL MODAL ANALYSIS USING AMBIENT AND EARTHQUAKE
VIBRATIONS: THEORY, SOFTWARE AND APPLICATIONS**

by

NTOSIOS EVANGELOS

Diploma in Mechanical Engineering, University of Thessaly, 2005

A Thesis
Submitted in Partial Fulfilment of the
Requirements for the Degree of
Master of Science
(in Mechanical Engineering)
2009



**ΠΑΝΕΠΙΣΤΗΜΙΟ ΘΕΣΣΑΛΙΑΣ
ΒΙΒΛΙΟΘΗΚΗ & ΚΕΝΤΡΟ ΠΛΗΡΟΦΟΡΗΣΗΣ
ΕΙΔΙΚΗ ΣΥΛΛΟΓΗ «ΓΚΡΙΖΑ ΒΙΒΛΙΟΓΡΑΦΙΑ»**

Αριθ. Εισ.: 7294/1
Ημερ. Εισ.: 21-07-2009
Δωρεά: Συγγραφέα
Ταξιθετικός Κωδικός: Δ
624.176 2
ΝΤΟ



UNIVERSITY OF THESSALY
SCHOOL OF ENGINEERING
DEPARTMENT OF MECHANICAL ENGINEERING

Master Thesis

**EXPERIMENTAL MODAL ANALYSIS USING AMBIENT AND EARTHQUAKE
VIBRATIONS: THEORY, SOFTWARE AND APPLICATIONS**

by

NTOTSIOS EVANGELOS

Diploma in Mechanical Engineering, University of Thessaly, 2005

A Thesis
Submitted in Partial Fulfilment of the
Requirements for the Degree of
Master of Science
(in Mechanical Engineering)
2009



**ΠΑΝΕΠΙΣΤΗΜΙΟ ΘΕΣΣΑΛΙΑΣ
ΠΟΛΥΤΕΧΝΙΚΗ ΣΧΟΛΗ
ΤΜΗΜΑ ΜΗΧΑΝΟΛΟΓΩΝ ΜΗΧΑΝΙΚΩΝ**

Μεταπτυχιακή Εργασία

**ΑΝΑΓΝΩΡΙΣΗ ΙΔΙΟΜΟΡΦΙΚΩΝ ΧΑΡΑΚΤΗΡΙΣΤΙΚΩΝ ΚΑΤΑΣΚΕΥΩΝ
ΒΑΣΕΙ ΜΕΤΡΗΣΕΩΝ ΤΩΝ ΤΑΛΑΝΤΩΣΕΩΝ ΣΕ ΠΕΡΙΒΑΛΛΟΝΤΙΚΕΣ ΚΑΙ
ΣΕΙΣΜΙΚΕΣ ΔΙΕΓΕΡΣΕΙΣ: ΘΕΩΡΙΑ, ΛΟΓΙΣΜΙΚΟ ΚΑΙ ΕΦΑΡΜΟΓΕΣ**

υπό

ΝΤΟΤΣΙΟΥ ΕΥΑΓΓΕΛΟΥ

Διπλωματούχου Μηχανολόγου Μηχανικού, Π.Θ., 2005

Υπεβλήθη για την εκπλήρωση μέρους των
απαιτήσεων για την απόκτηση του
Μεταπτυχιακού Διπλώματος Ειδίκευσης
2009

© 2009 Ντόσιος Ευάγγελος

Η έγκριση της μεταπτυχιακής εργασίας από το Τμήμα Μηχανολόγων Μηχανικών της Πολυτεχνικής Σχολής του Πανεπιστημίου Θεσσαλίας δεν υποδηλώνει αποδοχή των απόψεων του συγγραφέα (Ν. 5343/32 αρ. 202 παρ. 2).

This research was co-funded 75% from the European Union (European Social Fund), 25% from the Greek Ministry of Development (General Secretariat of Research and Technology) and from the private sector, in the context of measure 8.3 of the Operational Program Competitiveness (3rd Community Support Framework Program) under grant 03-EΔ-524 (PENED 2003). This support is gratefully acknowledged.

Εγκρίθηκε από τα Μέλη της Πενταμελούς Εξεταστικής Επιτροπής:

Πρώτος Εξεταστής (Επιβλέπων) Δρ. Παπαδημητρίου Κωνσταντίνος
Καθηγητής, Τμήμα Μηχανολόγων Μηχανικών, Πανεπιστήμιο Θεσσαλίας

Δεύτερος Εξεταστής Δρ. Σταματέλλος Αναστάσιος
Καθηγητής, Τμήμα Μηχανολόγων Μηχανικών, Πανεπιστήμιο Θεσσαλίας

Τρίτος Εξεταστής Δρ. Νασιάβας Σωτήριος
Καθηγητής, Τμήμα Μηχανολόγων Μηχανικών, Αριστοτέλειο
Πανεπιστήμιο Θεσσαλονίκης

Τέταρτος Εξεταστής Δρ. Τσόπελας Παναγιώτης
Αναπληρωτής Καθηγητής, Τμήμα Πολιτικών Μηχανικών, Πανεπιστήμιο
Θεσσαλίας

Πέμπτος Εξεταστής Δρ. Πανέτσος Παναγιώτης
Διδάσκων Π. Δ. 407/80, Τμήμα Πολιτικών Μηχανικών, Τμήμα
Αρχιτεκτόνων Μηχανικών, Πανεπιστήμιο Θεσσαλίας

Ευχαριστίες

Πρώτα απ' όλα, θα ήθελα να ευχαριστήσω τον επιβλέποντα της μεταπτυχιακής εργασίας μου, Καθηγητή κ. Παπαδημητρίου Κωνσταντίνο, για την πολύτιμη βοήθεια και καθοδήγησή του κατά τη διάρκεια της συνεργασίας μας. Επίσης, ευχαριστώ τα υπόλοιπα μέλη της εξεταστικής επιτροπής της μεταπτυχιακής εργασίας μου, Καθηγητές κκ. Σταματέλλο Αναστάσιο, Νασιάβα Σωτήριο, Τσόπελα Παναγιώτη και Πανέτσο Παναγιώτη για την προσεκτική ανάγνωση της εργασίας μου και για τις πολύτιμες υποδείξεις τους. Ευχαριστίες οφείλω σε όλους τους μεταπτυχιακούς και προπτυχιακούς φίλους και φοιτητές του Εργαστηρίου Δυναμικής Συστημάτων για την άριστη συνεργασία που είχαμε κατά τη διάρκεια της παρούσας μεταπτυχιακής εργασίας. Ευχαριστώ τους φίλους και φίλες μου για την υποστήριξή τους και για τις ωραίες στιγμές που περάσαμε.

Πάνω απ' όλα, είμαι ευγνώμων στους γονείς μου, Γιώργο και Παρασκευή για την ολόψυχη αγάπη και υπομονή τους όλα αυτά τα χρόνια καθώς και για τη υποστήριξη που μου έδωσαν να συνεχίσω τις σπουδές μου.

Ντόσιος Βαγγέλης

Abstract

This thesis addresses the problem of identifying the modal properties of structures using vibration measurements. Modal identification methodologies are proposed based on vibration measurements induced by artificial, ambient or earthquake loads applied on the structure. A modal model of the structure is identified using a weighted least-squares approach and measured time histories at selected locations of a structure. For artificially induced and ambient vibration measurements, the identification is performed in the frequency domain using respectively frequency response functions and cross power spectral densities. For earthquake induced vibrations, the identification is performed in both time and frequency domains. The modal identification methods presented in this work treat generalized non-classically damped modal models.

The identification of the modal parameter (modal frequencies, modal damping ratios, modeshape components and modal participation factors) is accomplished by introducing a computationally very efficient three step approach as follows. In the first step, stabilization diagrams are constructed containing frequency and damping information. The modeshape components and participation factors are estimated in a second least-squares step, based on the user selection of the stabilized poles. The first two steps involve non-iterative procedures and result in solving linear algebraic systems of equations. Finally, in order to improve the estimation of the modal characteristics, especially for the challenging case of closely spaced and overlapping modes, a third step is introduced to solve a fully nonlinear optimization problem using available iterative gradient-based optimization algorithms. In this thesis, theoretical developments as well as software implementation issues are presented.

The methodologies and software developed are applied for the identification of the modal characteristics of a small laboratory structure for the case of artificial induced vibration measurements, as well as the identification of the modal characteristics of three bridges, the under construction R/C bridge of Egnatia Odos located at Metsovo (Greece), and two other representative R/C bridges of Egnatia Odos located at Polymylos and Kavala (Greece) for the cases of ambient and earthquake induced vibration measurements. Results provide qualitative and quantitative information on the dynamic behaviour of the systems and their components under different types of excitations.

All modal identification methodologies presented in this work are implemented in user-friendly software, termed Modal Identification Tool (MITool). The software which includes graphical user interface allows the full exploration and analysis of signals that are measured on a structure when it is excited by artificial, ambient or earthquake loads. A user manual is also presented which gives details for the operations and prospects of the MITool software. Step-by-step examples of modal identification are presented to demonstrate the applicability of the software.

Contents

Chapter 1: Introduction	1
1.1 Overview of Operational Modal Analysis methods.....	4
1.2 Overview of Modal Analysis methods based on earthquake induced vibrations.....	5
1.3 Outline and organization of the thesis.....	6
Chapter 2: Linear system analysis in time and frequency domains	8
2.1 Introduction.....	8
2.2 Formulation for classically damped models.....	9
2.3 State space formulation of non-classically damped models.....	10
2.3.1 The eigenvalue problem.....	10
2.3.2 Orthogonality conditions.....	11
2.4 Observation equations.....	13
2.5 Modal model.....	13
2.5.1 State space equations.....	13
2.5.2 Observation equations.....	14
2.5.3 Summary of modal model equations.....	15
2.6 Special case: Classically damped model.....	17
2.7 The Frequency Response Function based on the modal model.....	18
Chapter 3: Cross power spectral densities in modal space	21
3.1 Introduction.....	21
3.2 Modal decomposition of cross power functions.....	21
3.3 Estimation of auto and cross power spectral densities.....	22
3.3.1 The periodogram approach.....	22
3.3.2 The correlogram approach.....	23
3.3.3 The 'positive' power spectra approach.....	25
3.3.4 Choosing reference responses.....	26
Appendix 3.A: Modal decomposition of cross power functions.....	27

Chapter 4: Least squares methodologies for modal identification	34
4.1 Introduction.....	34
4.2 Experimental Modal Analysis	36
4.3 Operational Modal Analysis.....	37
4.3.1 Identification based on the full spectra	37
4.3.2 Identification based on the half spectra.....	39
4.4 Earthquake induced vibrations	40
4.4.1 Identification in the time domain.....	41
4.4.2 Identification in the frequency domain.....	43
4.5 Identification of closely spaced modes using simulated measurement data	45
 Chapter 5: Applications on input-output and output-only modal identification	 48
5.1 Introduction.....	48
5.2 Application on a three-story laboratory structure.....	48
5.2.1 Description of the laboratory three-story structure and instrumentation	48
5.2.2 Modal identification results	51
5.3 Application on a Metsovo bridge during construction using ambient vibration measurements	59
5.3.1 Description of Metsovo bridge and instrumentation	59
5.3.2 Modal identification of Metsovo bridge	62
5.4 Application on Polymylos and Kavala bridges using ambient and earthquake induced vibration measurements.....	64
5.4.1 Description of bridge systems and instrumentation.....	64
5.4.2 Modal identification of Polymylos and Kavala bridges	67
 Chapter 6: Modal Identification Toolbox (MITool).....	 72
6.1 Introduction.....	72
6.2 MITool Software	73
6.2.1 Installation notes for MITool software	73
6.2.2 MITool Graphical User Interface (GUI)	74
6.2.2.1 Input files for MITool	75

6.2.2.2	The File menu.....	76
6.2.2.3	The Preferences dialog box.....	76
6.2.2.4	The View menu.....	79
6.2.2.5	The Options menu	80
6.2.2.6	The Identification Options dialog box	81
6.2.2.7	The MIMO Options dialog box.....	83
6.2.2.8	The Full Spectra Options and the Half Spectra Options dialog boxes	85
6.2.2.9	The Quasi-Newton Options dialog box.....	87
6.2.2.10	The Tools menu.....	88
6.2.2.11	The Post Processing menu.....	89
6.2.3	The Stabilization Diagrams.....	92
6.3	Step-by-step user guide to modal identification with MITool software	93
6.3.1	Modal identification application on G9 bridge at Polymylos using ambient vibration measurements	93
6.3.2	Modal identification application on G2 bridge at Kavala using simulated earthquake induced vibration measurements	106
Chapter 7: Conclusions		120
References		124

Introduction

During the last decade modal analysis has become a key technology in structural dynamics analysis. Starting from simple techniques for trouble shooting, it has evolved to an established technique to analyze the dynamical behaviour of complex mechanical structures. Beginning from the modal model, design improvements can be predicted and the structure can be optimized. Based on the academic principles of system identification, experimental modal analysis helps the engineers to get more physical insight from the identified models. Continuously expanding its application base, modal analysis is today successfully applied in civil engineering (buildings, bridges, off-shore platforms, dams), automotive engineering (engine, suspension, fully trimmed cars), aircraft engineering (in-flight tests, ground vibration tests, landing gear, control surfaces), spacecraft engineering (launchers, antennas, solid panels, satellites) and industrial machinery (pumps, compressors, turbines).

A great number of structures require certain specifications for safe and precise operation conditions, which usually form the most significant design parameters. In order to ensure a constantly accepted and reliable performance of a system, the knowledge of its dynamic behavior becomes essential in either case of operational or unpredictable extreme loads. For newly build structures, as well as for the ones that are already in operation for some time, the measurement of their dynamic properties, such as natural frequencies, damping factors and modeshapes is well desired, so as for the prediction of their behavior using a reliable model to be feasible.

The vibration of a structure originates from its resonance modes that are inherent properties of the structure. Small forces exciting the structure at one or more of these resonance frequencies can cause large vibration responses resulting in possible damage, discomfort and malfunctioning in the structure. These modes are determined by the geometry, the material properties (mass, damping and stiffness) and the boundary conditions of the structure. If the geometry, material properties or boundary conditions change, the structural modes change.

The modal model expresses the behaviour of a linear time-invariant mechanical system as a linear combination of these different resonance modes. Each mode is defined by a damped resonance frequency, modal damping and mode shape, i.e. the so-called modal parameters. Given the physical interpretation of the modes, engineers often prefer this mathematical model because it provides the best physical understanding for the system.

Experimental modal analysis (EMA) identifies a modal model from the measured forces applied to the test structure and the measured vibration responses. Classically, one applies an artificial, measurable input to the system and one measures the output. From these measurements, the experimental model can be obtained by a variety of parameter estimation methods. During an EMA, the structure is often removed from its operating environment and tested in laboratory conditions.

The latter experimental situation can differ significantly from the real-life operating conditions. Cases exist where it is rather difficult to apply an artificial force on a structure and one has to rely

on available ambient excitation sources. For these cases, system identification techniques were developed to identify the modal model from the structure under its operational conditions from vibration responses only. These techniques, referred as *operational modal analysis* (OMA) or output-only modal analysis, take advantage of the ambient excitation as e.g. wind, traffic and turbulence. OMA proved very useful in civil engineering, where it is very difficult and expensive to excite constructions such as bridges and buildings with a hammer or shaker and to obtain artificially induced vibration levels that exceed the natural vibrations due to traffic or wind. Also in mechanical engineering, OMA is successfully applied to obtain data-based dynamic models of, for instance, a vehicle during road testing or an aircraft during flight tests. Also, an important advantage of OMA is that the structure can remain in its normal operating condition. This allows the identification of more realistic modal models for in-operation structures.

For the cases of civil engineering structures, the response of the structure induced by an earthquake event can offer an opportunity to study quantitatively and qualitatively their dynamic behaviour within the resulting vibration levels. For the case of earthquake-induced vibrations, the modal characteristics are estimated from the measured portion of the excitation occurred to the structure and the measured vibration responses. These measurements are usually the acceleration of the structure obtained by accelerometers optimal placed on the structure (Papadimitriou et al. 2000; Papadimitriou 2005; Ntotsios et al. 2006). It has been observed from response measurements of large structures to potentially damaging excitations that the dynamic properties of many structures are markedly different during response to strong ground motion than in small amplitude ambient and forced vibration tests. Hence, it is of considerable interest and importance to extract information about structural behavior from strong motion data.

The identified modal model of a structure can be used for the following applications:

- **Response prediction:** The modal models are often used for the purpose of predicting the response of the structure to given dynamic loadings representing the real-life operating conditions. This allows designers to check the performance of a developed product under a variety of working conditions (Papadimitriou et al. 2001).
- **Load identification:** The modal model can be used to identify the unknown forces (full time history or other characteristics such as power spectra) using measured response time histories. This is also an inverse problem that has high practical value (Parloo et al. 2003).
- **Model validation and updating:** The modal properties, mainly identified modal frequencies and modeshapes, can be used to validate a finite element model (FEM) as well as update the values of various properties of the FEM, such as material properties, geometrical properties and boundary conditions, in order to obtain a reliable FEM model of the structure consistent with the measured data (Motterhead and Friswell 1993; Bohle and Fritzen 2003; Taughels et al. 2003; Lam et al. 2004; Christodoulou and Papadimitriou 2007; Christodoulou et al. 2008). This updated finite element model can be used to carry out updated response predictions consistent with the test data.
- **Structural health monitoring and damage detection:** The modal properties of a modal model can be used for detecting damage in a structure by continuously monitoring the structure and exploiting the vibration measurements from the healthy and damage state of the structure (Farrar et al. 1994; Doebling et al. 1996; Fritzen et al. 1998; Vanik et al. 2000; Taughels and De Roeck 2005; Ntotsios et al. 2008). The idea is that damage may be cause stiffness reduction at some

locations of the structure. These stiffness reductions, which results from the onset of cracks or loosening of a connection, will cause changes in the modal properties of the structure. By monitoring these changes in the modal properties and coupling these changes with the finite element model, one should be able to detect the onset of damage in the structure as well as identify the location and the size of damage.

- **Sub-structuring:** The identified modal model can also be used to represent one or more substructures of a complex structure and then construct hybrid models of the full structure (Giagopoulos and Natsiavas 2007) using sub-structuring techniques (Maia and Silva 1997). Given the modal model of different components of a complex structure, the dynamical behavior of the complete structure can be computed.

There are certain limitations in the effectiveness and reliability of the modal model identification techniques. These limitations are summarized as follows.

- **Insufficient measurement data:** This is due to the limited number of sensors placed in the structure. As a result only estimates of the partial modeshape of the structure are available at the measured degrees of freedom (DOF). Also, this is due to the usually limited range of the frequency band contained in the excitations forces that, as a result do not excite all modes of the structure and therefore some of the system's dynamic properties cannot be identified. The problem is more pronounced with the higher frequency modes since, from a testing point of view, it is more difficult to excite the higher frequency response of a structure since more energy is required to produce measurable response at these higher frequencies than at the lower frequencies. It should be noted that optimal sensor location strategies could be used to give the best possible information about the modes of the excited system.

- **Measurement error:** These are errors associated with the dynamic data measurements. It consists of bias errors caused by faulty instruments or noise caused by changes in the environmental conditions during testing or poor preprocessing of the initial data (for example, bias from windowing of the data). The effect of noise on the modal identification results is that it limits the number of modes that can be estimated reliably. This is more pronounced for higher modes where there exists the signal-to-noise ratio is relatively small. Thus, often the modal parameters can be identified only for the dominant modes in the measurement records.

- **Modal coupling:** It is often difficult to identify the closely spaced modes which are contributing to the measured response within the measured frequency range of interest. This difficulty is observed more commonly at the higher frequency portions of the spectrum where the modal density is typically greater.

- **Non-uniqueness:** This is due to the fact that the number of parameters is larger than needed or the available measurements are relatively limited. In such case, the optimal solution to the identification problem appears not to be unique.

- **Ill-Conditioning:** This is due to the lack of sensitivity of the measurement quantities to small changes in the modal parameters to be identified.

- **Model Error:** This is due to the fact that the chosen class of linear modal models chosen for identification is unable to exactly model the actual behavior of the structure (for example, due to nonlinear behavior of the structure at a portion of the frequency range).

1.1 Overview of Operational Modal Analysis methods

The peak-picking method (Felber 1993) is the simplest method to estimate the modal parameters of a structure subjected to ambient loading. It is based on the power spectra that are obtained from the measured time histories using discrete Fourier transform. The locations of the peaks of the power spectra give an estimate of the modal frequencies. The mode shapes are determined by computing the cross power spectral density functions between all outputs and a reference sensor. The method requires that the damping is low and the modes are well-separated. Violation of these two assumptions may lead to erroneous results. A disadvantage of the method is the subjective selection of modal frequencies and the lack of accurate damping estimates. However, the major advantage of the method is its speed. In general, the method identifies the operational deflection shapes instead of mode shapes, since there is no modal model that is fitted to the measured data. In particular, for the case of closely spaced modes such operational deflection shapes will be the superposition of the modeshapes of the multiple closely-spaced modes.

Nowadays, the stochastic subspace identification (Van Overschee and De Moor 1996, Hermans and Van der Auweraer 1999, Peeters and De Roeck 1999, Basseville et al. 2001) has been well developed and widely used for identifying the modal properties from ambient vibration measurements. In this method, a stochastic state space model is identified directly from measured output data or output correlations. It can be shown that this stochastic state space model is a good representation of a vibrating structure, provided that the unknown excitation forces can be modeled by white noise processes. Successful real-life modal analysis applications of stochastic subspace identification can be found in the literature (e.g. Hermans and Van der Auweraer 1999; Peeters 2000; Basseville et al. 2001).

Statistical methods for the estimation of the modal parameters based on output-only measurements have also been proposed. Frequency-domain maximum likelihood approaches for the estimation of modal parameters from output-only data were proposed by Hermans et al. (1998), Guillaume et al. (1999), Verboten (2002), Parloo (2003) and Cauberghe (2004). A Bayesian statistical approach for modal identification has also been proposed by Katafygiotis and Yuen (2001) using ambient data. The method is based on the statistics of an estimator of the spectral density. This approach allows for the direct calculation of the probability density functions (PDF) of the modal parameters which can then be approximated by an appropriately selected multi-variant Gaussian distribution.

Besides the aforementioned modal identification approaches, several methods proposed are based on fitting directly the measured data with modal model predicted data using least-squares type of approaches. In Beck et al. (1994) a methodology for modal identification is proposed using time-domain least-squares methods based on correlation functions of the output time histories. In Brinker et al. (2001), Verboten (2002) and Cauberghe (2004) frequency-domain least-squares methods based on full cross-power spectral densities (CPSD) are proposed. Finally, Peeters and Van der Auweraer (2005) have proposed a frequency-domain least-squares modal identification methods based on half spectra.

There are certain advantages for using output only measurements for identifying the structural modes. In operational modal analysis there is no need to use artificial devices for exciting the structure (Farrar et al. 1994). Instead, the modes are identified from the vibrations obtained during the operation of the structure. This has certain advantages for massive civil structures for which large exciters have to be used to excite the structure. The use of exciters is not only very

costly but it is also time-consuming and impractical (Peeters and De Roeck, 1999) for structural health monitoring applications. Ambient vibration measurement can directly be used for continuously monitoring the civil engineering structures (Peeters, 2000; Peeters and De Roeck, 2001). Such ambient vibration measurements have also been recently used in identifying the modal characteristics of ground and air vehicles (Peeters et al., 2004; Souty 2008; Boswald and Govers 2008, Klepka and Tadeusz 2008, Peeters et al. 2009). Finally, it is worth noting that the OMA methods provide the modal properties that correspond to the real operation conditions of the structure. These conditions may differ significantly from the ones obtained during laboratory forced excitation tests. Examples of this situation include the modal properties obtained for bridges using large exciters. Such modal analyses are usually performed under closed traffic conditions. For bridges that are open in traffic, one should expect changes in mass loading due to the vehicles passing through the bridge (Kim et al., 2001; Roberts, 2001). These changes alter the modal properties of the structure.

The disadvantages of the operational modal analysis methods are the broadband assumptions on the unknown input and the low signal to noise ratios for the low level vibrations on which usually the measurements are made. In particular, all operational modal analysis methods are based on the fact that the unknown input forces can be adequately modeled by white noise processes. This condition is often violated since excitation forces may contain harmonic components which will appear as peaks in the spectra and may be erroneously identified by the methods as structural modes.

1.2 Overview of Modal Analysis methods based on earthquake induced vibrations

For the case of earthquake-induced vibrations, modal identification algorithms provide estimates of the modal frequencies, modal damping ratios, modeshapes at the measured DOFs and modal participation factors using classically-damped or non-classically damped modal models. Modal identification methods have been developed in time domain (Beck 1978; Beck and Jennings 1980) and in frequency domain (McVerry 1980), based on a minimization of the measure of fit between the time history or its Fourier transform of the acceleration responses estimated from the measurements and the corresponding ones predicted from a classically-damped modal model of the structure. These methodologies have also been extended to treat non-classically damped modal models, since damping may not be proportionally distributed in various structural components.

Specifically, Beck (1978) and Beck and Jennings (1980) had presented an output-error approach for the identification of linear, time-invariant models from strong motion records. McVerry (1980) has applied an output-error approach in the frequency domain, using the Fast Fourier Transform (FFT) of the acceleration response time histories to estimate the modal properties through least-squares matching. Werner et al. (1987) formulated a methodology in the time domain for the case of measured input excitation, such as earthquake excitation, for an elastic system with classical normal modes and with motion measurements from any number of input and system response DOFs. Their procedure was an extension of the least-squares-output-error method which was used by Beck (1978). Extensions for identifying non classically-damped modal models in the frequency domain have been developed by Chaudhary et al. (2002). Tan and Cheng (1993) proposed an iterative identification algorithm, which was based on the modal sweep concept and

the band-pass filtering process, to identify the modal parameters of a non-classically damped linear structure from its recorded earthquake response. Mahmoudabadi et al. (2007) developed a method for parametric system identification in frequency domain for classically and non-classically damped linear systems subjected up to six components of earthquake ground motions, which is able to work in multi-input/multi-output (MIMO) case. Nikolaou (2008) has recently extended the work by Beck (1978) and McVerry (1980) to the use of non-classically damped models. A novel aspect of Nikolaou (2008) method is to use a three step approach to distinguish the physical from the mathematical poles using stabilization diagrams and reduce the computational time for estimating the modal parameters of the physical modes by re-formulating the optimization problems in terms of quadratic objective functions.

1.3 Outline and organization of the thesis

In this thesis modal identification methodologies for estimating the dynamic modal characteristics of structures have been developed. A generalized non-classically damped modal model of the structure is considered and the identification is based of vibration measurements induced by artificial-, ambient- and earthquake-induced excitations. An output error formulation is used in which the modal parameters are identified through least-squares matching between the output measured response of the structure and the predicted by a modal model of the structure subjected to the different excitation types. A three step approach is proposed to solve the output error optimization problem. The first step provides estimates of the modal frequencies and modal damping ratios by solving a system of linear algebraic equations. Stabilization diagrams are used to distinguish between physical and mathematical modes. The second step provides estimates of the modeshapes and the modal participation factors by solving a system of linear algebraic equations. The first two steps usually give accurate estimates of the modal characteristics. A third step is added to improve these estimates, if needed, by efficiently solving the full nonlinear optimization problem with initial estimates of the modal parameters those obtained from the first and second steps.

The identification algorithms have been implemented in the software Modal Identification Tool (MITool) with Graphical User Interface (GUI) environment. The MITool has been developed in the System Dynamics Laboratory of the Department of Mechanical Engineering of the University of Thessaly. The GUI is fully adaptable to satisfy the user' s requirements by allowing the resetting of most of its operational parameters. The effectiveness and applicability of all identification algorithms and software are using simulated measurements, as well as real measurement from laboratory model structures and fully operational bridges.

The thesis is divided into seven chapters.

Chapter 2 presents the linear system theory that is used to describe the characteristics of the response of linear structures in the time and frequency domains in terms of the modal coordinates. Several mathematical models are discussed that can be used to describe the dynamical behavior of a structure with a limited number of modal parameters. The formulation is presented for the general case of non-classically damped modes. The classically damped case is then formulated as a special case. Both continuous and discrete time formulations are presented. The Frequency Response Functions (FRF) are formulated using different mathematical models like state space models and matrix fraction polynomial models.

Chapter 3 deals with the modal decomposition of output-only data in the frequency domain. It is shown that, analogous to FRF data, modal parameters can be identified from cross power spectra of output-only data. For this, available methods are used for the estimation of auto and cross power spectra from measured response data sets.

In Chapter 4 several modal identification methodologies are proposed to solve the modal identification problem for the cases of artificial, ambient and earthquake induced vibrations. These modal identification methodologies provide estimates of the modal properties (e.g. modal frequencies, modal damping ratios, modeshapes and modal participation factors) of a structure. All these methodologies introduced are based on the minimization of an error function using a least squares minimization approach. The formulation is presented for the general case of non-classically damped modal model. The proposed modal identification methodologies use a three step approach to solve the output error minimization problem. The first step provides estimates of the modal frequencies and modal damping ratios. In addition, using stabilization diagrams, the physical poles are distinguished from the mathematical poles. The second step provides estimates of the modeshapes and the modal participation factors and the third step improves these estimates by solving a nonlinear optimization problem. A modal identification example using simulated measurements is presented for the case of a structure with closely and overlapping modes showing the efficiency of the proposed three step identification approach and the need to use the third step for the case of closely spaced and overlapping modes.

In Chapter 5 the proposed identification methodologies are applied to real structures. The purpose of this chapter is to demonstrate and compare the applicability and effectiveness of the modal identification methodologies. The dynamic modal characteristics are estimated for a small scale laboratory structure using artificially (impulse hammer) excited vibration measurements and for three bridges on the Egnatia Odos motorway (G9 Polymylos, G2 Kabala and Metsovo bridges) using both ambient and earthquake induced vibration measurements.

Finally, Chapter 6 presents the MITool software that has been developed to implement all the identification algorithms discussed in the present thesis. All the operations and prospects of the MITool software are presented in details. A step-by-step user guide is also presented for identifying the modal characteristics of two bridges using real ambient vibration response measurements and earthquake induced vibration response measurements.

Conclusions of this work are summarised in Chapter 7.

Linear system analysis in time and frequency domains

2.1 Introduction

This section uses linear system theory to solve the equations of motion that govern the response (displacement, velocity and acceleration) of structures. Modal analysis is used to describe the response at the measured (observable) degrees of freedom of the structure in terms of the eigenproperties (eigenvalues and eigenvectors) and the excitation. The analysis is used in subsequent Chapters for solving the inverse problem of identifying the eigenproperties given input-output and output-only measurements.

Using a spatial discretization method, such as finite element analysis, the equations of motion for a linear structure are given by the following set of n second order differential equations

$$M\ddot{\underline{q}}(t) + C_0\dot{\underline{q}}(t) + K\underline{q}(t) = \underline{L}f(t) \quad (2.1)$$

where $\underline{q}(t) \in \mathbb{R}^{n \times 1}$ is the displacement vector, M , C_0 and $K \in \mathbb{R}^{n \times n}$ are respectively the mass, damping and stiffness matrices, $\underline{f}(t) \in \mathbb{R}^{N_m \times 1}$ is the applied force vector at the N_m DOFs, and $\underline{L} \in \mathbb{R}^{n \times N_m}$ is a matrix comprised of zeros and ones that maps the N_m excited DOFs to the n output DOFs. Throughout the analysis, it is assumed that the system matrices M , C_0 and K are symmetric.

Linear system theory is used with the objective to describe the solution of the system in the time domain in terms of the modal coordinates. The formulation is presented for the general case of non-classically damped modes. The classically damped case is then formulated as a special case. Both continuous and discrete time formulations are presented. All results given in this Chapter are well known. Their presentation is given herein in order to make this Thesis self-contained.

The presentation is divided into the following sections. Section 2.2 gives known modal analysis results for formulating the response of the structure in terms of real modal coordinates for a classically-damped model (2.1). Sections 2.3 to 2.5 extend the formulation to the general case of a non-classically damped model (2.1). For this, the state space form of system (2.1) is used and the corresponding complex-valued modal analysis results are presented. Section 2.5.3 gives a summary of the formulas that describe the response of the structure at the measured locations in terms of the complex eigenproperties (eigenvalues and eigenvectors). Section 2.6 presents the modal analysis formulation for the classically damped modal models as a special case of the non-classically damped modal models. Finally, Section 2.7 presents the formulation for the transfer function between the output and the input DOFs using the non-classically damped modal model.

2.2 Formulation for classically damped models

Assuming that the structure is classically damped and that the system matrices M , C_0 and $K \in \mathbb{R}^{n \times n}$ are symmetric, the solution for the displacement response $\underline{q}(t) \in \mathbb{R}^{n \times 1}$ in the modal space can be written in the form:

$$\underline{q}(t) = \sum_{r=1}^n \underline{\phi}_r \xi_r(t) = \Phi \underline{\xi}(t) \quad (2.2)$$

The modal coordinates $\xi_r(t)$ are given by the modal equations

$$\ddot{\xi}_r(t) + 2\zeta_r \omega_r \dot{\xi}_r(t) + \omega_r^2 \xi_r(t) = \underline{\phi}_r^T L f(t) \quad (2.3)$$

where ω_r is the modal frequency, ζ_r is the modal damping ratio and $\underline{\phi}_r$ is the modeshape vector for the r mode. The modeshapes $\underline{\phi}_r, r = 1, \dots, n$, are real and satisfy the orthogonality conditions

$$\underline{\phi}_r^T M \underline{\phi}_s = \delta_{rs} \quad r = 1, \dots, n, s = 1, \dots, n \quad (2.4)$$

$$\underline{\phi}_r^T K \underline{\phi}_s = \omega_r^2 \delta_{rs} \quad r = 1, \dots, n, s = 1, \dots, n \quad (2.5)$$

where

$$\delta_{rs} = \begin{cases} 1, & r = s \\ 0, & r \neq s \end{cases} \quad (2.6)$$

is the Kronecker delta. Equivalently, in matrix form the orthogonality condition (2.4) and (2.5) are written as

$$\Phi^T M \Phi = I \quad (2.7)$$

$$\Phi^T K \Phi = \Omega^2 \quad (2.8)$$

where $\Phi = [\underline{\phi}_1 \quad \dots \quad \underline{\phi}_n]$ is the matrix of modeshapes and Ω^2 is a diagonal matrix of the squares of the modal frequencies given by

$$\Omega^2 = \begin{bmatrix} \omega_1^2 & & 0 \\ & \ddots & \\ 0 & & \omega_n^2 \end{bmatrix} \quad (2.9)$$

Note that all variables involved in the classically damped analysis presented in this section are real and the modal equations are second order differential equations. In contrast, the variables in the non-classically damped modal analysis presented in Section 2.3 are in general complex, while the modal equations are first order differential equations. It can be shown that the two formulations for describing the response in the modal space are equivalent.

2.3 State space formulation of non-classically damped models

In the general case where the system is non-classically damped the set of equations (2.1) must be converted to a set of first order state space formulation. This is accomplished by introducing the complementary equation

$$M\ddot{\underline{q}}(t) = M\dot{\underline{q}}(t) \quad (2.10)$$

and the state vector

$$\underline{x} = \begin{bmatrix} \underline{q} \\ \dot{\underline{q}} \end{bmatrix} \quad (2.11)$$

Equations (2.1) and (2.10) can be written in the state space form

$$P\dot{\underline{x}} + Q\underline{x} = \begin{bmatrix} L \\ 0 \end{bmatrix} \underline{f}(t) \quad (2.12)$$

where the matrices P and Q are given by

$$P = \begin{bmatrix} C_0 & M \\ M & 0 \end{bmatrix}, \quad Q = \begin{bmatrix} K & 0 \\ 0 & -M \end{bmatrix} \quad (2.13)$$

2.3.1 The eigenvalue problem

The eigenvectors $\underline{\psi}_r$ and the corresponding eigenvalues λ_r satisfy the eigenproblem

$$(P\lambda + Q)\underline{\psi} = \underline{0} \quad (2.14)$$

The eigenvalues λ_r and the eigenvectors $\underline{\psi}_r$ are complex and it can be shown that if λ_r and $\underline{\psi}_r$ are the eigenvalues and eigenvectors of the eigenproblem then λ_r^* and $\underline{\psi}_r^*$ are also eigenvalues and eigenvectors of the same eigenproblem.

Introducing the eigenmatrix $\Psi = [\underline{\psi}_1 \ \dots \ \underline{\psi}_n \ \underline{\psi}_1^* \ \dots \ \underline{\psi}_n^*] \in \mathbb{C}^{2n \times 2n}$ it can easily be shown that the eigenmatrix of the eigenproblem (2.14) is given by

$$\Psi = \begin{bmatrix} \Phi & \Phi^* \\ \Phi\Lambda & \Phi^*\Lambda^* \end{bmatrix} \in \mathbb{C}^{2n \times 2n} \quad (2.15)$$

where Φ , λ satisfy the second order eigenproblem

$$M\Phi\lambda^2 + C_0\Phi\lambda + K\Phi = 0 \quad (2.16)$$

The eigenvalues λ_r are given by

$$\lambda_r = -\zeta_r\omega_r \pm j\omega_r\sqrt{1-\zeta_r^2} \quad (2.17)$$

where

$$\omega_r = |\lambda_r| \quad \text{and} \quad \zeta_r = -\frac{\text{Re}\{\lambda_r\}}{\omega_r} \quad (2.18)$$

The eigenvalue matrix for the first order linear system (2.12) is given by

$$\Lambda_c = \begin{bmatrix} \Lambda & 0 \\ 0 & \Lambda^* \end{bmatrix} = \text{diagonal} \in C^{2n \times 2n} \quad (2.19)$$

where Λ is the diagonal matrix

$$\Lambda = \begin{bmatrix} \lambda_1 & & 0 \\ & \ddots & \\ 0 & & \lambda_n \end{bmatrix} \quad (2.20)$$

2.3.2 Orthogonality conditions

The complex eigenvectors satisfy the orthogonality condition

$$\Psi^T P \Psi = \text{diag}[a_r] \quad (2.21)$$

that can be written as

$$P = \Psi^{-T} \text{diag}[a_r] \Psi^{-1} \quad (2.22)$$

The eigenvectors also satisfy the orthogonality condition

$$\Psi^T Q \Psi = \text{diag}[\beta_r] \quad (2.23)$$

that respectively can be written as

$$Q = \Psi^{-T} \text{diag}[\beta_r] \Psi^{-1} \quad (2.24)$$

Pre-multiplying (2.14) by $\underline{\psi}^T$ yields

$$\underline{\psi}^T P \underline{\psi} \lambda + \underline{\psi}^T Q \underline{\psi} = 0 \quad (2.25)$$

and solving for λ gives

$$\lambda = -\frac{\underline{\psi}^T Q \underline{\psi}}{\underline{\psi}^T P \underline{\psi}} \quad (2.26)$$

For the r-th eigenvalue and eigenvector, the last expression gives

$$\lambda_r = -\frac{\underline{\psi}_r^T Q \underline{\psi}_r}{\underline{\psi}_r^T P \underline{\psi}_r} \quad (2.27)$$

The r-th eigenvalue is finally given by

$$\lambda_r = -\beta_r / \alpha_r \quad (2.28)$$

where

$$\begin{aligned} \beta_r &= \underline{\psi}_r^T Q \underline{\psi}_r \\ \alpha_r &= \underline{\psi}_r^T P \underline{\psi}_r \end{aligned} \quad (2.29)$$

and the eigenvalue matrix is given by

$$\Lambda_c = \text{diag} \left[\frac{1}{\alpha_r} \right] \text{diag} [\beta_r] \quad (2.30)$$

The normalized state space formulation is obtained by pre-multiplying equation (2.12) by P^{-1} .

$$P^{-1} = \begin{bmatrix} 0 & M^{-1} \\ M^{-1} & -M^{-1}C_0M^{-1} \end{bmatrix} \quad (2.31)$$

The normalized state space equations take the form

$$\dot{\underline{x}} = A_c \underline{x} + B_c \underline{f}(t) \quad (2.32)$$

where

$$A_c = -P^{-1}Q = \begin{bmatrix} 0 & M^{-1} \\ M^{-1} & -M^{-1}C_0M^{-1} \end{bmatrix} \begin{bmatrix} K & 0 \\ 0 & -M \end{bmatrix} = \begin{bmatrix} 0 & I \\ -M^{-1}K & -M^{-1}C_0 \end{bmatrix} \quad (2.33)$$

is the state space matrix and

$$B_c = -P^{-1} \begin{bmatrix} L \\ 0 \end{bmatrix} = \begin{bmatrix} 0 & M^{-1} \\ M^{-1} & -M^{-1}C_0M^{-1} \end{bmatrix} \begin{bmatrix} L \\ 0 \end{bmatrix} = \begin{bmatrix} 0 \\ -M^{-1}L \end{bmatrix} \quad (2.34)$$

Based on the eigenproblem (2.14) and pre-multiplying (2.14) by P^{-1} yields

$$(-P^{-1}Q - \lambda I)\underline{\psi} = \underline{0} \Rightarrow (A_c - \lambda I)\underline{\psi} = \underline{0} \quad (2.35)$$

For the r -th eigenvalue and eigenvector, the last expression can be written in the form

$$A_c \underline{\psi}_r = \lambda_r \underline{\psi}_r, \quad r = 1, \dots, 2n \quad (2.36)$$

In matrix form, the set of $2n$ equations (2.36) can be written in the form

$$A_c \Psi = \Psi \Lambda_c \quad (2.37)$$

that gives

$$A_c = \Psi \Lambda_c \Psi^{-1} \quad (2.38)$$

Formulation (2.37) shows that the matrices Λ_c and Ψ contain the eigenvalues and eigenvectors of the state space matrix A_c .

2.4 Observation equations

Let $\underline{y}(t) \in \mathbb{R}^{N_0}$ be the response vector of interest. These responses, in general case, are a linear combination of the accelerations, velocities and displacements of the system. The generalized observation equation is given in the form

$$\underline{y}(t) = C_\alpha \underline{\ddot{q}}(t) + C_v \underline{\dot{q}}(t) + C_d \underline{q}(t) \quad (2.39)$$

By writing $\underline{\ddot{q}}(t)$ as a function of $\underline{\dot{q}}(t)$ and $\underline{q}(t)$ using (2.1) and substituting in (2.39) yields

$$\underline{y}(t) = C_c \underline{x} + D_c \underline{f}(t) \quad (2.40)$$

where

$$C_c = [C_d - C_\alpha M^{-1} K \mid C_v - C_\alpha M^{-1} C_0] \quad (2.41)$$

and

$$D_c = C_\alpha M^{-1} L \quad (2.42)$$

2.5 Modal model

2.5.1 State space equations

For the realization of modal analysis method the following transformation is introduced

$$\underline{x}(t) = \Psi \underline{\xi}(t) \quad (2.43)$$

where $\underline{\xi}$ is the vector of the main modal coordinates. Substituting eq. (2.43) in (2.32) and pre-multiplying by Ψ^{-1} the following expressions are obtained

$$\Psi \underline{\dot{\xi}} = A_c \Psi \underline{\xi} + B_c \underline{f}(t) \quad (2.44)$$

or equivalently

$$\underline{\dot{\xi}} = \Psi^{-1} A_c \Psi \underline{\xi} + \Psi^{-1} B_c \underline{f}(t) \quad (2.45)$$

Using the eigenvalue problem (2.37), one finally obtains the equations

$$\underline{\dot{\xi}} = \Lambda_c \underline{\xi} + L_c \underline{f}(t) \quad (2.46)$$

where

$$L_c = \Psi^{-1} B_c \quad (2.47)$$

The last equation (2.46) is the state space equations for the modal coordinates $\underline{\xi}(t)$. The L_c term can be simplified using equation (2.22) which is solved with respect to Ψ^{-1} to yield

$$\Psi^{-1} = \text{diag} \left[\frac{1}{a_r} \right] \Psi^T P \quad (2.48)$$

By substituting the last expression in (2.47) and using (2.15) and (2.13) results in

$$\begin{aligned}
L_c &= \Psi^{-1} B_c = \text{diag} \left[\frac{1}{a_r} \right] \Psi^T P \begin{bmatrix} 0 \\ M^{-1} L \end{bmatrix} = \\
&= \text{diag} \left[\frac{1}{a_r} \right] \left[\begin{array}{c|c} \Phi & \Phi^* \\ \hline \Phi \Lambda & \Phi^* \Lambda^* \end{array} \right]^T \begin{bmatrix} C_0 & M \\ M & 0 \end{bmatrix} \begin{bmatrix} 0 \\ M^{-1} L \end{bmatrix}
\end{aligned} \tag{2.49}$$

Carrying out the matrix multiplications, the above equation finally simplifies to

$$L_c = \text{diag} \left[\frac{1}{a_r} \right] \begin{bmatrix} \Phi^T \\ \Phi^{*T} \end{bmatrix} L \tag{2.50}$$

The L_c matrix is the participation factor matrix. Using modal coordinates equations (2.50) result in

$$\dot{\xi}_r(t) = \lambda_r \xi_r(t) + \frac{1}{\alpha_r} \phi_r^T L f(t), \quad r = 1, \dots, n \tag{2.51}$$

$$\dot{\xi}_{n+r}(t) = \lambda_r^* \xi_{n+r}(t) + \frac{1}{\alpha_{n+r}} \phi_{n+r}^{*T} L f(t), \quad r = 1, \dots, n \tag{2.52}$$

with

$$\xi_{n+r} = \xi_r^* \quad \text{and} \quad \alpha_{n+r} = \alpha_r^* \tag{2.53}$$

Note that the complex equation (2.52) is the complex conjugate of the complex model equation (2.51).

2.5.2 Observation equations

The response $\underline{y}(t)$ defined in (2.40) can be expressed using modal coordinates by substituting the transformation (2.43) in (2.40) to yield

$$\underline{y}(t) = C_c \Psi \underline{\xi}(t) + D_c \underline{f}(t) \tag{2.54}$$

or equivalently

$$\underline{y}(t) = V_c \underline{\xi}(t) + D_c \underline{f}(t) \tag{2.55}$$

where

$$V_c = C_c \Psi \tag{2.56}$$

The matrix $V_c \in \mathbb{C}^{N_o \times 2n}$ is called the modal response observation matrix and can be simplified using equations (2.41) and (2.15) into the form

$$V_c = \left[C_d - C_\alpha M^{-1} K \mid C_v - C_\alpha M^{-1} C_0 \right] \left[\begin{array}{c|c} \Phi & \Phi^* \\ \hline \Phi \Lambda & \Phi^* \Lambda^* \end{array} \right] \tag{2.57}$$

Let us now consider the following three special cases:

The response $\underline{y}(t)$ consists of the displacements only, that is $C_a = C_v = 0$ and $C_d \neq 0$. The V_c matrix takes the final form

$$V_c = [C_d \mid 0] \left[\begin{array}{c|c} \Phi & \Phi^* \\ \hline \Phi\Lambda & \Phi^*\Lambda^* \end{array} \right] = C_d [\Phi \mid \Phi^*] \quad (2.58)$$

The response $\underline{y}(t)$ consists of the velocities only, that is $C_a = C_d = 0$ and $C_v \neq 0$. The V_c matrix takes the final form

$$V_c = C_v [\Phi\Lambda \mid \Phi^*\Lambda^*] \quad (2.59)$$

The response $\underline{y}(t)$ consists of the accelerations only, that is $C_v = C_d = 0$ and $C_a \neq 0$. The V_c matrix takes the final form

$$\begin{aligned} V_c &= -C_a [M^{-1}K \mid M^{-1}C_0] \left[\begin{array}{c|c} \Phi & \Phi^* \\ \hline \Phi\Lambda & \Phi^*\Lambda^* \end{array} \right] \\ &= -C_a [M^{-1}K\Phi + M^{-1}C_0\Phi\Lambda \mid M^{-1}K\Phi^* + M^{-1}C_0\Phi^*\Lambda^*] \end{aligned} \quad (2.60)$$

that can be simplified further using the eigenproblem (2.16). Specifically, from (2.16) one has

$$M^{-1}K\Phi + M^{-1}C_0\Phi\Lambda = -\Phi\Lambda^2 \quad (2.61)$$

or equivalently by taking complex conjugates

$$M^{-1}K\Phi^* + M^{-1}C_0\Phi^*\Lambda^* = -\Phi^*\Lambda^{*2} \quad (2.62)$$

Substituting the last two expressions into (2.60), V_c is given by

$$V_c = C_a [\Phi\Lambda^2 \mid \Phi^*\Lambda^{*2}] \quad (2.63)$$

2.5.3 Summary of modal model equations

Summarizing, for the case of general non classically damped systems, the modal model consists of the modal state space equations (2.46) and the modal observation equations (2.55), that is,

$$\dot{\underline{\xi}} = \Lambda_c \underline{\xi} + L_c \underline{f}(t) \quad (2.64)$$

$$\underline{y}(t) = V_c \underline{\xi}(t) + D_c \underline{f}(t) \quad (2.65)$$

where

$$\underline{\xi}(t) = \begin{Bmatrix} \xi_1(t) \\ \vdots \\ \xi_n(t) \\ \xi_1^*(t) \\ \vdots \\ \xi_n^*(t) \end{Bmatrix} \in C^{2n \times 1} \quad (2.66)$$

is the modal coordinates vector

$$\Lambda_c = \begin{bmatrix} \Lambda & 0 \\ 0 & \Lambda^* \end{bmatrix} \quad (2.67)$$

is the matrix that consists of the complex eigenvalues λ_r of the system,

$$L_c = \Psi^{-1} B_c = \text{diag} \left[\frac{1}{a_r} \right] \begin{bmatrix} \Phi^T \\ \Phi^{*T} \end{bmatrix} L \in C^{2n \times N_m} \quad (2.68)$$

is the participation factor matrix,

$$\underline{f}(t) \in \mathbb{R}^{N_m} \quad (2.69)$$

is the independent vector of excitations,

$$D_c = C_a M^{-1} L \in \mathbb{R}^{N_o \times N_m} \quad (2.70)$$

is a matrix that is zero if no accelerations are contained in the response vector $\underline{y}(t)$, and $V_c \in C^{N_o \times 2n}$ is a matrix given by

$$V_c = C_d \begin{bmatrix} \Phi & \Phi^* \end{bmatrix} \quad \text{for displacements} \quad (2.71)$$

$$V_c = C_v \begin{bmatrix} \Phi \Lambda & \Phi^* \Lambda^* \end{bmatrix} \quad \text{for velocities} \quad (2.72)$$

$$V_c = C_a \begin{bmatrix} \Phi \Lambda^2 & \Phi^* \Lambda^{*2} \end{bmatrix} \quad \text{for accelerations} \quad (2.73)$$

Consider next the case for which C_d , C_v and C_a in (2.39) are observation matrices that assign a correspondence between the model degrees of freedom and the observation (measured) degrees of freedom. In this case note that:

$$U = C_d \Theta = [\underline{u}_1 \quad \cdots \quad \underline{u}_n] \quad (2.74)$$

is the eigenvector matrix at the desirable (measured) degrees of freedom that are included in the response vector $\underline{y}(t)$ for the displacements. Similarly, taking into account that Λ is diagonal yields

$$C_v \Theta \Lambda = [\lambda_1 \underline{u}_1 \quad \cdots \quad \lambda_n \underline{u}_n] \quad (2.75)$$

is the eigenvector matrix at the desirable degrees of freedom that are included in the response vector $\underline{y}(t)$ for the velocities. Similarly, taking into account that Λ^2 is a diagonal matrix,

$$C_d \Theta \Lambda^2 = \begin{bmatrix} \lambda_1^2 \underline{u}_1 & \cdots & \lambda_n^2 \underline{u}_n \end{bmatrix} \quad (2.76)$$

is the eigenvector matrix at the desirable degrees of freedom that are included in the response vector $\underline{y}(t)$ for the accelerations.

Based on the above formulations the response $\underline{y}(t) \in \mathbb{R}^{N_o}$ at the N_o degrees of freedom of the linear model is given by

$$\underline{y}(t) = \begin{bmatrix} U & U^* \end{bmatrix} \underline{\xi}(t) + D_c \underline{f}(t) \quad (2.77)$$

where

$$U = \begin{bmatrix} \underline{u}_1, \dots, \underline{u}_n \end{bmatrix} \in C^{N_o \times n} \quad (2.78)$$

is the eigenvector matrix at the desirable degrees of freedom. Consequently, the system response for either displacements or velocities or accelerations is fully defined when the elements of the matrices Λ_c , L_c , U and D_c are known.

From the previous analysis, it is evident that the response $\underline{y}(t)$ of the linear structure at selected degrees of freedom can be completely defined by knowing the parameters set $\underline{\theta}$ that includes all entries involved in the matrices Λ_c , L_c , V_c and D_c .

2.6 Special case: Classically damped model

The aforementioned equations for the general case of non-classically damped system are simplified in this paragraph for the case of classically damped systems and assuming that the structure matrices M , C_n and $K \in \mathbb{R}^{n \times n}$ are symmetric. From the analysis of classically damped structures with symmetric matrices, it is known that the response is given by

$$\underline{q} = \underline{\phi} e^{\lambda t} \quad (2.79)$$

where $\underline{\phi} \in \mathbb{R}^n$ is a real modeshape vector. In this case the matrix of modeshapes $\Phi \in \mathbb{R}^{n \times n}$, defined in (2.15), is also a real matrix.

Consequently, substituting in (2.15) the complex modeshape matrix, Ψ is given by

$$\Psi = \begin{bmatrix} \Phi & \Phi \\ \Phi \Lambda & \Phi \Lambda^* \end{bmatrix} \quad (2.80)$$

Substituting the above equation into the orthogonality condition (2.21) yields

$$\text{diag}[a_r] = \Psi^T P \Psi = \begin{bmatrix} \text{diag} \left[2\omega_r \sqrt{1 - \zeta_r^2} \right] & 0 \\ 0 & -\text{diag} \left[2\omega_r \sqrt{1 - \zeta_r^2} \right] \end{bmatrix} \quad (2.81)$$

and substituting (2.81) in (2.68) yields

$$L_c = -j \begin{bmatrix} \text{diag} [2\omega_r \sqrt{1-\zeta_r^2}] & 0 \\ 0 & -\text{diag} [2\omega_r \sqrt{1-\zeta_r^2}] \end{bmatrix}^{-1} \begin{bmatrix} \Phi^T \\ \Phi^T \end{bmatrix} L \quad (2.82)$$

Using (2.51) and (2.52), the modal coordinates $\xi_r(t)$ and $\xi_r^*(t)$ are written in the form

$$\dot{\xi}_r(t) = \lambda_r \xi_r + \frac{1}{2\omega_r j \sqrt{1-\zeta_r^2}} \phi_r^T L f(t) \quad (2.83)$$

$$\dot{\xi}_r^*(t) = \lambda_r^* \xi_r^* + \frac{1}{-2\omega_r j \sqrt{1-\zeta_r^2}} \phi_r^T L f(t) \quad (2.84)$$

The system of equation (2.83) and (2.84) can thus be written in the complex form (2.64) where L_c is an *purely imaginary* matrix given by (2.82). Using (2.55) to (2.57) and (2.80), the response vector $\underline{y}(t)$ is given by the observation equation

$$\underline{y}(t) = V_c \underline{\xi}(t) + D_c f(t) \quad (2.85)$$

where

$$V_c = C_c \begin{bmatrix} \Phi & \Phi \\ \Phi \Lambda & \Phi \Lambda^* \end{bmatrix} \quad (2.86)$$

$$C_c = [C_d - C_\alpha M^{-1} K \mid C_v - C_\alpha M^{-1} C_0] \quad (2.87)$$

$$D_c = C_\alpha M^{-1} L \quad (2.88)$$

2.7 The Frequency Response Function based on the modal model

For the system that has resulted following the aforementioned analysis we will use Fourier transform that results in the frequency domain equivalent, and at the same time transforms the differential equations into algebraic. Generally, a function $g(t)$ can be analyzed using Fourier components

$$g(t) = \frac{1}{2\pi} \int_{-\infty}^{\infty} \hat{g}(\omega) e^{j\omega t} d\omega \quad (2.89)$$

where $\hat{g}(\omega)$ is the Fourier coefficient given by

$$\hat{g}(j\omega) = \int_{-\infty}^{\infty} g(t) e^{-j\omega t} dt \quad (2.90)$$

Applying the Fourier transform to equation (2.1) in the frequency domain yields

$$\hat{q}(j\omega) = H(j\omega) \hat{L}f(j\omega) \quad (2.91)$$

where

$$H(j\omega) = [M(j\omega)^2 + C(j\omega) + K]^{-1} \quad (2.92)$$

The matrix $H(j\omega)$ is called transfer function matrix.

It has already been mentioned that from the set of differential equations in (2.1) has resulted into a set of algebraic equations in (2.91).

The modal equations (2.46) and (2.55) can be formulated in the frequency domain

$$\underline{y}(t) = \sum_{r=1}^n (\underline{u}_r \underline{\xi}_r(t) + \underline{u}_r^* \underline{\xi}_r^*(t)) + \sum_{k=1}^{N_m} \underline{d}_k f_k(t) \quad (2.93)$$

where

$$\dot{\underline{\xi}}_r(t) = \lambda_r \underline{\xi}_r(t) + \underline{L}_r^T \underline{f}(t) \quad (2.94)$$

$$\dot{\underline{\xi}}_r^*(t) = \lambda_r^* \underline{\xi}_r^*(t) + \underline{L}_r^{*T} \underline{f}(t) \quad (2.95)$$

$$\lambda_r = -\zeta_r \omega_r \pm j\omega_r \sqrt{1 - \zeta_r^2} \quad (2.96)$$

and the vector \underline{d}_k is the k -th column of D_c

$$D_c = [\underline{d}_1 \quad \cdots \quad \underline{d}_{N_m}] \quad (2.97)$$

Using the Fourier transform, the relation between the response $\hat{\underline{y}}(j\omega)$ and the excitation $\hat{\underline{f}}(j\omega)$ in the frequency domain is given by

$$\hat{\underline{y}}(j\omega) = H(j\omega) \hat{\underline{f}}(j\omega) + D_c \hat{\underline{f}}(j\omega) \quad (2.98)$$

where

$$H(j\omega) = \sum_{r=1}^n \left[\frac{\underline{u}_r \underline{L}_r^T}{j\omega - \lambda_r} + \frac{\underline{u}_r^* \underline{L}_r^{*T}}{j\omega - \lambda_r^*} \right] \quad (2.99)$$

In matrix form equation (2.99) can be written as

$$H(j\omega) = U [j\omega I_n - \Lambda]^{-1} L_c^T + U^* [j\omega I_n - \Lambda^*]^{-1} L_c^{*T} \quad (2.100)$$

with

$$L_c = \begin{bmatrix} \underline{L}_1^T \\ \vdots \\ \underline{L}_n^T \end{bmatrix} \in R^{n \times n} \quad (2.101)$$

is the Transfer Function matrix that is formulated with respect to eigenvectors \underline{u}_r , participation factors \underline{l}_r and eigenvalues λ_r and define the Frequency Response Function (FRF) matrix between the n outputs and the N_m inputs.

It should be noted that the second term in the right-hand side of equation (2.98) is non-zero only if the response vector of interest $\underline{\hat{y}}(j\omega)$ include terms for the system acceleration.

Cross power spectral densities in modal space

3.1 Introduction

The following chapter will deal with the modal decomposition of output-only data in the frequency domain. It will be shown that, analogous to FRF data, modal parameters can be identified from cross power spectra of output-only data. The estimation of the power spectra between the outputs and the reference outputs is discussed. The auto and cross power spectral density functions are the primary data for model parameter identification based on output-only (ambient) measurements. Basically, two classical approaches exist for the estimation of auto and cross power spectral density functions. The periodogram estimator operates directly on the spectra of different time blocks resulting from a division of the time sequences. The correlogram approach first estimates the correlation functions in the time-domain and next the power spectra are obtained by transferring the correlations to the frequency-domain. Finally, the estimation of the half (or positive) power spectra is also discussed.

3.2 Modal decomposition of cross power functions

Consider a n DOF representation of a linear mechanical system given in (2.1). Let $\underline{f}(t) \in \mathbb{R}^{N_m}$ denote the force input vector at continuous time t and $\underline{x}(t) \in \mathbb{R}^n$ the output displacement vector. Let the $(n \times N_m)$ Frequency Response Function (FRF) matrix between the outputs and inputs be given by equation (2.99)

$$H(j\omega) = \sum_{r=1}^{N_m} \left[\frac{\underline{u}_r \underline{l}_r^T}{j\omega - \lambda_r} + \frac{\underline{u}_r^* \underline{l}_r^{*T}}{j\omega - \lambda_r^*} \right] \quad (3.1)$$

where λ_r , \underline{u}_r and \underline{l}_r are respectively the pole, mode shape and modal participation factor of mode r , and N_m is the number of contributing modes with $N_m \leq n$.

It is known from literature (Ljung, 1999) that for stationary stochastic processes the cross power spectral density matrix $S_{xx}(j\omega) \in \mathbb{C}^{N_{out} \times N_{out}}$ of the response vector $x(t)$ can be written as a function of the transfer function $H(j\omega)$ and the cross power spectral density matrix $S_{ff}(j\omega)$ of the (unknown) force vector $\underline{f}(t)$ as follows:

$$S_{xx}(j\omega) = H(j\omega)S_{ff}(j\omega)H^{*T}(j\omega) \quad (3.2)$$

Assuming that the forces acting on the structure are white noise sequences, then the cross power spectral density matrix of the forces is constant, independent of $j\omega$, given by $S_{ff}(j\omega) = S_0$ that is real. In this case equation (3.2) is written in the form

$$S_{xx}(j\omega) = H(j\omega)S_0(j\omega)H^{*T}(j\omega) \quad (3.3)$$

It is shown in the Appendix 3.A that by assuming white noise inputs and substituting (2.99) in (3.3) the matrix cross power spectral density matrix $S_{xx}(j\omega)$ of the responses evaluated at frequency ω , can be modally decomposed as follows

$$S_{xx}(j\omega) = \sum_{r=1}^{N_m} \left[\frac{\underline{u}_r \underline{g}_r^T}{j\omega - \lambda_r} + \frac{\underline{u}_r^* \underline{g}_r^{*T}}{j\omega - \lambda_r^*} + \frac{\underline{g}_r \underline{u}_r^T}{-j\omega - \lambda_r} + \frac{\underline{g}_r^* \underline{u}_r^{*T}}{-j\omega - \lambda_r^*} \right] \quad (3.4)$$

where \underline{u}_r is the complex modeshape of mode r of the linear system and \underline{g}_r is the operational reference vector for mode r given by eq. (3.28) in Appendix 3.A. This reference vector is a complex function of the cross power spectrum matrix of the unknown random input forces and the modal parameters of the structure but its physical interpretation is less obvious than the modal participation factors. It should be noticed that the modal decomposition of the power densities of the outputs has a symmetry in the poles i.e. both the positive and negative poles are present in the model. This symmetry is referred to as a 4-quadrant symmetry. Given this similarity between the modal decomposition of the cross spectral densities of the outputs and the modal decomposition of the FRFs, the modal parameter estimation techniques developed for FRFs can be extended to handle the case where the cross power spectral density matrix is available from output-only data.

3.3 Estimation of auto and cross power spectral densities

In order to use equation (3.4) for the identification of modal parameters from output-only data, accurate estimates of the cross power spectral densities, between the responses, are to be obtained from finite sequences of measured time samples. Basically, two classical methods exist for the estimation of auto and cross power spectral density estimates (Marple 1987), the periodogram and the correlogram approach. The periodogram (Marple 1987) method operates directly on the data set to yield power spectrum estimates. The correlogram approach (Blackman and Tukey 1958) first makes an estimate of the correlation functions in the time-domain and then proceeds by Fourier transforming the correlation sequences into power spectral densities. For both approaches, the user is faced with a tradeoff to produce statistically reliable estimates of highest possible spectral resolution from finite sequences of measured time data. For completeness, these methods are briefly presented. Parts of the presentation that follows have been taken from the work of Parloo (2003) and Cauberghe (2004).

3.3.1 The periodogram approach

The periodogram method is a popular method for the estimation of auto and cross power spectral densities (Marple 1987). Let $x_o(m)$, $m = 0, \dots, M-1$, $o = 1, \dots, N_{out}$ be an assembly of N_{out} discrete time-domain output sequences. Let $\underline{x}^{ref}(m)$ be a sub-vector of $\underline{x}(m)$ containing the time sequences of N_{ref} outputs which are serving as reference-responses for the measured data set. The basic idea of the periodogram method is to divide the data sequence for each measured output of M samples into P non-overlapping segments of D samples each, so that $DP \leq M$.

As an alternative to choosing no common samples between adjacent segments, a small overlap can be used (Welch, 1967). For each segment s , $s = 0, \dots, P-1$, the discrete Fourier transform of the signal $x_o(m)$ for all considered responses o , $o = 1, \dots, N_{out}$, weighted with a time window W of length D , can be computed as

$$X_o^s(j\omega) = T_s \left(\sum_{k=0}^{D-1} W(k) x_o(sD+k) e^{-j\omega k T_s} \right) \quad (3.5)$$

A similar expression can be found for all reference responses i , $i = 1, \dots, N_{ref}$, assembled in the sub-vectors $\underline{x}^{ref}(m)$

$$X_o^{s,ref}(j\omega) = T_s \left(\sum_{k=0}^{D-1} W(k) x_i^{ref}(sD+k) e^{-j\omega k T_s} \right) \quad (3.6)$$

An estimate of the entries of the $(N_{out} \times N_{ref})$ cross power spectral density matrix $S(j\omega)$ for each response reference-response combination, evaluated at discrete frequency ω , is given by

$$S_{o,i}(j\omega) = \frac{1}{P} \sum_{s=0}^{P-1} \left[X_o^s(j\omega) (X_i^{s,ref}(j\omega))^* \right] \quad (3.7)$$

where $X_o^s(j\omega)$ and $X_i^{s,ref}(j\omega)$ are respectively the $(N_{out} \times 1)$ and $(N_{ref} \times 1)$ vectors computed in (3.5) and (3.6).

The time window W (e.g., Hanning window) is used to reduce the negative effect of leakage. Choosing a higher amount of data samples D in each segment, at the expense of the number of averages P , will reduce the effect of leakage. Moreover, a higher spectral resolution will be obtained in the frequency-domain. However, the resulting decrease in the number of averages P leads to a higher stochastic uncertainty on the estimates. In practice, a trade-off will have to be made between these contradicting aspects.

Note that the basic idea behind allowing an overlap between the data segments consists in allowing a better contribution of all samples of the raw time history response data to the averaged estimate. If no overlap is considered, the contribution of samples near the edges of the segments will be suppressed by the presence of the Hanning window.

3.3.2 The correlogram approach

The periodogram approach can be used as an alternative to the periodogram method for the estimation of cross power spectra of the response signals. This method computes the unbiased discrete-time domain correlation estimate between the signal $x_o(m)$, $m = 0, \dots, M-1$, of a response o and the signal $x_i^{ref}(m)$ of a reference-response i . This correlation estimate is given by

$$\left\{ \begin{array}{l} R_{o,j}(k) = \frac{1}{M-k} \sum_{m=0}^{M-k-1} x_o(m+k)x_i^{ref}(m) \quad \text{for } 0 \leq k \leq M-1 \\ R_{o,j}(k) = \frac{1}{M-|k|} \sum_{m=0}^{M-|k|-1} x_i^{ref}(m+|k|)x_o(m) \quad \text{for } -(M-1) \leq k \leq 0 \end{array} \right. \quad (3.8)$$

with k the correlation time. The biased correlation estimate uses $1/M$ rather than $1/(M-k)$. The cross power spectral density function matrix estimates can then be obtained by Fourier transforming the correlation functions obtained from (3.8)

$$S_{o,j}(j\omega) = T_s \sum_{k=-M}^M W(k)R_{o,j}(k)e^{-j\omega T_s} \quad (3.9)$$

where $R(k)$ is the $(N_{out} \times N_{ref})$ matrix that contains the correlation estimates calculated in (3.8) and $W(k)$ is a $(2M+1)$ point time window.

The window reduces the effect of leakage due to the large side lobes of the implicit rectangular window and therefore the bias error in the cross power spectral density estimate. The use of an adequate window (e.g., Hanning, Hamming, etc), symmetric around the origin, is advisable. For instance, applying a Hanning window to the correlation estimate will force the correlation to zero at the higher lags. Moreover, the application of such a window reduces the stochastic uncertainty on the cross power estimate due to the presence of a higher stochastic uncertainty near the higher lags of the correlation function estimate. However, when applying a time window, the poles (and especially the damping) of the underlining system will be affected. However, for an exponential window, the poles can be compensated exactly for the added damping. This is not the case for other windows such as Hanning or Hamming.

Hence, for the purpose of modal parameter estimation, the correlogram approach is best combined with the use of an exponential window. Given the form of the correlation function estimates, a double sided exponential time data window centered around 0,

$$W_m = e^{-\beta|m|T_s} \quad \text{with} \quad -M \leq m \leq +M \quad (3.10)$$

with β a decay factor, can be used. The poles λ_r^{est} extracted from the estimates can be compensated (corrected) for the artificial damping added by the window by using the value of the β factor as follows

$$\lambda_r^{cor} = \lambda_r^{est} + \beta \quad (3.11)$$

Although an averaging procedure is usually not strictly required, the possibility exists to use an averaging similar to the periodogram approach. If the time history response sequences consist of M samples, every response sequence can be divided into P non-overlapping segments of D samples each so that $DP \leq M$. Correlogram estimates of the auto- and cross power spectra $S_{o,j}^s$, between the responses o , $o=1, \dots, N_{out}$, and a subset of reference responses i , $i=1, \dots, N_{ref}$, can be obtained using equations (3.8) and (3.9) for each segments s , $s=0, \dots, P-1$. An averaged correlogram estimate of the auto- and cross power spectra is then given by

$$S_{o,j} = \sum_{s=0}^{P-1} S_{o,j}^s \quad (3.12)$$

It should be noted that averaging the correlogram estimates decreases the spectral resolution of the resulting estimate. Reducing the number of samples used for the computation of the correlation functions also increases the bias error due to leakage on these estimates.

3.3.3 The 'positive' power spectra approach

For the identification of modal parameters from output-only measurements, several frequency-domain identification methods are based on the cross power spectral densities satisfying (3.4). However, this technique has several disadvantages:

- The power spectra have a 4-quadrant symmetry i.e. the modal model contains as poles the values λ_r , λ_r^* , $-\lambda_r$ and $-\lambda_r^*$. This results in a model order, which is twice the modal order needed to model FRFs. For all identification methods based on the full spectra, this higher model order results in an increasing calculation time and in a less good numerical conditioning.
- The power spectra contain both stable λ_r , λ_r^* and unstable poles $-\lambda_r$, $-\lambda_r^*$ poles in its model. This results in less interesting properties for the interpretation of stabilization diagrams, when distinguishing physical from mathematical poles.
- Power spectra estimated from a limited amount of data are typically characterized by high noise levels compared to FRFs. Therefore, an additional noise reduction would be preferable.
- When using the periodogram approach to estimate the power spectra, a tradeoff must be made between the stochastic uncertainties and the bias errors introduced by leakage.

Some of these disadvantages can be overcome by starting from the first M positive lags of the correlation function R_n given by (3.8). Using the correlogram approach it is sufficient to estimate the so called *positive spectra* (or half spectra), which are obtained by using only the correlation having a positive time lag (Cauberghe 2004, Peeters and Van der Auwearer 2005) in (3.9) as follows

$$S_{o,j}^{++}(j\omega) = \frac{W(0)R_{o,j}(0)}{2} + T_s \sum_{k=1}^M W(k)R_{o,j}(k)e^{-j\omega T_s} \quad (3.13)$$

The relation between half spectra (3.13) and the full spectra (3.9) is the following:

$$S_{o,j}(j\omega) = S_{o,j}^{++}(j\omega) + \left(S_{o,j}^{++}(j\omega)\right)^{*T} \quad (3.14)$$

The modal decomposition of these half spectra only consists of the first two terms in (3.4), that is,

$$S_{xx}^{++}(j\omega) = \sum_{r=1}^{N_m} \left[\frac{\mathbf{u}_r \mathbf{g}_r^T}{j\omega - \lambda_r} + \frac{\mathbf{u}_r^* \mathbf{g}_r^{*T}}{j\omega - \lambda_r^*} \right] \quad (3.15)$$

The advantage in modal analysis is that models of low order can be fitted without affecting the quality.

Under the white noise input assumption, the output correlations are equivalent to impulse response. So, just like in impact testing, it is logical to apply an exponential window $W(k)$ to the correlations before computing the DFT in equation (3.13). The exponential window reduces the effect of leakage and the influence of the higher time lags, which have a larger variance. Moreover, the application of an exponential window to impulse responses or correlations is compatible with the modal model and the pole estimates can be corrected using equation (3.11).

3.3.4 Choosing reference responses

Similar to choosing position(s) for the input force(s) (so-called references) during input-output modal testing, the choice of good reference response signals during output-only modal testing can be important for obtaining high quality data sets.

If all N_{out} responses of a structure under test are measured simultaneously, each of the structural responses can be used as a reference response. This approach results in a $N_{out} \times N_{out}$ power spectrum matrix $S(j\omega)$. If the number of outputs is large, the latter approach can lead to a high computational burden especially during the parametric estimation.

Instead of using all outputs as reference responses, a small number of responses in suitable locations of the structure can be chosen as reference responses. Note that the nodal points of structural modes should be avoided to be used as reference positions. Moreover, responses with a signal to noise ratio superior (or at least equal) compared to the other responses should be preferred when choosing reference responses in order to increase the quality of the auto and cross power spectral density estimates. If the reference response signals are chosen carefully, similar quality modal information can be extracted from data sets obtained with a limited number of references as from data sets where the maximum number of references was used.

The idea of the reference sensors can be used to obtain measurements for a structure using a small number of sensors compared to the measurement locations that one would like to identify the modeshape components. In this case the available sensors are divided into two groups. One group constitutes the reference group and the sensors are placed at reference locations which remain fixed during the measurements. The other group constitutes the moving group and the sensors in this group are moved from measurement to measurement to new locations until all desirable measurements locations are covered by the available number of moving sensors. The measurements from the moving sensors are combined into the vector $\underline{x}(m)$, while the measurements from the reference sensors constitute the vector of measurements $\underline{x}^{ref}(m)$. In choosing the reference locations care should be taken so that nodal points are avoided.

Appendix 3.A: Modal decomposition of cross power spectral density functions

The aim of this appendix is to show that the cross power matrix of the responses $S_{xx}(j\omega)$ can be modally decomposed in the form (3.4). For this, note that equation (2.99) can be written as

$$H(j\omega) = [U \quad U^*] \begin{bmatrix} h(j\omega) & 0 \\ 0 & h^*(j\omega) \end{bmatrix} \begin{bmatrix} L_c \\ L_c^* \end{bmatrix} \quad (3.16)$$

where U , L_c are given by (2.78) and (2.101)

$$h(j\omega) = \begin{bmatrix} \ddots & & 0 \\ & \frac{1}{j\omega - \lambda_r} & \\ 0 & & \ddots \end{bmatrix} \in \mathbb{C}^{m \times m} \quad (3.17)$$

$$h^*(j\omega) = \begin{bmatrix} \ddots & & 0 \\ & \frac{1}{j\omega - \lambda_r^*} & \\ 0 & & \ddots \end{bmatrix} \in \mathbb{C}^{m \times m} \quad (3.18)$$

Substituting equation (3.16) in (3.3) gives

$$S_{xx}(j\omega) = [U \quad U^*] \begin{bmatrix} h(j\omega) & 0 \\ 0 & h^*(j\omega) \end{bmatrix} \begin{bmatrix} L_c \\ L_c^* \end{bmatrix} S_0 \begin{bmatrix} L_c^{*T} & L_c^T \end{bmatrix} \begin{bmatrix} h^*(-j\omega) & 0 \\ 0 & h(-j\omega) \end{bmatrix} \begin{bmatrix} U^{*T} \\ U^T \end{bmatrix} \quad (3.19)$$

It should be noted that each component in the matrix $S_{xx}(j\omega)$ is a product of the four rational functions

$$\frac{1}{j\omega - \lambda_r}, \frac{1}{j\omega - \lambda_r^*}, \frac{1}{-j\omega - \lambda_r} \text{ and } \frac{1}{-j\omega - \lambda_r^*} \quad (3.20)$$

So partial fraction decomposition can be used to write each component of $S_{xx}(j\omega)$ as a sum of the rational functions (3.20) with coefficients in the sum to be determined.

Repeating this partial fraction decomposition for all components of the matrix $S_{xx}(j\omega)$, one finally has the following partial fraction decomposition for the cross power spectral density matrix $S_{xx}(j\omega)$:

$$S_{xx}(j\omega) = \sum_{r=1}^{N_m} \left[\Psi_{r1} \frac{1}{j\omega - \lambda_r} + \Psi_{r2} \frac{1}{j\omega - \lambda_r^*} + \Psi_{r3} \frac{1}{-j\omega - \lambda_r} + \Psi_{r4} \frac{1}{-j\omega - \lambda_r^*} \right] \quad (3.21)$$

where $\Psi_{r1} \in \mathbb{C}^{N_{out} \times N_{out}}$ are the matrix coefficients to be determined as follows.

Specifically, the matrix Ψ_{r1} is obtained by multiplying both sides of equation (3.21) by $j\omega - \lambda_r$ and evaluating the resulting equation at $j\omega = \lambda_r$. Thus, one obtains that

$$\Psi_{r1} = (j\omega - \lambda_r)S_{xx}(j\omega) = \begin{bmatrix} U & U^* \end{bmatrix} \begin{bmatrix} h(j\omega)(j\omega - \lambda_r) & 0 \\ 0 & h^*(j\omega)(j\omega - \lambda_r) \end{bmatrix} \Big|_{j\omega=\lambda_r} \begin{bmatrix} L_c^* & L_c^T \\ L_c^* & L_c^T \end{bmatrix} S_0 \begin{bmatrix} L_c^{*T} & L_c^T \\ L_c^* & L_c^T \end{bmatrix} \begin{bmatrix} h^*(-\lambda_r) & 0 \\ 0 & h(-\lambda_r) \end{bmatrix} \begin{bmatrix} U^{*T} \\ U^T \end{bmatrix} \quad (3.22)$$

This expression is further simplified by noting that

$$\left[(j\omega - \lambda_r)h(j\omega) \right]_{j\omega=\lambda_r} = \underline{\delta}_r \underline{\delta}_r^T \in \mathbb{R}^{m \times m} \quad (3.23)$$

and

$$\left[(j\omega - \lambda_r)h^*(j\omega) \right]_{j\omega=\lambda_r} = 0 \in \mathbb{R}^{m \times m} \quad (3.24)$$

where $\underline{\delta}_r \in \mathbb{R}^{m \times 1}$ is a vector with the r -th element equal to 1 and all other $m-1$ element equal to 0. Thus, the following expressions are simplified to

$$\begin{aligned} \left[\begin{bmatrix} U & U^* \end{bmatrix} \begin{bmatrix} h(j\omega) & 0 \\ 0 & h^*(j\omega) \end{bmatrix} (j\omega - \lambda_r) \right]_{j\omega=\lambda_r} &= \begin{bmatrix} U & U^* \end{bmatrix} \begin{bmatrix} \underline{\delta}_r \underline{\delta}_r^T & 0 \\ 0 & 0 \end{bmatrix} \\ &= \begin{bmatrix} \underline{0} & \dots & \underline{0} & \underline{u}_r & \underline{0} & \dots & \underline{0} \end{bmatrix} \in \mathbb{C}^{N_{out} \times 2m} \end{aligned} \quad (3.25)$$

and

$$\begin{aligned} \left[\begin{bmatrix} U & U^* \end{bmatrix} \begin{bmatrix} h(j\omega) & 0 \\ 0 & h^*(j\omega) \end{bmatrix} (j\omega - \lambda_r) \begin{bmatrix} L_c \\ L_c^* \end{bmatrix} \right]_{j\omega=\lambda_r} \\ = \begin{bmatrix} \underline{0} & \dots & \underline{0} & \underline{u}_r & \underline{0} & \dots & \underline{0} \end{bmatrix} \begin{bmatrix} L_c \\ L_c^* \end{bmatrix} = \underline{u}_r \underline{l}_r^T \in \mathbb{C}^{N_{out} \times 2m} \end{aligned} \quad (3.26)$$

Substituting in (3.22) gives

$$\Psi_{r1} = \underline{u}_r \underline{l}_r^T S_0 \begin{bmatrix} L_c^{*T} & L_c^T \\ L_c^* & L_c^T \end{bmatrix} \begin{bmatrix} h^*(-\lambda_r) & 0 \\ 0 & h(-\lambda_r) \end{bmatrix} \begin{bmatrix} U^{*T} \\ U^T \end{bmatrix} \in \mathbb{C}^{N_{out} \times N_{out}} \quad (3.27)$$

Introducing the vector

$$\underline{g}_r^T = \underline{l}_r^T S_0 \begin{bmatrix} L_c^{*T} & L_c^T \\ L_c^* & L_c^T \end{bmatrix} \begin{bmatrix} h^*(-\lambda_r) & 0 \\ 0 & h(-\lambda_r) \end{bmatrix} \begin{bmatrix} U^{*T} \\ U^T \end{bmatrix} \in \mathbb{C}^{1 \times N_{out}} \quad (3.28)$$

the coefficient matrix simplifies to

$$\Psi_{r1} = \underline{u}_r \underline{g}_r^T \quad (3.29)$$

Similarly, multiplying both sides of equation (3.21) by $j\omega - \lambda_r^*$ and evaluating the expression at $j\omega = \lambda_r^*$ one obtains that

$$\Psi_{r,2} = (j\omega - \lambda_r^*)S_{xr}(j\omega) = \begin{bmatrix} U & U^* \end{bmatrix} \begin{bmatrix} h(j\omega)(j\omega - \lambda_r^*) & 0 \\ 0 & h^*(j\omega)(j\omega - \lambda_r^*) \end{bmatrix} \underset{j\omega = \lambda_r^*}{\begin{bmatrix} L_c \\ L_c^* \end{bmatrix}} S_0 \begin{bmatrix} L_c^{*T} & L_c^T \end{bmatrix} \begin{bmatrix} h^*(-\lambda_r^*) & 0 \\ 0 & h(-\lambda_r^*) \end{bmatrix} \begin{bmatrix} U^{*T} \\ U^T \end{bmatrix} \quad (3.30)$$

This expression is further simplified by noting that

$$\left[(j\omega - \lambda_r^*)h(j\omega) \right]_{j\omega = \lambda_r^*} = 0 \in \mathbb{R}^{m \times m} \quad (3.31)$$

and

$$\left[(j\omega - \lambda_r^*)h^*(j\omega) \right]_{j\omega = \lambda_r^*} = \underline{\delta}_r \underline{\delta}_r^T \in \mathbb{R}^{m \times m} \quad (3.32)$$

The following simplification follows

$$\begin{aligned} & \left[\begin{bmatrix} U & U^* \end{bmatrix} \begin{bmatrix} h(j\omega) & 0 \\ 0 & h^*(j\omega) \end{bmatrix} (j\omega - \lambda_r^*) \begin{bmatrix} L_c \\ L_c^* \end{bmatrix} \right]_{j\omega = \lambda_r^*} = \begin{bmatrix} U & U^* \end{bmatrix} \begin{bmatrix} 0 & 0 \\ 0 & \underline{\delta}_r \underline{\delta}_r^T \end{bmatrix} \begin{bmatrix} L_c \\ L_c^* \end{bmatrix} \\ & = \begin{bmatrix} \underline{0} & \dots & \underline{0} & \underline{u}_r^* & \underline{0} & \dots & \underline{0} \end{bmatrix} \begin{bmatrix} L_c \\ L_c^* \end{bmatrix} = \underline{u}_r^* \underline{l}_r^{*T} \in \mathbb{C}^{N_{out} \times 2m} \end{aligned} \quad (3.33)$$

Substituting in (3.30), one obtains that

$$\Psi_{r,2} = \underline{u}_r^* \underline{l}_r^{*T} S_0 \begin{bmatrix} L_c^{*T} & L_c^T \end{bmatrix} \begin{bmatrix} h^*(-\lambda_r^*) & 0 \\ 0 & h(-\lambda_r^*) \end{bmatrix} \begin{bmatrix} U^{*T} \\ U^T \end{bmatrix} \in \mathbb{C}^{N_{out} \times N_{out}} \quad (3.34)$$

Introducing the vector

$$\underline{p}_r^T = \underline{l}_r^{*T} S_0 \begin{bmatrix} L_c^{*T} & L_c^T \end{bmatrix} \begin{bmatrix} h^*(-\lambda_r^*) & 0 \\ 0 & h(-\lambda_r^*) \end{bmatrix} \begin{bmatrix} U^{*T} \\ U^T \end{bmatrix} \in \mathbb{C}^{1 \times N_{out}} \quad (3.35)$$

then

$$\Psi_{r,2} = \underline{u}_r^* \underline{p}_r^T \quad (3.36)$$

Proposition: The following equation holds which relates the vectors \underline{p}_r and \underline{g}_r involved in equations (3.29) and (3.36)

$$\underline{p}_r^T = \underline{g}_r^{*T} \quad (3.37)$$

Proof: Starting from the definition of \underline{p}_r in (3.35), one has that

$$\underline{p}_r^T = \underline{l}_r^{*T} S_0 \begin{bmatrix} L_c^{*T} & L_c^T \end{bmatrix} \begin{bmatrix} h^*(-\lambda_r^*) U^{*T} \\ h(-\lambda_r^*) U^T \end{bmatrix} = \underline{l}_r^{*T} S_0 \{ L_c^{*T} h^*(-\lambda_r^*) U^{*T} + L_c^T h(-\lambda_r^*) U^T \} \quad (3.38)$$

Also, starting from the definition of \underline{g}_r in (3.29), one has that

$$\begin{aligned} \underline{g}_r^{*T} &= \underline{l}_r^{*T} S_0 \begin{bmatrix} L_c^T & L_c^{*T} \end{bmatrix} \begin{bmatrix} [h^*(-\lambda_r)]^* & 0 \\ 0 & [h(-\lambda_r)]^* \end{bmatrix} \begin{bmatrix} U^T \\ U^{*T} \end{bmatrix} \\ &= \underline{l}_r^{*T} S_0 \begin{bmatrix} L_c^T & L_c^{*T} \end{bmatrix} \begin{bmatrix} [h^*(-\lambda_r)]^* U^T \\ [h(-\lambda_r)]^* U^{*T} \end{bmatrix} \\ &= \underline{l}_r^{*T} S_0 \left\{ L_c^T [h^*(-\lambda_r)]^* U^T + L_c^{*T} [h(-\lambda_r)]^* U^{*T} \right\} \end{aligned} \quad (3.39)$$

Note that the above equation assumes that $S_0^* = S_0$ which is true for the case of the excitation vector is a superposition of independent white noise processes.

Using (3.18) for $j\omega = -\lambda_r$, one has that

$$h^*(-\lambda_r) = \begin{bmatrix} \ddots & & 0 \\ & \frac{1}{-\lambda_r - \lambda_r^*} & \\ 0 & & \ddots \end{bmatrix} \quad (3.40)$$

and taking the complex conjugate, one derives that

$$[h^*(-\lambda_r)]^* = \begin{bmatrix} \ddots & & 0 \\ & \frac{1}{-\lambda_r^* - \lambda_r} & \\ 0 & & \ddots \end{bmatrix} \quad (3.41)$$

Using (3.17) for $j\omega = -\lambda_r^*$, it can be seen that

$$[h^*(-\lambda_r)]^* = h(-\lambda_r^*) \quad (3.42)$$

Using (3.17) for $j\omega = -\lambda_r$, one has that

$$h(-\lambda_r) = \begin{bmatrix} \ddots & & 0 \\ & \frac{1}{-\lambda_r - \lambda_r} & \\ 0 & & \ddots \end{bmatrix} \quad (3.43)$$

and taking the complex conjugate, one derives that

$$[h(-\lambda_r)]^* = \begin{bmatrix} \ddots & & 0 \\ & \frac{1}{-\lambda_r^* - \lambda_r} & \\ 0 & & \ddots \end{bmatrix} \quad (3.44)$$

Using (3.18) for $j\omega = -\lambda_r^*$ it can be seen that

$$[h(-\lambda_r)]^* = h^*(-\lambda_r^*) \quad (3.45)$$

Substituting (3.42) and (3.45) into (3.39) one readily derives that the right hand side of (3.39) is the same with the right hand side of (3.38) and thus

$$\underline{p}_r^T = \underline{g}_r^{*T} \quad (3.46)$$

which completes the proof of the proposition.

Using (3.36) and (3.37) one has

$$\Psi_{r2} = \underline{u}_r^* \underline{g}_r^{*T} \quad (3.47)$$

Moreover, comparing with (3.36) one has that

$$\Psi_{r2} = \Psi_{r1}^* \quad (3.48)$$

Similarly, the matrix Ψ_{r3} is obtained by multiplying both sides of equation (3.21) by $(-j\omega - \lambda_r)$ and evaluating the resulting equation at $j\omega = -\lambda_r$. Thus one obtains that

$$\begin{aligned} \Psi_{r3} &= (-j\omega - \lambda_r) S_{xx}(j\omega) = \\ & \begin{bmatrix} U & U^* \end{bmatrix} \begin{bmatrix} h(j\omega)(-j\omega - \lambda_r) & 0 \\ 0 & h^*(j\omega)(-j\omega - \lambda_r) \end{bmatrix} \Big|_{j\omega = -\lambda_r} \begin{bmatrix} L_c \\ L_c^* \end{bmatrix} S_0 \begin{bmatrix} L_c^{*T} & L_c^T \end{bmatrix} \begin{bmatrix} h^*(\lambda_r) & 0 \\ 0 & h(\lambda_r) \end{bmatrix} \begin{bmatrix} U^{*T} \\ U^T \end{bmatrix} \end{aligned} \quad (3.49)$$

This expression is further simplified by noting that

$$\left[(-j\omega - \lambda_r) h^*(-j\omega) \right]_{j\omega = -\lambda_r} = 0 \in \mathbb{R}^{m \times m} \quad (3.50)$$

and

$$\left[(-j\omega - \lambda_r) h(j\omega) \right]_{j\omega = -\lambda_r} = \underline{\delta}_r \underline{\delta}_r^T \in \mathbb{R}^{m \times m} \quad (3.51)$$

Thus, the following expression is obtained

$$\begin{aligned} & \left[\begin{array}{cc} L_c^{*T} & L_c^T \end{array} \right] \begin{bmatrix} h^*(j\omega) & 0 \\ 0 & h(j\omega) \end{bmatrix} (-j\omega - \lambda_r) \begin{bmatrix} U^{*T} \\ U^T \end{bmatrix} \Big|_{j\omega = -\lambda_r} \\ & = \begin{bmatrix} \underline{0} & \dots & \underline{0} & \underline{l}_r & \underline{0} & \dots & \underline{0} \end{bmatrix} \begin{bmatrix} U^{*T} \\ U^T \end{bmatrix} = \underline{l}_r \underline{u}_r^T \in \mathbb{C}^{N_{out} \times 2m} \end{aligned} \quad (3.52)$$

Substituting in (3.49) gives

$$\Psi_{r3} = \begin{bmatrix} U & U^* \end{bmatrix} \begin{bmatrix} h(-\lambda_r) & 0 \\ 0 & h^*(-\lambda_r) \end{bmatrix} \begin{bmatrix} L_c \\ L_c^* \end{bmatrix} S_0 \underline{l}_r \underline{u}_r^T \in \mathbb{C}^{N_{out} \times N_{out}} \quad (3.53)$$

and taking the complex conjugate transpose of equation (3.35) one has

$$\underline{p}_r^* = \begin{bmatrix} U & U^* \end{bmatrix} \begin{bmatrix} h(-\lambda_r) & 0 \\ 0 & h^*(-\lambda_r) \end{bmatrix} \begin{bmatrix} L_c \\ L_c^* \end{bmatrix} S_0 \underline{l}_r \quad (3.54)$$

that can be substituted in equation (3.53) to give

$$\Psi_{r3} = \underline{p}_r^* \underline{u}_r^T \quad (3.55)$$

Using equation (3.37), one has

$$\Psi_{r3} = \underline{g}_r \underline{u}_r^T \quad (3.56)$$

Similarly, multiplying both sides of equation (3.21) by $-j\omega - \lambda_r^*$ and evaluating the expression at $j\omega = -\lambda_r^*$ one obtains that

$$\begin{aligned} \Psi_{r4} &= (-j\omega - \lambda_r^*) S_{xx}(j\omega) = \\ & \begin{bmatrix} U & U^* \end{bmatrix} \begin{bmatrix} h(j\omega)(-j\omega - \lambda_r^*) & 0 \\ 0 & h^*(j\omega)(-j\omega - \lambda_r^*) \end{bmatrix} \begin{bmatrix} L_c \\ L_c^* \end{bmatrix} S_0 \begin{bmatrix} L_c^{*T} & L_c^T \end{bmatrix} \begin{bmatrix} h^*(\lambda_r^*) & 0 \\ 0 & h(\lambda_r^*) \end{bmatrix} \begin{bmatrix} U^{*T} \\ U^T \end{bmatrix} \Big|_{j\omega = -\lambda_r^*} \end{aligned} \quad (3.57)$$

This expression is further simplified by noting that

$$\left[(-j\omega - \lambda_r^*) h^*(-j\omega) \right]_{j\omega = -\lambda_r^*} = \underline{\delta}_r \underline{\delta}_r^T \in \mathbb{R}^{m \times m} \quad (3.58)$$

and

$$\left[(-j\omega - \lambda_r^*) h(-j\omega) \right]_{j\omega = -\lambda_r^*} = 0 \in \mathbb{R}^{m \times m} \quad (3.59)$$

The following simplification follows

$$\begin{aligned} & \left[\begin{bmatrix} L_c^{*T} & L_c^T \end{bmatrix} \begin{bmatrix} h^*(-j\omega) & 0 \\ 0 & h(-j\omega) \end{bmatrix} (-j\omega - \lambda_r^*) \begin{bmatrix} U^{*T} \\ U^T \end{bmatrix} \right]_{j\omega = -\lambda_r^*} \\ & = \begin{bmatrix} \underline{0} & \cdots & \underline{0} & \underline{l}_r^* & \underline{0} & \cdots & \underline{0} \end{bmatrix} \begin{bmatrix} U^{*T} \\ U^T \end{bmatrix} = \underline{p}_r^* \underline{u}_r^{*T} \in \mathbb{C}^{N_{out} \times 2m} \end{aligned} \quad (3.60)$$

Substituting in (3.57) gives

$$\Psi_{r4} = \begin{bmatrix} U & U^* \end{bmatrix} \begin{bmatrix} h(-\lambda_r^*) & 0 \\ 0 & h^*(-\lambda_r^*) \end{bmatrix} \begin{bmatrix} L_c \\ L_c^* \end{bmatrix} S_0 \underline{l}_r^* \underline{u}_r^{*T} \in \mathbb{C}^{N_{out} \times N_{out}} \quad (3.61)$$

and taking the complex conjugate transpose of equation (3.28) one has

$$\underline{g}_r^* = \begin{bmatrix} U & U^* \end{bmatrix} \begin{bmatrix} h(-\lambda_r^*) & 0 \\ 0 & h^*(-\lambda_r^*) \end{bmatrix} \begin{bmatrix} L_c \\ L_c^* \end{bmatrix} S_0 \underline{l}_r^* \quad (3.62)$$

that can be substituted in equation (3.61) giving

$$\Psi_{r4} = \underline{g}_r^* \underline{u}_r^{*T} \quad (3.63)$$

Finally, substituting the expressions (3.29), (3.47), (3.56) and (3.63) for the matrices Ψ_{r1} , Ψ_{r2} , Ψ_{r3} and Ψ_{r4} , respectively, into equation (3.21) results in the final form for $S_{cr}(j\omega)$ given in (3.4) with \underline{g}_r^T given by (3.28).

Chapter 4

Least squares output error methodologies for modal identification

4.1 Introduction

This chapter discusses several Modal Identification methodologies proposed to estimate the modal properties for the cases of EMA, OMA and earthquake induced vibrations. Modal identification methodologies are used for the estimation of modal frequencies, modal damping ratios, modeshapes and modal participation factors of a structure. All these methodologies introduced are based on the minimization of an output error function using a least squares minimization approach. The formulation is presented for the general case of non-classically damped modal model.

Specifically, the proposed modal identification methodologies use a three step approach to solve the error minimization problem. The first step provides estimates of the modal frequencies and modal damping ratios by solving a system of linear algebraic equations using the right-matrix fraction model or the common denominator model (Verboten 2002; Cauberghe 2004). Stabilization diagrams are used to distinguish between physical and mathematical modes. For the cases of OMA and MIMO this method (first step) is an extension of the PolyMAX or polyreference least-squares complex frequency domain method, developed by Peeters et al. (2004). The second step provides estimates of the modeshapes and the participation factors by solving a system of linear algebraic equations. It should be noted that two different approaches have been developed for the computation of the modeshapes and participation factors in this second step. In the first approach the modal properties are derived directly by Singular Value Decomposition (SVD) of the resulting numerator matrix. In the second approach, advantages taken from the fact that the error function is quadratic with respect to the modeshapes. So the modeshapes are computed by taking stationary conditions in order to develop a linear system of equations from which the modeshapes are derived. The first two steps usually give accurate estimates of the modal characteristics. However, a third step is often recommended to improve these estimates, especially for closely spaced and overlapping modes, by efficiently solving the full nonlinear optimization problem with initial estimates of the modal parameters those obtained from the first and second steps. A schematic diagram summarizing this three step modal identification algorithm is presented in Figure 4.1.

This chapter is organized as follows. Section 4.2 describes the identification methodology for the case of EMA. In the next Section 4.3 the identification methodologies for OMA are discussed for the cases involving the Full and the Half spectra functions. The case of modal identification based on earthquake induced (base excitation) vibrations is presented in the time and frequency domain in Section 4.4. Finally, a modal identification example using simulated ambient vibration measurements is presented for the case of a structure with closely and overlapping modes showing the efficiency of the proposed three step identification approach.

Output-error least-squares minimization modal identification methodologies

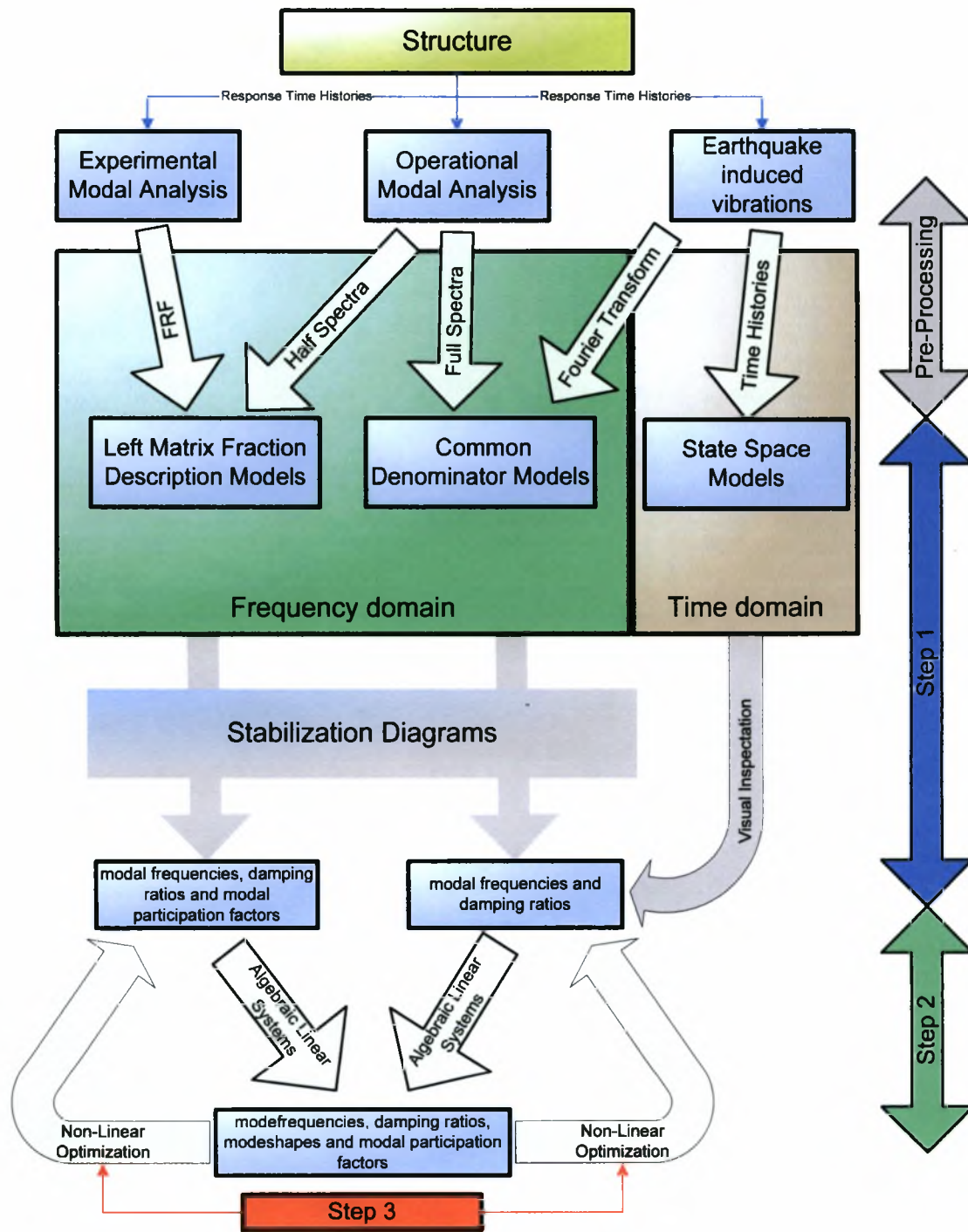


Figure 4.1: Schematic diagram of the three step modal identification algorithm

4.2 Experimental Modal Analysis

The estimation of the modal characteristics using vibration data induced by a measured force applied on a structure is based on a least squares minimization of the measure of fit

$$E(\underline{\theta}) = \sum_{k=1}^{N_m} \text{tr} \left[\left(H(k\Delta\omega; \underline{\theta}) - \hat{H}(k\Delta\omega) \right)^* \left(H(k\Delta\omega; \underline{\theta}) - \hat{H}(k\Delta\omega) \right) \right] \quad (4.1)$$

between the Frequency Response Function (FRF) matrix $\hat{H}(k\Delta\omega) \in \mathbb{C}^{N_0 \times N_m}$ estimated from the measured output acceleration time histories and the FRF matrix $H(k\Delta\omega; \underline{\theta}) \in \mathbb{C}^{N_0 \times N_m}$ predicted by a modal model, where N_0 is the number of measured DOFs, N_m is the number of excited DOFs, $\Delta\omega$ is the discretization step in the frequency domain, $k = \{1, \dots, N_\omega\}$ is the index set corresponding to frequency values $\omega = k\Delta\omega$, N_ω is the number of data in the indexed set, and $\underline{\theta}$ is the parameter set to be estimated. Assuming general non-classically damped modes, the FRF matrix $H(k\Delta\omega; \underline{\theta})$ based on the modal model of the structure is given by (2.99) written alternatively as

$$H(j\omega, \underline{\theta}) = \sum_{r=1}^m \left[\frac{\underline{u}_r \underline{l}_r^T}{j\omega - \lambda_r} + \frac{\underline{u}_r^* \underline{l}_r^{*T}}{j\omega - \lambda_r^*} \right] + A + \frac{B}{(j\omega)^2} \quad (4.2)$$

where m is the number of contributing modes in the frequency range of interest, $\lambda_r = -\zeta_r \omega_r \pm j\omega_r \sqrt{1 - \zeta_r^2}$ is the complex eigenvalue of the r -th contributing mode, ω_r is the r -th modal frequency, ζ_r is the r -th modal damping ratio, $\underline{u}_r \in \mathbb{C}^{N_0}$ is the complex modeshape of the r -th mode, $A \in \mathbb{R}^{N_0 \times N_m}$, $B \in \mathbb{R}^{N_0 \times N_m}$ are real symmetric matrices called the upper and lower residual terms accounting for the approximate contribution of the out-of-bound modes to the selected frequency range of interest (Heylen et al. 1997), and $\underline{l}_r \in \mathbb{C}^{N_m}$ are the participation factors, while the symbol z^* denotes the complex conjugate of a complex number z .

The modal parameter set $\underline{\theta}$ to be identified contains the parameters ω_r , ζ_r , \underline{u}_r , \underline{l}_r , $r = 1, \dots, m$, A and B that completely define the FRF matrix in eq. (4.2). The total number of parameters is $2m(1 + 2N_0) + N_0^2 + N_0$ for non-classically damped modal models.

A three step approach is used to identify the number of contributing modes and to estimate the values of the modal properties given the FRF $\hat{H}(k\Delta\omega)$ estimated from the measured input-output response time histories. In the first step, conventional least squares complex frequency algorithms using the right matrix fraction polynomial model (Verboten 2002; Cauberghe 2004) are employed, along with stabilization diagrams, to obtain estimates of the modal frequencies ω_r , modal damping ratios ζ_r and participation factors \underline{l}_r , as well as distinguish between the physical and the mathematical modes. In the second step by recognizing that the error function in (4.1) is quadratic with respect to the complex modeshapes \underline{u}_r and the elements in the matrices A and B explicit expressions that relate the parameters \underline{u}_r , A and B to the vectors \underline{l}_r , the modal frequencies ω_r and the damping ratios ζ_r are obtained. These values in most cases are very

close to the optimal values. Alternatively, in the second step, given the values of ω_r and ζ_r , the values of the residue matrices $R_r = \underline{u}_r \underline{l}_r^T \in \mathbb{C}^{N_0 \times N_m}$ in eq. (4.2) are obtained by first recognizing that the objective function in (4.1) is quadratic with respect to R_r , A and B , then formulating and solving the resulting linear system of equations for R_r , A and B , and finally applying SVD to obtain estimates of \underline{u}_r and \underline{l}_r from R_r . Usually, this two-step approach gives results that are very close to the optimal estimates. However, for closely-spaced and overlapping modes it is often recommended to solve the original nonlinear optimization problem with objective function given by (4.1).

In the third step, the minimization of the objective function (4.1) can be carried out efficiently, significantly reducing the computational cost, by recognizing that the error function in (4.1) is quadratic with respect to the complex modeshapes \underline{u}_r and the elements in the matrices A and B . This observation is used to develop explicit expressions that relate the parameters \underline{u}_r , A and B to the vectors \underline{l}_r , the modal frequencies ω_r and the damping ratios ζ_r , so that the number of parameters involved in the optimization is reduced from $2m(1+2N_0)+N_0^2$ to $2m(N_0+1)$. This reduction is considerable for a relatively large number of measurement points. Applying the optimality conditions in eq. (4.1) with respect to the components of \underline{u}_r , A and B , a linear system of equations results for obtaining \underline{u}_r , A and B with respect to the \underline{l}_r , ω_r and ζ_r , $r = 1, \dots, m$. The resulting nonlinear optimization problem with respect to the remaining variables \underline{l}_r , ω_r and ζ_r , $r = 1, \dots, m$, is solved in Matlab using available gradient-based optimisation algorithms. The starting values of the parameters required in the optimization are obtained from the estimates provided by the first and second steps. These starting values are usually very close to the optimal values for most of the modes and thus the optimization algorithm converges in a relatively few iterations.

4.3 Operational Modal Analysis

In this case, the input measurements are not known. They are assumed to be modeled by white noise processes. The modal identification is based on either the full or the half spectra as follows.

4.3.1 Identification based on the full spectra

The estimation of the modal characteristics using vibration data induced by ambient unknown excitation forces applied on a structure is based on a least squares minimization of the measure of fit

$$E(\underline{\theta}) = \sum_{k=1}^{N_m} \text{tr} \left[\left(S(k\Delta\omega; \underline{\theta}) - \hat{S}(k\Delta\omega) \right)^* \left(S(k\Delta\omega; \underline{\theta}) - \hat{S}(k\Delta\omega) \right) \right] \quad (4.3)$$

between the Cross Power Spectral Density (CPSD) function matrix $\hat{S}(k\Delta\omega) \in \mathbb{C}^{N_0 \times N_0}$ estimated using the techniques described in Chapter 3 from the measured output acceleration time histories

and the CPSD fraction matrix $S(k\Delta\omega; \underline{\theta}) \in \mathbb{C}^{N_0 \times N_0}$ predicted by a modal model, where N_0 is the number of measured DOFs, $\Delta\omega$ is the discretization step in the frequency domain, $k = \{1, \dots, N_\omega\}$ is the index set corresponding to frequency values $\omega = k\Delta\omega$, N_ω is the number of data in the indexed set, and $\underline{\theta}$ is the parameter set to be estimate. Assuming general non-classically damped modes, the CPSD function matrix $S(k\Delta\omega; \underline{\theta})$ based on the modal model of the structure is given by (3.4), written alternatively as

$$S(j\omega, \underline{\theta}) = \sum_{r=1}^m \left[\frac{\underline{u}_r \underline{g}_r^T}{j\omega - \lambda_r} + \frac{\underline{u}_r^* \underline{g}_r^{*T}}{j\omega - \lambda_r^*} + \frac{\underline{g}_r \underline{u}_r^T}{-j\omega - \lambda_r} + \frac{\underline{g}_r^* \underline{u}_r^{*T}}{-j\omega - \lambda_r^*} \right] + \frac{A}{(j\omega)^4} + B \quad (4.4)$$

where m is the number of contributing modes in the frequency range of interest, $\lambda_r = -\zeta_r \omega_r \pm j\omega_r \sqrt{1 - \zeta_r^2}$ is the complex eigenvalue of the r -th contributing mode, ω_r is the r -th modal frequency, ζ_r is the r -th modal damping ratio, $\underline{u}_r \in \mathbb{C}^{N_0}$ is the complex modeshape of the r -th mode, $A \in \mathbb{R}^{N_0 \times N_0}$, $B \in \mathbb{R}^{N_0 \times N_0}$ are real symmetric matrices called the upper and lower residual term accounting for the approximate contribution of the out-of-bound modes to the selected frequency range of interest (Heylen et al. 1997), and $\underline{g}_r \in \mathbb{C}^{N_0}$ are vector quantities called operational reference vector given in Chapter 3, that depend on the characteristics of the modal model and the CPSD of the white noise input vector, while the symbol z^* denotes the complex conjugate of a complex number z .

The modal parameter set $\underline{\theta}$ to be identified contains the parameters ω_r , ζ_r , \underline{u}_r , \underline{g}_r , $r = 1, \dots, m$, A and B that completely define the CPSD fraction matrix in eq. (4.4). The total number of parameters is $2m(1 + 2N_0) + N_0^2 + N_0$ for non-classically damped modal models.

A three step approach is used to identify the number of contributing modes and to estimate the values of the modal properties given the CPSD functions $\tilde{S}(k\Delta\omega)$ estimated from the measured output response time histories. In the first step, conventional least squares complex frequency algorithms using the common denominator model (Verboten 2002) are employed, along with stabilization diagrams, to obtain estimates of the modal frequencies ω_r and modal damping ratios ζ_r as well as distinguish between the physical and the mathematical modes. In the second step by recognizing that the error function in (4.3) is quadratic with respect to the complex modeshapes \underline{u}_r and the elements in the matrices A and B explicit expressions that relate the parameters \underline{u}_r , A and B to the vectors \underline{g}_r , the modal frequencies ω_r and the damping ratios ζ_r are obtained. These values in most cases are very close to the optimal values. Alternatively, in the second step, given the values of ω_r and ζ_r , the values of the residue matrices $R_r = \underline{u}_r \underline{g}_r^T \in \mathbb{C}^{N_0 \times N_0}$ in eq. (4.4) are obtained by first recognizing that the objective function in (4.1) is quadratic with respect to R_r , A and B , then formulating and solving the resulting linear system of equations for R_r , A and B , and finally applying SVD to obtain estimates of \underline{u}_r and \underline{g}_r from R_r . Usually, this two-step approach gives results that are very close to the optimal

estimates. However, for closely-spaced and overlapping modes it is often recommended to solve the original nonlinear optimization problem with objective function given by (4.3).

The minimization of the objective function (4.3) can be carried out efficiently, significantly reducing the computational cost, by recognizing that the error function in (4.3) is quadratic with respect to the complex modeshapes \underline{u}_r and the elements in the matrices A and B . This observation is used to develop explicit expressions that relate the parameters \underline{u}_r , A and B to the vectors \underline{g}_r , the modal frequencies ω_r and the damping ratios ζ_r , so that the number of parameters involved in the optimization is reduced from $2m(1 + 2N_0) + N_0^2 + N_0$ to $2m(N_0 + 1)$. This reduction is considerable for a relatively large number of measurement points. Applying the optimality conditions in eq. (4.3) with respect to the components of \underline{u}_r , A and B , a linear system of equations results for obtaining \underline{u}_r , A and B with respect to the \underline{g}_r , ω_r and ζ_r , $r = 1, \dots, m$. The resulting nonlinear optimization problem with respect to the remaining variables \underline{g}_r , ω_r and ζ_r , $r = 1, \dots, m$, is solved in Matlab using available gradient-based optimisation algorithms. The starting values of the parameters required in the optimization are obtained from the estimates provided by the first and second steps. These starting values are usually very close to the optimal values for most of the modes and thus the optimization algorithm converges in a relatively few iterations.

4.3.2 Identification based on the half spectra

In the previous section the estimation of the modal characteristics using vibration data induced by ambient unknown excitation forces applied on a structure was based on a methodology that use the CPSD functions of the measured response signals. In this section the modal identification methodology is based on a similar approach but using the half CPSD functions (or half positive spectra) of the measured response signals. This approach is presented in the work by Peeters and Van Auweraer (2005). Specifically, the methodology is based on a least squares minimization of the measure of fit

$$E(\underline{\theta}) = \sum_{k=1}^{N_\omega} \text{tr} \left[\left(S^{++}(k\Delta\omega; \underline{\theta}) - \widehat{S}^{++}(k\Delta\omega) \right)^* \left(S^{++}(k\Delta\omega; \underline{\theta}) - \widehat{S}^{++}(k\Delta\omega) \right) \right] \quad (4.5)$$

between the half spectra matrix $\widehat{S}^{++}(k\Delta\omega) \in C^{N_0 \times N_0}$ estimated using the techniques described in Chapter 3 from the measured output acceleration time histories and the half spectra matrix $S^{++}(k\Delta\omega; \underline{\theta}) \in C^{N_0 \times N_0}$ predicted by a modal model, where N_0 is the number of measured DOFs, $\Delta\omega$ is the discretization step in the frequency domain, $k = \{1, \dots, N_\omega\}$ is the index set corresponding to frequency values $\omega = k\Delta\omega$, N_ω is the number of data in the indexed set, and $\underline{\theta}$ is the parameter set to be estimate. Assuming general non-classically damped modes, the half spectra matrix $S^{++}(k\Delta\omega; \underline{\theta})$ based on the modal model of the structure is given by (3.4) written alternatively as

$$S^{++}(j\omega, \underline{\theta}) = \sum_{r=1}^m \left[\frac{\underline{u}_r \underline{g}_r^T}{j\omega - \lambda_r} + \frac{\underline{u}_r^* \underline{g}_r^{*T}}{j\omega - \lambda_r^*} \right] + \frac{A}{j\omega} + (j\omega)B \quad (4.6)$$

where m is the number of contributing modes in the frequency range of interest, $\lambda_r = -\zeta_r \omega_r \pm j\omega_r \sqrt{1 - \zeta_r^2}$ is the complex eigenvalue of the r -th contributing mode, ω_r is the r -th modal frequency, ζ_r is the r -th modal damping ratio, $\underline{u}_r \in \mathbb{C}^{N_0}$ is the complex modeshape of the r -th mode, $A \in \mathbb{R}^{N_0 \times N_0}$, $B \in \mathbb{R}^{N_0 \times N_0}$ are real symmetric matrices called the upper and lower residual term accounting for the approximate contribution of the out-of-bound modes to the selected frequency range of interest and $\underline{g}_r \in \mathbb{C}^{N_0}$ are vector quantities called operational reference vector given in Chapter 3, that depend on the characteristics of the modal model and the CPSD of the white noise input vector, while the symbol z^* denotes the complex conjugate of a complex number z .

The modal parameter set $\underline{\theta}$ to be identified contains the parameters ω_r , ζ_r , \underline{u}_r , \underline{g}_r , $r=1, \dots, m$, A and B that completely define the half CPSD matrix in eq. (4.6). The total number of parameters is $2m(1 + 2N_0) + N_0^2$ for non-classically damped modal models.

Recognizing that (4.5) and (4.6) has exactly the same structure with (4.1) and (4.2) respectively, one can directly apply for this problem the same optimization procedure described in Section 4.3.1. The only difference is in the coefficients A and B which can be readily taken into account in the formulation.

4.4 Earthquake induced vibrations

In this section, a time and a frequency domain methodology are presented for identifying the modal parameters of non-classically damped modal models used to describe the response of linear structures subjected to multiple base excitations. The modal parameters to be identified include the modal frequencies, the modal damping ratios, the modeshapes and the participation factors. The proposed structural modal identification methodology is applicable to civil engineering structures such as buildings, towers, bridges, offshore structures, etc., subjected to earthquake excitations. The identification methodology for the time domain methodology uses measured input acceleration time history data at the base DOFs and output acceleration time history data at several model DOFs of the structure. The identification methodology for the frequency domain methodology uses the Discrete Fourier Transform (DFT) of the measured input acceleration time history data at the base DOFs and the output acceleration time history data at the model DOFs of the structure. An output error formulation is presented, in which the modal parameters are identified through least-squares matching between the output measured responses and the responses predicted by a modal model of the structure subjected to the measured base inputs. All these methodologies have been described in full details in the thesis by Nikolaou (2008).

The methods developed by McVerry (1980) in the frequency domain and Beck and Jennings (1980) in the time domain have been extended to treat non-classically damped modal models, since damping may not be proportionally distributed in various structural components, especially

due to the energy dissipation mechanism provided locally by the elastomeric bearings and the foundation soil. The modal identification methodology also accounts for different support excitations encountered in civil engineering structures.

4.4.1 Identification in the time domain

Let $\underline{y}(k\Delta t, \underline{\theta})$ be a vector of the sampled response of a linear structure obtained from a modal model involving a parameter set $\underline{\theta}$ and m modes. The variable Δt denotes the time discretization step and $k = \{1, 2, \dots, N\}$ is an index set and N the total number of sample data over the response duration T . The parameters in $\underline{\theta}$ include the modal characteristics such as modal frequencies, modal damping ratios, and modeshape components at the measured locations, modal participation factors, and other parameters that completely define the response vector $\underline{y}(k\Delta t, \underline{\theta})$.

A modal model output-error identification approach seeks the optimal values of the parameter set $\underline{\theta}$ that minimize a measure of fit between the modal model predictions $\underline{y}(k\Delta t, \underline{\theta})$ and the corresponding response $\hat{\underline{y}}(k\Delta t)$ estimated from the measured data. That is, the modal model identification is formulated as a minimization problem of finding the values of $\underline{\theta}$ that minimizes the measure of fit

$$J(\underline{\theta}) = \frac{1}{V} \sum_{k=0}^N [\underline{y}(k\Delta t; \underline{\theta}) - \hat{\underline{y}}(k\Delta t)]^T [\underline{y}(k\Delta t; \underline{\theta}) - \hat{\underline{y}}(k\Delta t)] \quad (4.7)$$

where $\hat{\underline{y}}(k\Delta t)$ is the measured response time histories at the N_0 measured DOF, $\underline{y}(k\Delta t; \underline{\theta})$ is the response time histories at the measured N_0 DOF predicted by the modal model.

The normalization factor for time domain is given by

$$V = \sum_{k=0}^N [\hat{\underline{y}}(k\Delta t)]^T [\hat{\underline{y}}(k\Delta t)] \quad (4.8)$$

Using the analysis in Chapter 2, the vector $\underline{y}(t; \underline{\theta})$ of the acceleration responses at the N_0 measured degrees of freedom, based on the non-classically damped modal models, can be written in the form

$$\underline{y}(t) = [U \quad U^*] \underline{\xi}(t) + D_c \underline{u}(t) \quad (4.9)$$

where $D_c \in \mathbb{R}^{N_0 \times N_m}$ is a real matrix, $\underline{u}(t)$ is the vector of the base excitation time histories measured at the N_m locations,

$$U = [\underline{u}_1, \dots, \underline{u}_m] \in C^{N_{out} \times m} \quad (4.10)$$

is the matrix of the complex eigenvectors \underline{u}_r , $r = 1, \dots, m$, at N_0 DOFs, and

$$\underline{\xi}(t) = \begin{Bmatrix} \xi_1(t) \\ \vdots \\ \xi_m(t) \\ \xi_1^*(t) \\ \vdots \\ \xi_m^*(t) \end{Bmatrix} \in C^{2m \times 1} \quad (4.11)$$

is the complex vector of modal coordinates satisfying the complex modal state space equations

$$\begin{aligned} \dot{\xi}_r(t) &= \lambda_r \xi_r(t) + l_r^T \underline{u}(t) \\ \dot{\xi}_r^*(t) &= \lambda_r^* \xi_r^*(t) + l_r^{*T} \underline{u}(t) \end{aligned} \quad , r = 1, \dots, m \quad (4.12)$$

where $l_r^T \in C^{1 \times N_m}$ is the complex vector of the modal participation factors relating the N_m inputs to the r mode of the system, and

$$\lambda_r = -\zeta_r \omega_r \pm j \omega_r \sqrt{1 - \zeta_r^2} = -a_r \pm j b_r \quad , r = 1, \dots, m \quad (4.13)$$

are the complex eigenvalues of the structure. The modal response $\xi_r(t)$ can be obtained by solving (4.12) using the complex-valued initial conditions $\xi_r(0)$.

The parameters set $\underline{\theta}$ in the notation $\underline{y}(t; \underline{\theta})$ contains the parameters that completely define the response vector $\underline{y}(t; \underline{\theta})$ using the modal analysis. From equations (4.9) to (4.13), it is evident that the parameter set $\underline{\theta}$ contains the complex eigenvalue λ_r of the r mode, the complex modeshapes $\underline{u}_r \in C^{N_0 \times 1}$, the modal participation factor vectors $l_r^T \in C^{1 \times N_m}$, the initial conditions $\xi_r(0) = \xi_r^0$, and the entries of the real matrix $D_c \in \mathbb{R}^{N_0 \times N_m}$, that is

$$\underline{\theta} : \{ \lambda_r, \underline{u}_r, l_r^T, \xi_r^0, r = 1, \dots, m, D_c \} \quad (4.14)$$

where m is the number of contributing modes which is also unknown in the modal identification process.

The minimization of the objective function (4.7) can be carried out efficiently, significantly reducing computational cost, by recognizing that the error function in (4.7) is quadratic with respect to the complex modeshapes \underline{u}_r and the elements in the real matrix D_c . This observation is used to develop explicit expressions that relate the parameters \underline{u}_r and D_c to the rest of the model parameters appearing in the parameter set $\underline{\theta}$.

This formulation is an extension to the non-classically damped modes of the time domain formulation developed by Beck (1978) assuming classically damped modes. Basically, the problem being solved is the one of minimizing the cost function $J(\underline{\theta})$ in (4.7) with respect to the parameters $\underline{\theta}$. For this case, gradient-based optimization method is implemented that requires initial estimates for the parameters. It should also be noted that modal sweep approaches (Werner et al. 1987) are also implemented to improve the effectiveness of the proposed algorithm.

4.4.2 Identification in the frequency domain

Let $\underline{y}(k\Delta\omega, \underline{\theta})$ be a vector of the sampled Fourier Transform of the response of a linear structure predicted from a modal model involving a parameter set $\underline{\theta}$ and m modes at N_0 measured DOFs. The variable $\Delta\omega$ denotes the frequency discretization step and $k = \{1, 2, \dots, N_\omega\}$ is an index set and N_ω the total number of sample data over the response frequency band. The parameters in $\underline{\theta}$ include the modal characteristics such as modal frequencies, modal damping ratios and modeshape components at the measured locations, modal participation factors, and other parameters that completely define the response vector $\underline{y}(k\Delta\omega, \underline{\theta})$.

A modal model output-error identification approach seeks the optimal values of the parameter set $\underline{\theta}$ that minimize a measure of fit between the Fourier Transform of the acceleration $\underline{y}(k\Delta\omega, \underline{\theta})$ predicted by the modal model of the structure and the Fourier Transform of the corresponding response acceleration $\hat{\underline{y}}(k\Delta\omega)$ estimated from the measured data. Thus, the output-error measure $J(\underline{\theta})$ between measurement data and model predictions that correspond to a certain value of $\underline{\theta}$, is described similar to (4.7) by

$$J(\underline{\theta}) = \frac{1}{V} \sum_{k=0}^N \left[\underline{y}(k\Delta\omega, \underline{\theta}) - \hat{\underline{y}}(k\Delta\omega) \right]^{*T} \left[\underline{y}(k\Delta\omega, \underline{\theta}) - \hat{\underline{y}}(k\Delta\omega) \right] \quad (4.15)$$

Where V is the normalization factor for time domain given by:

$$V = \sum_{k=0}^N \left[\hat{\underline{y}}(k\Delta\omega) \right]^{*T} \left[\hat{\underline{y}}(k\Delta\omega) \right] \quad (4.16)$$

The Fourier transform vector $\underline{y}(k\Delta\omega; \underline{\theta}) \in \mathbb{C}^{N_0}$ of the acceleration responses based on the non-classically damped modal model can be obtained in the form

$$\underline{y}(j\omega; \underline{\theta}) \in \mathbb{C}^{N_0} = \left\{ \sum_{r=1}^m \left[\frac{\underline{u}_r \underline{l}_r^T}{(j\omega) - \lambda_r} + \frac{\underline{u}_r^* \underline{l}_r^{*T}}{(j\omega) - \lambda_r^*} \right] + P \right\} \underline{f}(j\omega) \quad (4.17)$$

where the vector $\underline{f}(j\omega)$ contains the Fourier transforms of the input (base) acceleration time histories at the N_m locations and m is the number of contributing modes which is also unknown in the modal identification process.

The parameter set $\underline{\theta}$ to be identified contains the modal frequencies ω_r , the modal damping ratios ζ_r , the complex modeshapes \underline{u}_r , the modal participation factor vectors \underline{l}_r , $r = 1, \dots, m$, and the constant matrix P which contains the pseudostatic response of the structure due to multiple differential base excitations. The total number of parameters is $2m(1 + N_0 + N_m) + N_0 N_m$ for non-classically damped modal models. The formulation in eq. (4.17) assumes that measured vibrations start from zero. Non-zero starting vibration levels have also been accounted for by adding additional terms in eq. (4.17) and augmenting the parameter set $\underline{\theta}$ to include parameters that account for the initial conditions of the modal equations.

The optimal values of the parameter set $\underline{\theta}$ are obtained by minimizing the objective function (4.15). This procedure is accomplished by applying a three step approach similar with the cases of identification based on artificial and ambient induced vibrations. Specifically, in the first step, conventional least squares complex frequency algorithms using the common denominator model (Verboten 2002) are employed, along with stabilization diagrams, to obtain estimates of the modal frequencies ω_r and modal damping ratios ζ_r , as well as distinguish between the physical and the mathematical modes. In the second step by recognizing that the error function in (4.15) is quadratic with respect to the complex modeshapes \underline{u}_r and the elements in the real matrix P explicit expressions that relate the parameters \underline{u}_r and P to the vectors \underline{l}_r , the modal frequencies ω_r and the damping ratios ζ_r are obtained. These values in most cases are very close to the optimal values. Alternatively, in the second step, given the values of ω_r and ζ_r , the values of the residue matrices $R_r = \underline{u}_r \underline{l}_r^T \in \mathbb{C}^{N_0 \times N_m}$ in eq. (4.17) are obtained by first recognizing that the objective function in (4.1) is quadratic with respect to R_r and P , then formulating and solving the resulting linear system of equations for R_r and P , and finally applying SVD to obtain estimates of \underline{u}_r and \underline{l}_r from R_r . Usually, this two-step approach gives results that are very close to the optimal estimates. However, for closely-spaced and overlapping modes it is often recommended to solve the original nonlinear optimization problem with objective function given by (4.15).

In the third step, the minimization of the objective function (4.15) can be carried out efficiently, significantly reducing the computational cost, by recognizing that the objective function in (4.15) is quadratic with respect to the complex modeshapes \underline{u}_r and the real matrix P . Applying the optimality conditions in eq. (4.15) with respect to the components of \underline{u}_r and P , a linear system of equations results for obtaining \underline{u}_r and P with respect to the vectors \underline{l}_r , ω_r and ζ_r . The resulting nonlinear optimization is reduced to the $2m(3 + N_m)$ parameters \underline{l}_r , ω_r and ζ_r , $r = 1, \dots, m$. This reduction is considerable for a relatively large number of measurement points. Applying the optimality conditions in eq. (4.15) with respect to the components of \underline{u}_r and P a linear system of equations results for obtaining \underline{u}_r and P with respect to the \underline{l}_r , ω_r and ζ_r , $r = 1, \dots, m$. The resulting nonlinear optimization problem with respect to the remaining variables \underline{l}_r , ω_r and ζ_r , $r = 1, \dots, m$, is solved in Matlab using available gradient-based optimisation algorithms. The starting values of the parameters required in the optimization are obtained from the estimates provided by the first and second steps. These starting values are usually very close to the optimal values for most of the modes and thus the optimization algorithm converges in a relatively few iterations. The derivatives of the objective function with respect to the modal parameters are evaluated analytically, accelerating the convergence of the algorithm. Modal sweep approaches (Werner et al. 1987) are also implemented to improve the effectiveness of the proposed algorithm.

4.5 Identification of closely spaced modes using simulated measurement data

The modal identification of a structure that has closely and overlapping modes is always a challenging problem. This problem is studied in this section in detail. Specifically, the proposed three step algorithm is applied and its efficiency is tested for the identification of closely spaced modes using simulated measurement data of the response of a model structure. In the literature, the usage of two step algorithms is commonly used for modal identification. This example demonstrates that the first two identification steps are sometimes inadequate especially for the case of closely and overlapping modes. For this case the application of the third step is necessary and is shown to improve significantly the modal identification results.

A model of a two-span bridge-like structure, shown in Figure 4.2, is considered in the simulation studies. The two spans are weakly connected and almost similar in properties. This has an effect of having two very closely bending modes. The behavior of the two span bridge resembles the behavior observed for the four span G2 Kavala bridge of Egnatia Odos Motorway. The four-span Kavala bridge has four closely spaced bending modes due to the almost similar properties of the four spans and the fact that these spans are weakly connected with each other. A finite element model for the simulated two-span bridge is constructed. The simulated measurement data used for the modal identification are the vibration responses predicted at several locations by a finite element model of a structure. These vibrations are induced by excitation forces applied at the deck and modeled by white noise processes. The model of the structure has been properly selected to have closely spaced and overlapping modes.

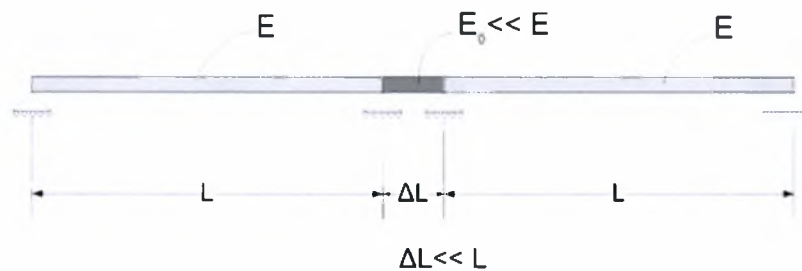


Figure 4.2: Two-span model of a bridge-like structure.

In generating the simulated acceleration response time signals to be used for identification using OMA, it should be noted that in order to clearly identify the closely spaced modes, the time duration of these responses should be several times greater than $(2\pi / \Delta\omega)$, where $\Delta\omega$ is the distance between the modal frequencies of the closely spaced modes. It is expected that the larger the duration of the measured response in relation to $(2\pi / \Delta\omega)$, the better the estimates of the closely spaced modal properties. As the duration is increased, the measurements tend to contain the necessary information for the distinction of the closely and overlapped modes.

The CPSD function matrix of the acceleration response of the model are first estimated using the methodologies described in Chapter 3 and then the first two steps of the proposed identification algorithm described in Section 4.3.1 are applied in the frequency band that contain the closely spaced modes for identifying the modal properties ω_r , ζ_r , \underline{u}_r , \underline{g}_r , A and B that define the CPSD matrix. The third step of the algorithm is also applied, where the original non-linear optimization problem (4.3) is solved with respect to the parameters ω_r , ζ_r and \underline{g}_r , using as initial values for the minimization (gradient based) algorithm the values of the parameters already computed by the first two steps of the identification algorithm. Figure 4.3 shows the comparison between the absolute value $\|\hat{S}(k\Delta\omega)\|$ of the measured CPSD functions and the absolute value $\|S(k\Delta\omega;\underline{\theta})\|$ of the CPSD functions predicted by the identified modal model for two measurement DOFs. Comparisons are shown for the case of applying the first two steps of the algorithm and for the case of applying all three steps. In this figure it can be easily observed that the modal model identified by applying only the first two steps of the algorithm is quite inadequate compared with the modal model resulted when the third step is also applied.

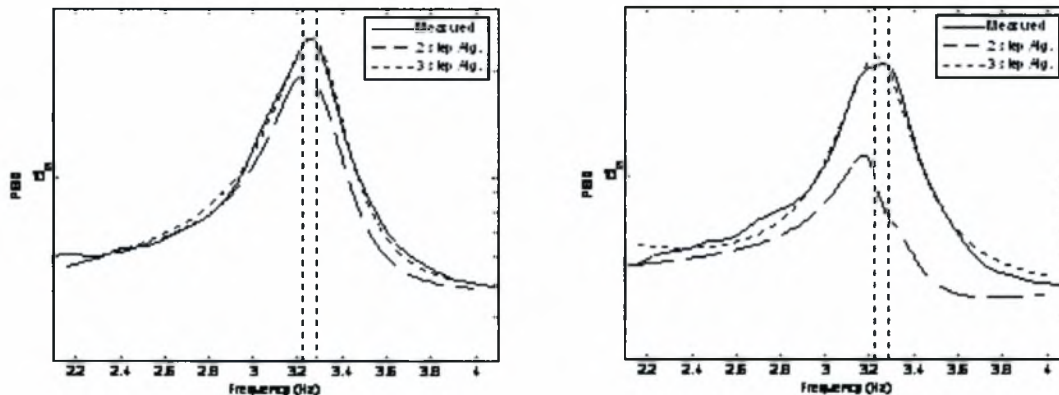


Figure 4.3: Comparison between the measured CPSD function and the CPSD functions predicted by the modal model that was identified by applying the two step and the three step algorithms for two measurement locations

The previous results were obtained for a duration of the response equal to $a(2\pi / \Delta\omega)$, where a is chosen to be $a = 100$. In order to study the effect of the duration on the reliability of the estimates, the results are repeated for a duration $2a(2\pi / \Delta\omega)$ which is twice as much the previous duration. Comparisons are shown in Figure 4.4. An improvement of the fit is observed for the three step approach, while significant discrepancies are still evident between the measured and the model predicted CPSD using the two step approach.

It should be noted that signals with large durations may cause other problems concerning with the storage requirements and the transfer of the measured data. They also increase significantly the computational time for estimating the CPSD functions from the measured time response.

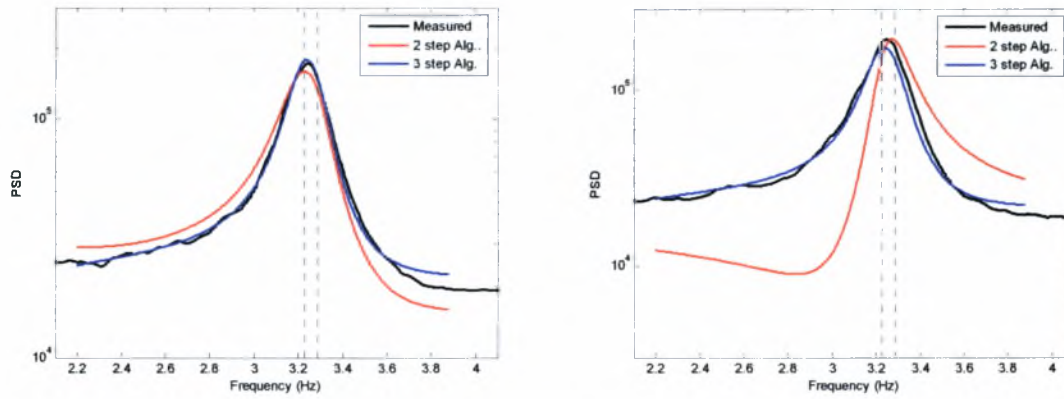


Figure 4.4: Comparison between the measured CPD function and the CPD functions predicted by the modal model that was identified by applying the two step and the three step algorithms for two measurement locations (duration of response is twice the duration used in the results shown in Figure 4.3)

Applications on input-output and output-only modal identification

5.1 Introduction

In the present study, the modal identification methodologies and software developed are used to analyze the dynamic modal characteristics of structures using real dynamic data. The purpose of this chapter is to demonstrate and compare the applicability and effectiveness the modal identification methodologies by applying them for estimating the dynamic modal characteristics of a small scale laboratory structure using artificially (impulse hammer) excited vibration measurements and of three bridges of the Egnatia Odos motorway, using both ambient and earthquake induced vibration measurements.

The chapter is organized as follows. The modal identification methodology is first applied on a three-story small laboratory structure using artificially excited vibration measurements is presented in Section 5.2. In Section 5.3 the proposed ambient identification methodologies are applied to the under construction R/C bridge of Egnatia Odos at Metsovo using ambient vibration measurements. Finally, in Section 5.4 the proposed identification methodologies are also applied to two representative R/C bridges of Egnatia Odos, the first at Kavala using ambient vibration measurements and the second at Polymylos using ambient vibration measurements and vibration measurements for the low level, magnitude $M_L = 4.6$, earthquake event that occurred on 21/2/2007 (2:04:38 GMT) at a distance 35km Northeast of the bridge.

5.2 Application on a three-story laboratory structure

This section applies the developed modal identification methodologies for estimating the dynamic modal characteristics of a three-story small laboratory structure using artificially excited vibration measurements. The structure was built and tested in the System Dynamics Laboratory of the University of Thessaly. The experimental modal identification methodology applied was that of Single-Input Multiple-Output (SIMO) described in Section 4.2. The identification of modes is based on the fit between the measured and the modal model predicted Frequency Response Functions (FRF).

5.2.1 Description of the laboratory three-story structure and instrumentation

The three-story laboratory structure is composed by three identical one-story components made of aluminum elements bonded with steel elements. A picture of the front view and side view of the fully composed three-story laboratory structure are given in Figure 5.1. A schematic diagram of the side and the front views of the individual (one-story) components of the laboratory structure with the material and geometric properties are given in Figure 5.2.



Figure 5.1: Three-story laboratory structure, (a) front view, (b) side view

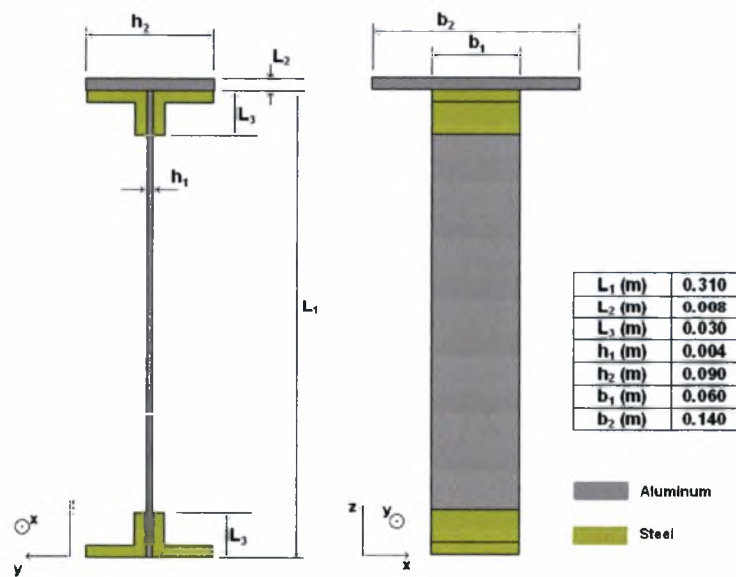


Figure 5.2: Schematic diagram of individual structure component

Modal identification results are presented for the case of artificially induced vibration data, generated by hitting the structure with an impulse hammer and recording the acceleration time histories and the excitation force. The recorded data for the structure include data sets obtained using an array of six accelerometers and the force transducer on the impulse hammer.

The experiment was conducted for the purpose of a case study for predicting the dynamic response of the whole three-story structure using finite element models by analysing the response of the separate structural components of the structure. Specifically, the modal identification methodology was applied for the separate parts of the structure. Three data sets for three different states of the structure respectively were available. The first data set contained the measurements for the one-story structure, the second data set contained the measurements for the two-story structure and the third data set contained the measurements for the whole three-story structure as shown in Figure 5.3(a). Sensor locations have been chosen in such a way so as to gather as more information as possible about the structure's modal response. Applying the array of sensors shown in Figure 5.3(b) all major modeshapes along the strong direction (y axis) can be identified using the developed modal analysis methodology. Figure 5.4 shows one indicative acceleration time history, from 0 to 20 seconds, obtained from sensor 1 measuring along y (strong) direction during a hammer test experiment, for the three-story structure.

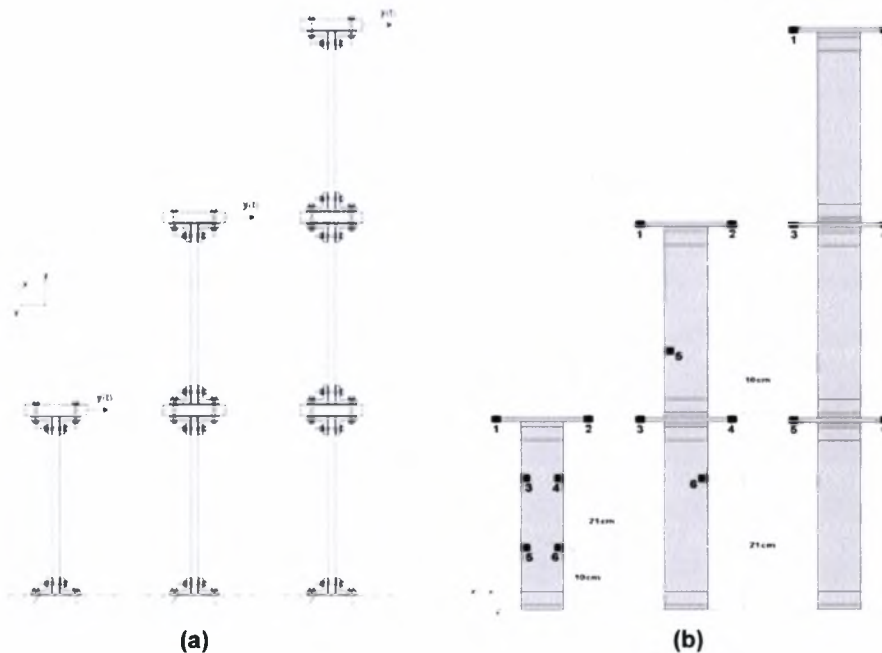


Figure 5.3: Three-story laboratory structure, (a) different states of the structure, (b) sensor locations

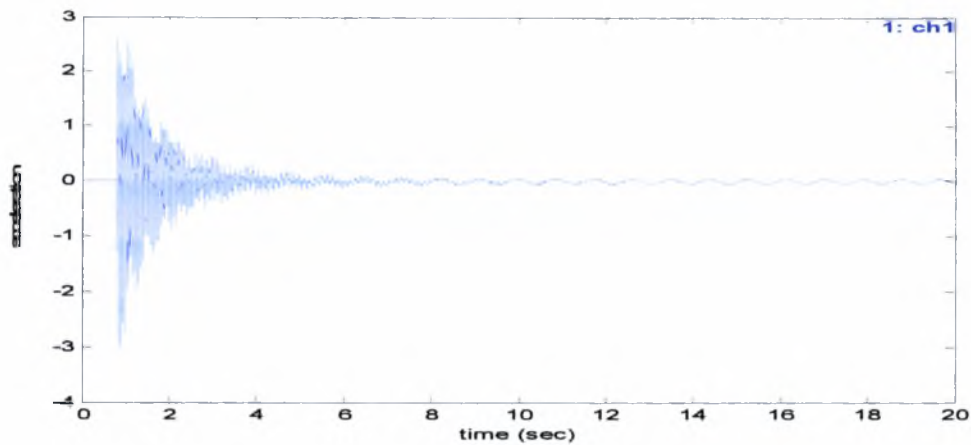


Figure 5.4: Measured acceleration timehistory from sensor 1 for the case of the tree-story structure

5.2.2 Modal identification results

Using the six available acceleration sensors which monitor the artificially induced vibrations and the measurement of the applied impulse force the Frequency Response Functions of the measured DOFs are evaluated. These Frequency Response Functions are evaluated by the MITool software that is used for the estimation of the modal properties. The values of the modal frequencies, modal damping ratios, modeshape components and modal participation factors resulted from Stabilization Diagrams after distinguishing the physical from the mathematical poles. Figure 5.5 presents an indicative Stabilization Diagram evaluated for the case of the first data set containing measurements for one-story structure in the 0 to 140 Hz frequency bandwidth.

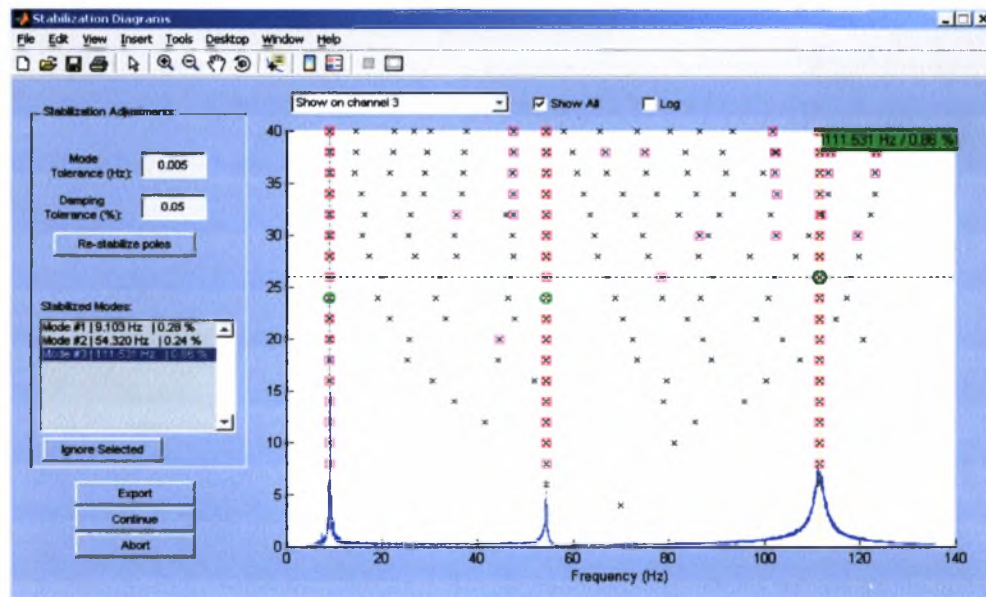


Figure 5.5: Stabilization Diagram for the case of one-story structure measurements

The values of the modal characteristics (modal frequencies, modal damping ratios and modal participation factors) resulted from the Stabilization Diagrams are used for the estimation of the modeshape components using the second step of the algorithm described in Section 4.2. Finally, the fit between the measured and the estimated modal model predicted FRFs is improved by evaluating the third step of the algorithm described in Section 4.2 using the estimates of the first two steps as starting values for the optimization algorithm. Table 5.1 presents the modal identification results for all three vibration data sets corresponding to the one-, two- and three-story structures. Figure 5.6 and 5.7 compares the measured FRFs with the FRFs predicted by the identified optimal modal models for selected sensors and for the case of the three-story structure. As it is seen, the fit of the measured FRF is very good which validates the effectiveness of the proposed modal identification software.

Table 5.1: Modal identification results (modal frequencies and modal damping ratios) for the three-story structure

No	Mode	Modefrequency (Hz)	Damping Ratio (%)
One-story structure			
1	1 st Bending	9.1075	0.247%
2	1 st Rotational	54.3350	0.218%
3	2 nd Bending	111.5299	0.883%
4	3 rd Bending	319.8724	0.865%
Two-story structure			
1	1 st Bending	2.6636	0.108%
2	2 nd Bending	15.8865	0.463%
3	1 st Rotational	31.3313	0.293%
4	2 nd Rotational	78.2356	0.170%
5	3 rd Bending	82.7008	0.656%
6	4 th Bending	149.6037	0.479%
7	5 th Bending	284.0000	0.378%
Three-story structure			
1	1 st Bending	1.1353	0.024%
2	2 nd Bending	7.6409	0.465%
3	3 rd Bending	20.6040	0.412%
4	1 st Rotational	21.7205	0.412%
5	2 nd Rotational	59.9910	0.346%
6	4 th Bending	74.6917	0.572%
7	3 rd Rotational	84.2906	0.280%
8	5 th Bending	114.0648	0.700%
9	6 th Bending	155.1758	0.734%

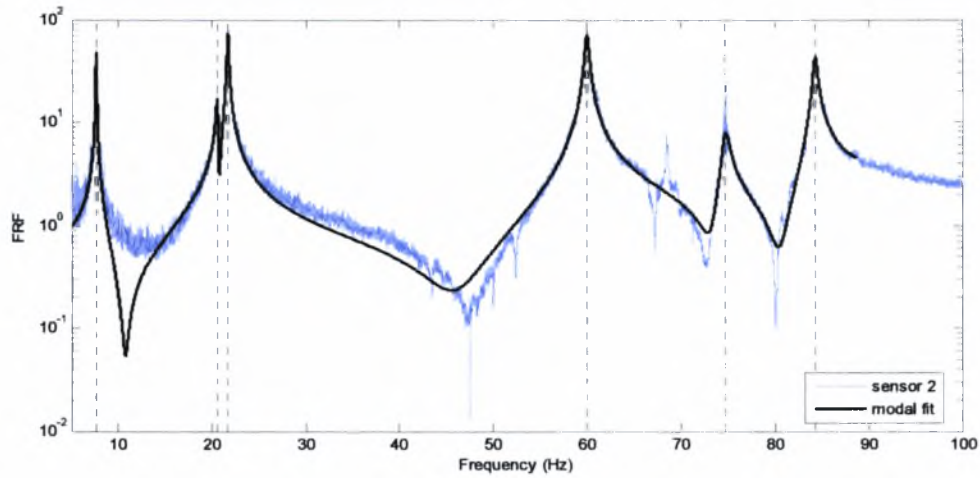


Figure 5.6: Comparison between measured at sensor 2 and optimal modal model predicted FRF

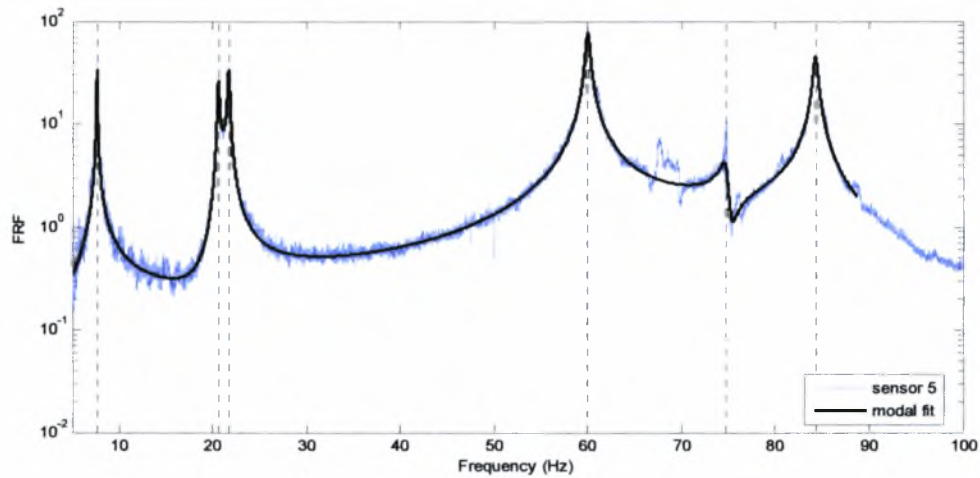


Figure 5.7: Comparison between measured at sensor 5 and optimal modal model predicted FRF

The modes identified were in the frequency band from 0 to 350 Hz. The modal damping ratios identified are significantly low varying according to Table 5.1 from 0.02% for the case of the three-story structure to 0.88% for the case of the one-story structure. For all the identified modes, the modeshape components at the measurement points were also estimated. For the case of one-story structure four modes were identified, three of them are bending modes and one rotational around the vertical axis (z axis). For the case of the two-story structure seven modes were identified, five of them are bending and two rotational modes. Finally, for the case of the three-story structure nine modes were identified, six of them are bending and three rotational modes. In Figures 5.8 to 5.16 graphical illustrations of the modeshape components for the first three identified modes are presented. The arrows are placed in measuring points and their length is proportional to the respective value of the normalized modal component. The modeshape components for each mode are compared with the corresponding modeshape predicted by the Finite Element (FE) models constructed for the three structures.

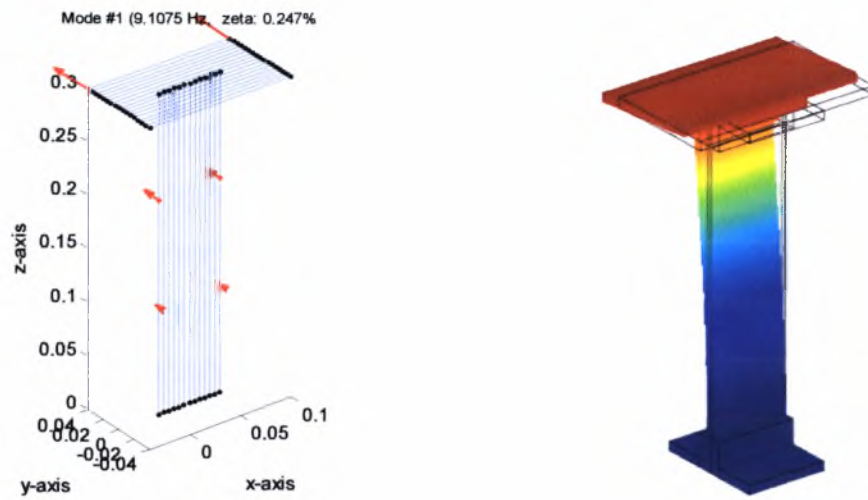


Figure 5.8: Graphical illustration of the modeshape components for the first mode compared with the modeshape predicted by the FE model, for the cases of one-story structure

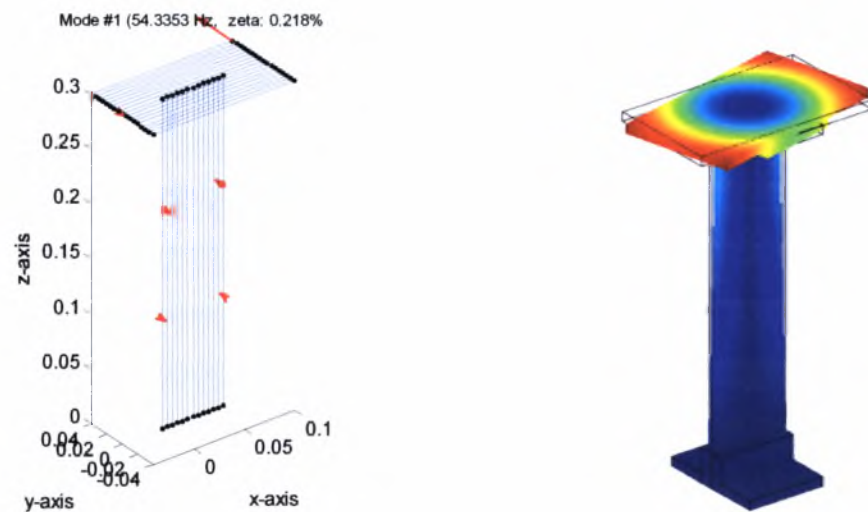


Figure 5.9: Graphical illustration of the modeshape components for the second mode compared with the modeshape predicted by the FE model, for the cases of one-story structure

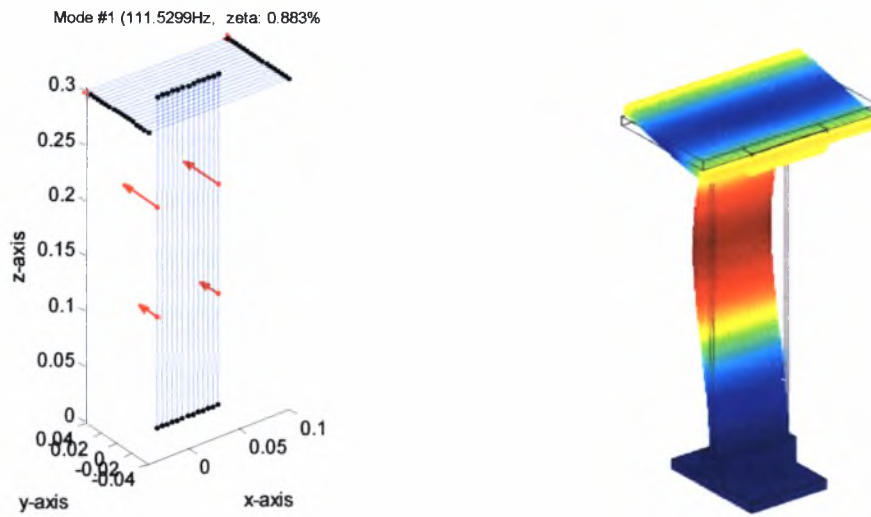


Figure 5.10: Graphical illustration of the modeshape components for the third mode compared with the modeshape predicted by the FE model, for the cases of one-story structure

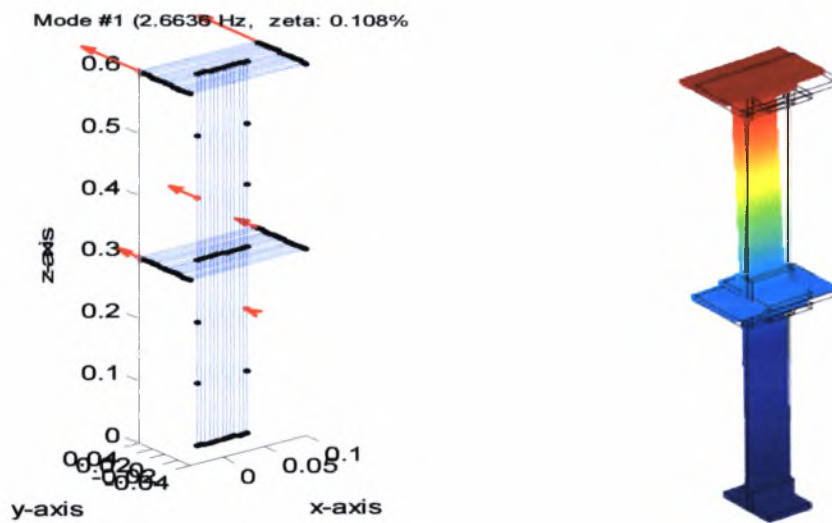


Figure 5.11: Graphical illustration of the modeshape components for the first mode compared with the modeshape predicted by the FE model, for the cases of two-story structure

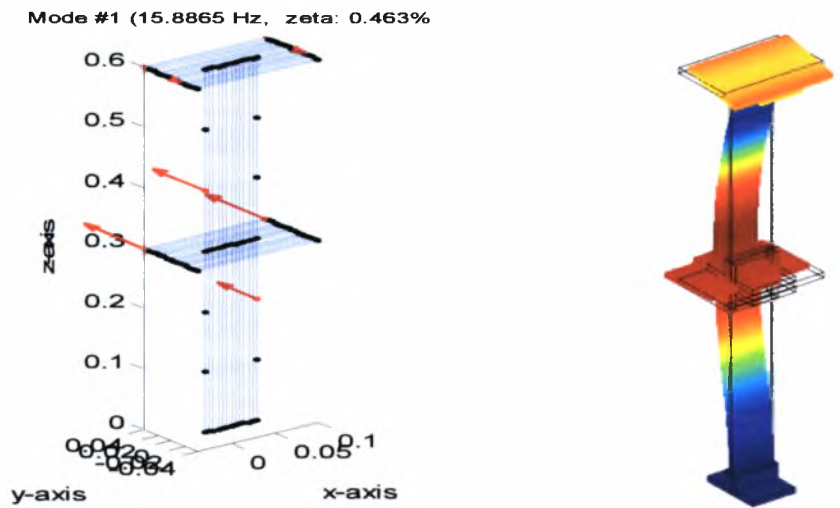


Figure 5.12: Graphical illustration of the modeshape components for the second mode compared with the modeshape predicted by the FE model, for the cases of two-story structure

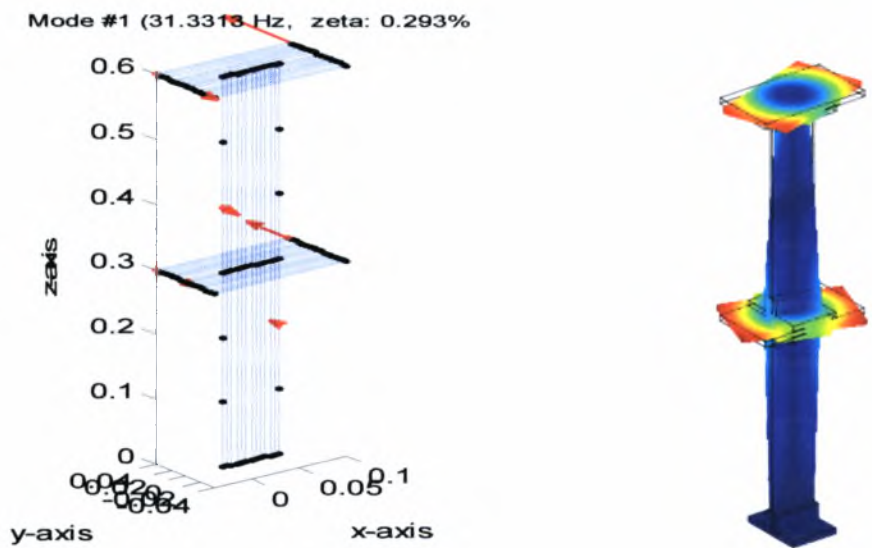


Figure 5.13: Graphical illustration of the modeshape components for the third mode compared with the modeshape predicted by the FE model, for the cases of two-story structure

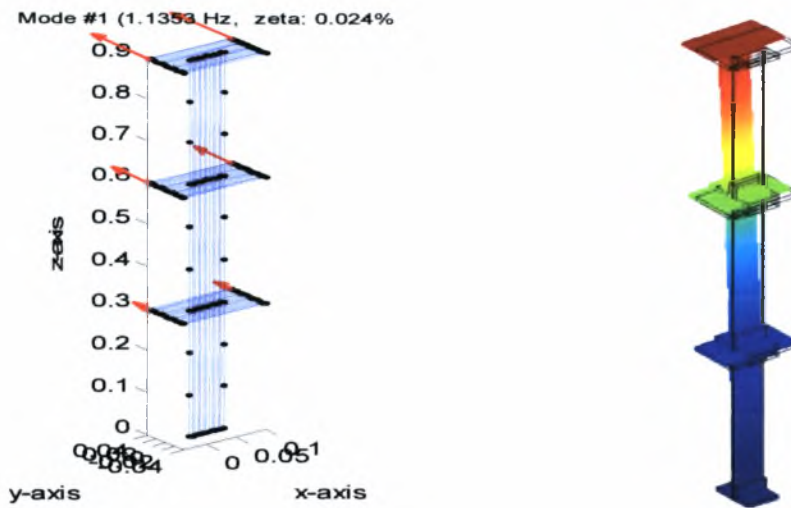


Figure 5.14: Graphical illustration of the modeshape components for the first mode compared with the modeshape predicted by the FE model, for the cases of three-story structure

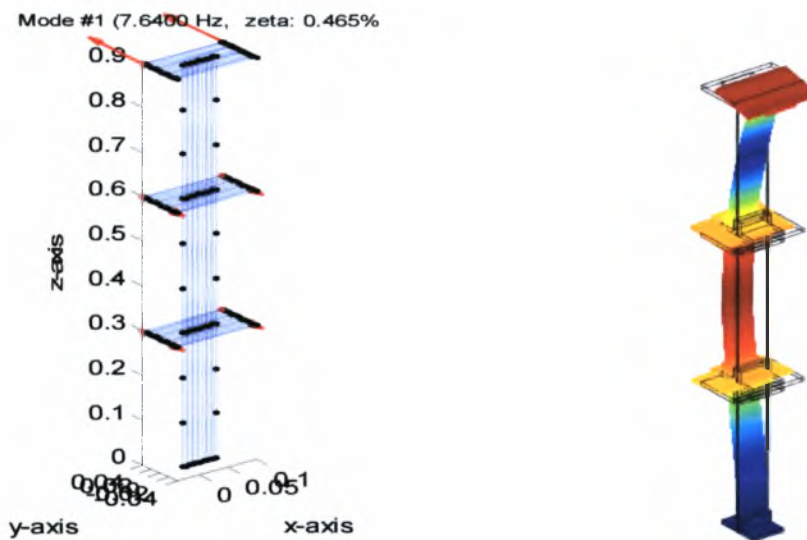


Figure 5.15: Graphical illustration of the modeshape components for the second mode compared with the modeshape predicted by the FE model, for the cases of three-story structure

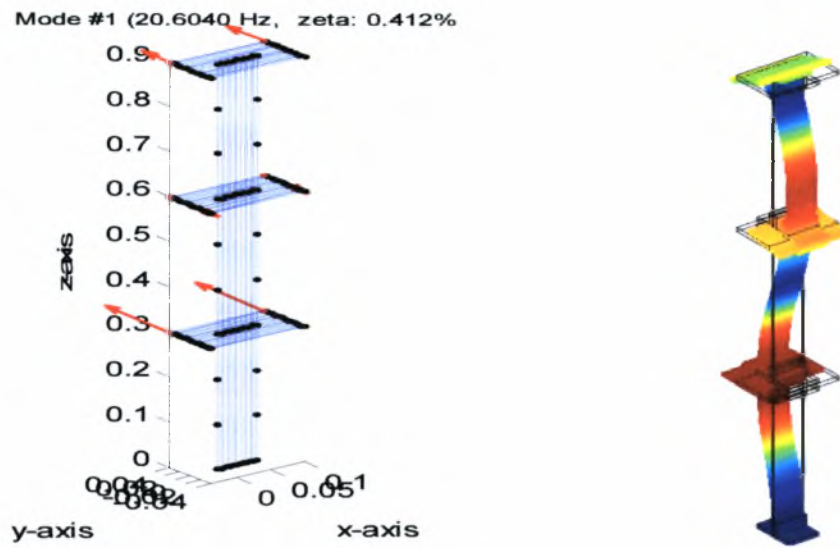


Figure 5.16: Graphical illustration of the modeshape components for the third mode compared with the modeshape predicted by the FE model, for the cases of three-story structure

5.3 Application on a Metsovo bridge during construction using ambient vibration measurements

This section applies the developed modal identification methodologies for estimating the dynamic modal characteristics of a ravine bridge of Egnatia Motorway at Metsovo during construction using ambient vibration measurements. The operational modal analysis methodology developed for output-only measurements was described in Section 4.3.

5.3.1 Description of Metsovo bridge and instrumentation

The new under construction ravine bridge of Metsovo (Figure 5.17), in section 3.2 (Anthohori tunnel-Anilio tunnel) of Egnatia Motorway., is crossing the deep ravine of Metsovitikos river, 150 m over the riverbed. This is the higher bridge of Egnatia Motorway., with the height of the taller pier M2 equal to 110 m. The total length of the bridge is 357 m. As a consequence of the strong inequality of the heights of the two basic piers of the bridge, M2 and M3 (110 m to 35 m), the very long central span of 235 m, is even longer during construction, as the pier M2 balanced cantilever is 250 m long, due to the eccentric position of the key segment. The key of the central span is not in midspan due to the different heights of the superstructure at its supports to the adjacent piers (13.0 m in pier M2 and 11.50 m in pier M3) for redistributing mass and load in favor of the short pier M3 and thus relaxing strong structural abnormality. The last was the main reason of this bridge to be designed to resist earthquakes fully elastic (q factor equal to 1).

The bridge has 4 spans, of length 44.78 m /117.87 m /235.00 m/140.00 m and three piers of which M1, 45 m high, supports the boxbeam superstructure through pot bearings (movable in both horizontal directions), while M2, M3 piers connect monolithically to the superstructure. The bridge is being constructed by the balanced cantilever method of construction and according to the constructional phases shown in Figures 5.18 and 5.19 (November 2007). A general view of the bridge completed (November 2008) is shown in figure 5.20. The total width of the deck is 13.95 m, for each carriageway. The superstructure is limited prestressed of single boxbeam section, of height varying from the maximum 13.5 m in its support to pier M2 to the minimum 4.00 m in key section.

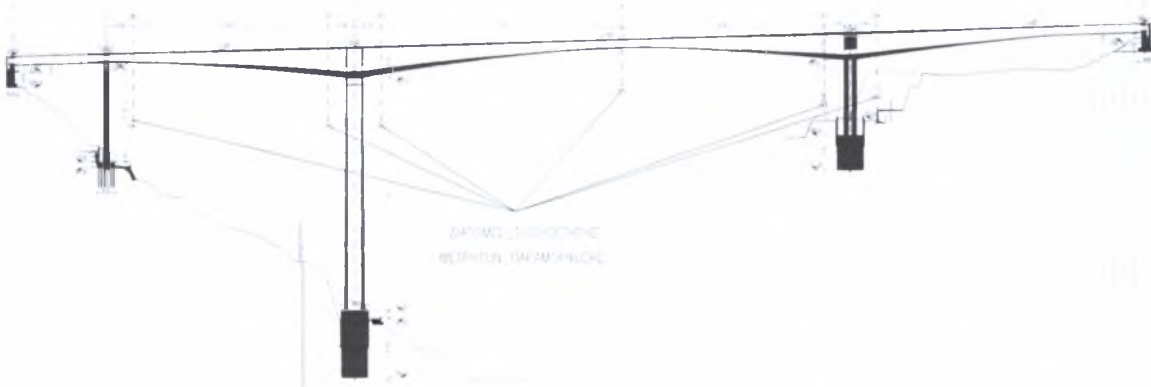


Figure 5.17: Longitudinal section of Metsovo ravine bridge of Egnatia Motorway.



Figure 5.18: General view of under construction Metsovo ravine bridge (November 2007)



Figure 5.19: Key of central span of under construction Metsovo ravine bridge



Figure 5.20: General view of Metsovo ravine bridge (November 2008)

The pier M3 balanced cantilever has been instrumented after the construction of all its segments and before the construction of the key segment that will join with the balanced cantilever of pier M2 (Figure 5.19). The total length of M3 cantilever was at the time of its instrumentation 215 m while its total height is 35 m. Piers M2, M3 are founded on huge circular $\varnothing 12.0$ m rock sockets in the steep slopes of the ravine of the Metsovitikos river, in a depth of 25 m and 15 m, respectively.

Six uniaxial accelerometers were installed inside the box beam cantilever M3 of the left carriageway of Metsovo ravine bridge. The accelerometer arrays, are shown in Figure 5.21. Due to the symmetry of the construction method (balanced cantilevering) and as the same number of segments were completed on both sides of pier M3, the instrumentation was limited to the right cantilever of pier M3, following two basic arrangements. According to the 1st arrangement two (2) sensors were supported on the head of pier M3, one measuring longitudinal and the other transverse accelerations (M3L, M3T), while the remaining four (4) accelerometers were supported on the right and the left internal sides of the box beam's webs, two (2) distant 46m and two (2) distant 68m from M3 axis, respectively (LV3, RV4, LV5, RV6). All four were measuring vertical acceleration. According to the 2nd arrangement the last two sensors of the 1st arrangement were fixed in a section near the cantilever edge, distant 93m from M3 axis, while the other four remain in the same positions. In both arrangements the sixth sensor was adjusted to alternatively measure both in vertical and in transverse horizontal direction (RV6 or RT6).

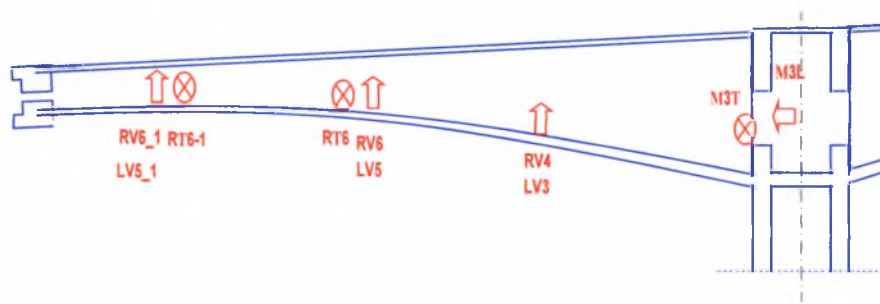


Figure 5.21: Accelerometer installation arrangements.

5.3.2 Modal identification of Metsovo bridge

The response of the cantilever structure subjected to ambient loads such as the wind, and loads induced by construction activities such as the crossing of light vehicles placing the prestressing cables inside the tendon tubes, was as expected of very low intensity (0,6% of the acceleration of gravity). The acceleration response time histories, measured from the 6 channel arrays, were analyzed using the modal identification software MITool. All the basic modal frequencies, modeshapes and damping ratios of the bridge were identified.

Table 5.2: Identified modes of the Metsovo ravine bridge

No	Identified Modes	Hz	Damping %
1	1 st rotational, z axis	0.15	2.93
2	1 st longitudinal	0.30	0.18
3	1 st transverse	0.62	0.43
4	2 nd longitudinal	0.68	0.42
5	1 st bending (deck)	0.90	0.25
6	2 nd transverse	1.30	0.40
7	2 nd bending (deck)	1.43	0.43
8	2 nd rotational, z axis	1.46	0.47
9	3 rd bending (deck)	2.28	0.40
10	3 rd transverse	2.58	1.27
11		2.94	0.49
12		3.24	0.31
13		4.63	0.35
14		4.94	0.63
15	1 st rotational, x axis	5.14	0.22

The identified values of the modal frequencies, the type and the corresponding values of the damping ratios are shown in Table 5.2. The modal damping ratios in Table 5.2, it is observed that the values of damping are of the order of 0.2% to 2.9%. Due to the small number of available sensors (six) the type of some of the modeshapes were not identified with confidence. Three indicative modeshapes are presented in Figure 5.22. The arrows are placed in measuring points

and their length is proportional to the respective value of the normalized modal component. The accuracy in the estimation of the modal characteristics is shown in Figure 5.23 comparing the measured with the modal model predicted CPSD. As it is seen, the fit of the measured power spectral density is very good which validates the effectiveness of the proposed modal identification software based on ambient vibrations.

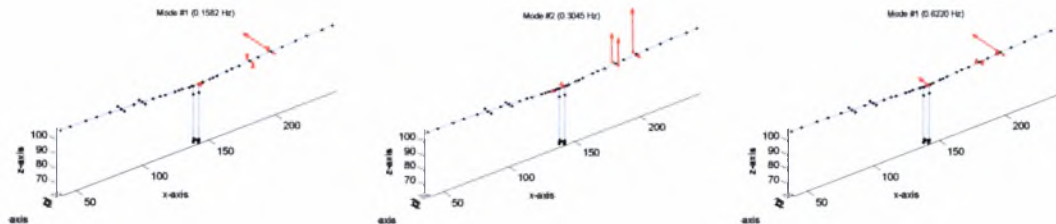


Figure 5.22: The three first identified modeshapes of Metsovo bridge.

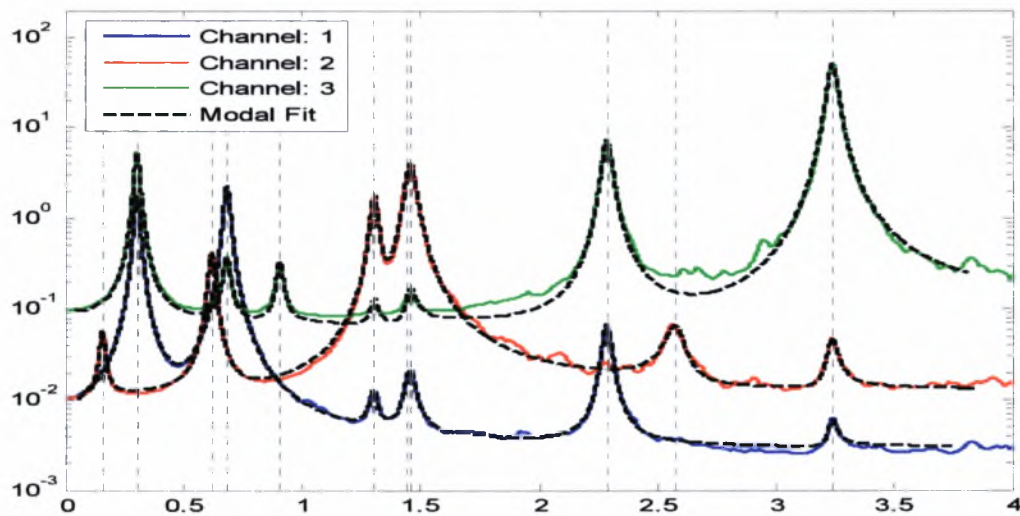


Figure 5.23: Comparison between measured and modal model predicted CPSD.

5.4 Application on Polymylos and Kavala bridges using ambient and earthquake induced vibration measurements

The last section of this applications chapter applies the developed modal identification methodologies for estimating the dynamic modal characteristics of two ravine bridges of Egnatia Motorway at Metsovo, the first at Kavala using ambient vibration measurements and the second at Polymylos using ambient vibration measurements and vibration measurements for the low level earthquake event. The operational modal analysis methodology (Output-only) for the ambient vibrations applied was described in section 4.3 and the modal analysis methodology for the earthquake induced vibrations (Multi-Input Multi-output) applied was described in section 4.4.

5.4.1 Description of bridge systems and instrumentation

Egnatia Motorway is a new, 670 km long highway, that transverses Northern Greece in an E-W direction. The two R/C bridges that were instrumented with special accelerometer arrays are the 9th Ravine Bridge on the Veria - Polymylos section (Figure 5.24) and the 2nd Kavala Bypass Ravine Bridge (Figure 5.25). Both bridges have two, almost identical, statically independent branches, one for each traffic direction, one of which was instrumented in each case.

The T-shaped 9th Polymylos bridge is curved in plan and has a total length of 170 m. The deck cross section is a box girder of height varying parabolically from 9 m at the central pier to 4 m at the two abutments. It is supported monolithically by a central pier (M1), of 35 m height, which is founded on a massive rectangular R/C rock socket at its basement and continues with two transverse flanges for the rest of its height. Each of the two 85 m long cantilever parts of the deck girder rests on each abutment through special elastomeric bearings that allow free sliding in the longitudinal direction (to accommodate thermal expansions/contractions), while functioning as normal elastomeric pads in the transverse (radial) direction.



Figure 5.24: View of 9th Polymylos bridge

The 2nd Kavala Bypass Ravine Bridge, with a total length of 170 m, comprises four identical simply supported spans of 42.5 m, each span built with four precast post-tensioned I-beams of 2.80m height, supporting a 26 cm thick deck, which is continuous throughout the bridge length. The I-beams are supported through laminated elastomeric bearings on the two abutments and the three piers. The piers have a 4m×4m square cross-section with 40 cm wall thickness and heights of 30 m (M1, M3) and 50 m (M2). The four spans of the deck are interconnected through a 2 m long-20 cm thick continuity slab over the piers.



Figure 5.25: View of 2nd Kavala bridge

Two 12-channel Kinometrics K2 ® recording units were installed on the northern branch of the 9th Polymylos bridge (on deck level at the middle of the total bridge deck), each supporting 12 uniaxial Kinometrics Episensor ® accelerometers ($\pm 2g$ full scale) installed on both sides of the bridge deck. The recording units have a 19-bit resolution, a sampling rate capacity of up to 200sps and a dynamic range of 108 dB @ 200 sps. Fifteen sensors were installed on the deck, three on the basement of the central pier and three on each of the two abutments (at the support level of the elastomeric bearings), as shown in Figure 5.26a. Thus, the nine sensors monitor the earthquake-induced excitations at the two abutments and the basement of the pier. The particular layout of the instrumentation permits the analysis of both ambient and earthquake-induced response of the bridge. The 3 to 4-letter sensor labels follow the following convention: The last letter denotes the orientation of the uniaxial sensor (L: longitudinal, T: transverse, V: vertical). The previous one denotes the side of the bridge deck on which the sensor lies (R: right, L: left). Finally, the first one or two letters denote the bridge section that the sensor lies on (first letters U1 and U3 refer here to the abutment level where the elastomeric bearings are seated, U2 refers to the base of the central pier and all other letters refer to positions on the level of the bridge deck). The numbers next to each sensor label denotes the length of the cable used to connect the

sensor to each recording unit. Among the 15 accelerometers located on the bridge deck, 8 record in the vertical, 1 in the longitudinal and the rest 6 in the transverse direction.

A similar, 24-accelerometer special array was used for the instrumentation of the southern branch of the 2nd Kavala Bypass Ravine Bridge. The two recording units were installed one at each deck side, at the middle of the total bridge span. The accelerometers were installed on both edges of the bridge deck (external sidewalk and internal New Jersey barrier). As shown in Figure 5.16b, of the 24 sensors, 18 were installed on the deck and 2 at the top of each of the three piers (6 in all) next to the elastomeric bearings so that adequate information is provided to distinguish between the pier and bearing stiffness. The sensor labels in Figure 5.26b follow the same convention used for the previous instrumentation case (Figure 5.26a): letters U1, U2 and U3 refer to the top of the piers, all the rest refer to positions on the deck of the bridge. The particular layout of the instrumentation permits the recording of the dynamic response of the bridge under ambient (traffic and wind) loads.

Both recording systems have common start / common trigger capabilities to enable synchronous data acquisition. The trigger threshold can be set independently for each sensor, and the user can define the sensors that will cause a system trigger. The systems are equipped with GPS boards as well as with external GSM/GPRS cellular modems that allowed telematic control and data transfer to the user offices.

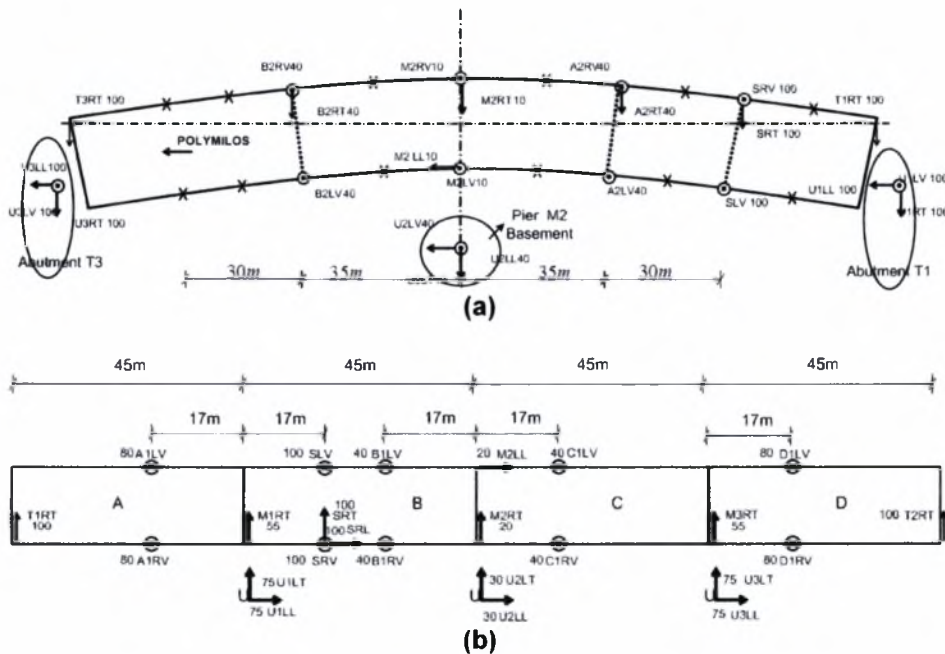


Figure 5.26: Instrumentation layout of (a) Polymylos and (b) Kavala bridges

5.4.2 Modal identification of Polymylos and Kavala bridges

Modal identification results (modal frequencies and modal damping ratios) for the Polymylos and Kavala bridges are shown in Table 5.3 and 5.4 for ambient vibration data of approximately 30 minutes duration each. Also, for the Polymylos bridge, modal identification results are shown in Table 5.5 for a low level, magnitude $M_L = 4.6$, earthquake event that occurred on 21/2/2007 (2:04:38 GMT) at a distance 35 km Northeast of the bridge. The 20 sec earthquake recordings are clear and not hidden by the ambient vibrations since the latter are much smaller in amplitude due to the fact that the earthquake occurred after midnight, so the traffic of the bridge was scarce. It is noted that eight modes were successfully and reliably identified for the Polymylos bridge: five transverse modes and three bending modes (Table 5.3). From the earthquake vibration data, in addition to these modes, one more longitudinal mode was identified (Table 5.4). Representative measured modeshapes (1st bending and 2nd transverse) are shown in Figure 5.27 for the Polymylos bridge. For the Kavala bridge, seven modes were reliably estimated from the ambient vibration data: two transverse, one longitudinal, and four closely-spaced bending modes (Table 5.6). The four closely-spaced modes, predicted also by the design finite element model of the structure, are due to the weak connection of the four spans through the 2-meter-long 20cm-thick continuity slabs described in Section 5.4.1.

Table 5.3: Identified modes of the 9th Polymylos bridge using ambient-induced vibration data

No	Identified Modes	Hz	Damping %
1	1 st Transverse	1.13	2.0
2	2 nd Transverse	1.20	5.6
3	1 st Bending (deck)	2.13	0.6
4	3 rd Transverse	2.22	1.1
5	2 nd Bending (deck)	3.07	0.4
6	4 th Transverse	4.10	0.8
7	3 rd Bending (deck)	6.66	0.5
8	5 th Transverse	6.78	0.8

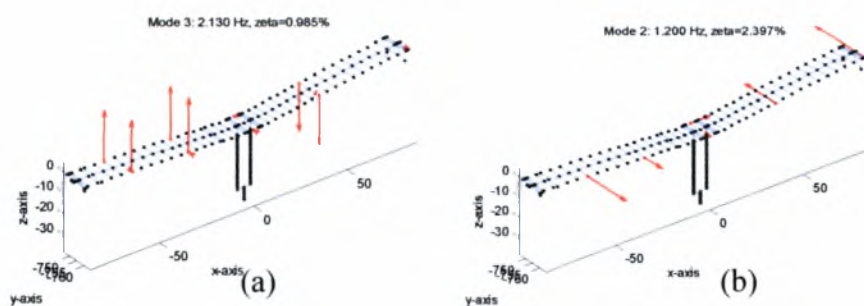


Figure 5.27: (a) 1st bending and (b) 2nd transverse modeshape of the Polymylos bridge

Table 5.4: Identified modes of the 9th Polymylos bridge using earthquake-induced vibration data

No	Identified Modes	Hz	Damping %
1	1 st Transverse	1.29	1.8
2	1 st Longitudinal	1.17	1.8
3	2 nd Transverse	1.30	5.9
4	1 st Bending (deck)	2.20	0.6
5	3 rd Transverse	2.56	3.5
6	2 nd Bending (deck)	3.20	0.7
7	4 th Transverse	4.23	3.2
8	3 rd Bending (deck)	6.89	0.6
9	5 th Transverse	7.24	1.2

Table 5.5: Identified modes of the 2nd Kavala bridge using ambient-induced vibration data

No	Identified Modes	Hz	Damping %
1	1 st Transverse	0.81	1.4
2	1 st Longitudinal	1.29	5.6
3	2 nd Transverse	1.61	5.2
4	1 st Bending (deck)	3.40	0.6
5	2 nd Bending (deck)	3.46	0.7
6	3 rd Bending (deck)	3.47	0.4
7	4 th Bending (deck)	3.51	0.5

Comparing the modal damping ratios in Tables 5.3, 5.4 and 5.5, it is observed that the bending modes have significantly lower values of damping, of the order of 0.4% to 0.7% for the Polymylos and Kavala bridges, than the damping values of the lower transverse and longitudinal modes which are of the order of 0.8% to 5.9% for the Polymylos bridge and of the order of 1.4% to 5.6% for the Kavala bridge. The higher damping values observed for the lower transverse and longitudinal modes can be attributed to the energy dissipation arising from the higher modal deformation levels of the elastomeric bearings at the ends of the bridges which dominate the motion of these modes. Also, soil damping could also have contributed to the higher damping values observed for these modes.

For the Polymylos bridge, Table 5.6 compares the measured peak acceleration responses and the root mean square (RMS) acceleration responses for the ambient and the earthquake excitations. The results for only twelve out of the fifteen sensors installed on the deck are reported in Table 5.6 since three out of the eight sensors recording along the vertical direction malfunctioned during the earthquake event. Also, Table 5.6 reports the ratio between the ambient and the earthquake vibrations for the peak and the RMS responses for each output channel.

Figure 5.28 gives a comparison between the ambient and the earthquake acceleration time histories for two representative recordings along the vertical (sensor B2RV) and the transverse (sensor SRT) directions.

Table 5.6: Comparison of Peak and RMS acceleration response obtained from Ambient (AV) and Earthquake induced Vibrations (EV) for the Polymylos bridge

Channel	Peak response (cm/sec ²)			RMS (cm/sec ²)		
	AV	EV	AV/EV	AV	EV	AV/EV
B2LV	23.2470	7.1062	3.2714	0.9181	1.9397	0.4733
M2LL	2.1767	1.0009	2.1747	0.0922	0.2407	0.3830
M2LV	11.2310	2.9575	3.7975	0.6044	0.7350	0.8223
SLV	15.9950	6.6148	2.4181	0.8847	2.0163	0.4388
T3RT	5.9160	3.3652	1.7580	0.1825	0.7129	0.2561
B2RV	26.9220	7.3206	3.6776	0.9704	1.7120	0.5668
B2RT	7.7054	2.3919	3.2215	0.2928	0.6667	0.4392
M2RT	4.3362	2.5179	1.7221	0.2582	0.6141	0.4204
A2RT	5.5674	2.5210	2.2084	0.2559	0.5911	0.4329
SRV	17.4100	12.3900	1.4052	0.9418	2.5206	0.3737
SRT	4.9252	2.5542	1.9283	0.2783	0.5786	0.4810
T1RT	1.2481	2.3865	0.5230	0.0401	0.6104	0.0657

From the Polymylos results in Tables 5.3 and 5.4, it is observed that the modal frequencies due to earthquake vibrations are 4% to 15% higher than the modal frequencies identified from the ambient vibrations. No conclusive explanation can be given for these differences without making assumptions about the bridge behavior within the measured vibration levels. These differences could be attributed to the nonlinear softening hysteretic behavior of the structural components, especially the elastomeric bearings. The results in Table 5.6 reveal that the peak acceleration responses for the earthquake induced vibrations are 1.4 to 3.8 times lower than the peak acceleration responses of the ambient vibrations. Accepting that the estimation of the equivalent modal frequencies is dominated by the peak vibration levels, this could justify a higher secant stiffness of the elastomeric bearings for the lower earthquake peak vibration levels which results in stiffer structures and thus justifies the increase in the equivalent values of the modal frequencies observed in Table 5.4 for earthquake induced vibrations. However, this explanation cannot be used to justify the higher modal frequency values observed for the modes associated with bending of the deck since these modes are not affected by the bearing stiffness. It is unlikely that similar softening nonlinear effects will arise by the deformation of the pier and deck elements in these low vibration levels.

To further support the above argument, the values of the modal frequencies were also identified using much shorter duration segments of the ambient vibrations recordings shown in Figure 5.28, selected so that the peak acceleration levels are approximately the same as or smaller than the peak acceleration of the earthquake recordings. The estimated values of the modal frequencies obtained by analyzing these short duration segments were found to be almost identical to the

values of the modal frequencies that were estimated using the whole, approximate 30 minutes in duration, segment of the records shown in Figure 5.28. This verifies that at the low vibration levels considered, the aforementioned differences in the peak acceleration levels between the ambient and the earthquake induced vibrations cannot justify the large differences in the modal frequencies observed in Tables 5.3 and 5.4.

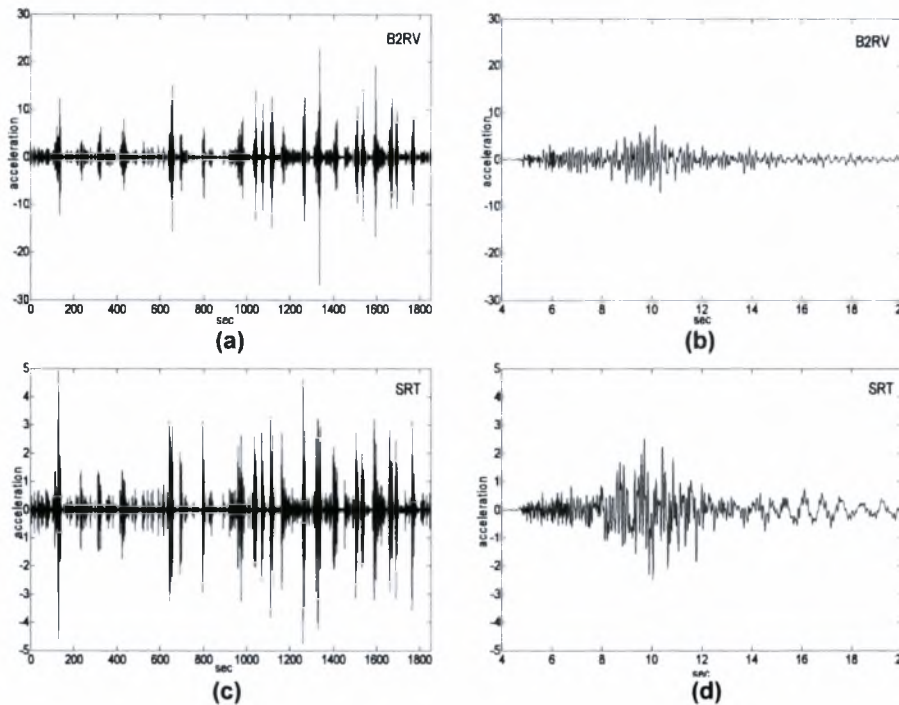


Figure 5.28: Accelerations time history measurements from ambient and earthquake vibrations at sensors B2RV and SRT, (a,c) ambient, (b,d) earthquake

In contrast to the peak vibration levels, the levels of the RMS response in Table 5.6 of the approximately 30 minutes ambient acceleration measurements are 0.25 to 0.82 times the corresponding root mean square earthquake response levels. Accepting that the estimation of the equivalent modal frequencies in Table 5.3 is dominated by the RMS vibration levels, the modal frequencies due to higher RMS earthquake vibration levels are expected to decrease if softening of the elastomeric bearings takes place, which is not consistent with the opposite increasing trend observed in Table 5.4.

A more reasonable explanation that can account for the differences between Table 5.3 and Table 5.4 is soil structure interaction effects (Safak 1995). Specifically, ignoring the rigid body rotation of the central pier foundation at the low vibration levels measured, the modal frequencies identified by the earthquake vibration measurements using as input accelerations the recordings at the abutments and the base of the central pier, are those of the fixed base bridge so that soil structure interaction effects are not participating in the identified dynamics of the bridge system. In contrast, the modal frequencies obtained from the ambient measurements due to excitations from the traffic and wind loads correspond to the dynamic characteristics of the combined system consisting of the bridge and accounting for soil structure interaction effects. This is also supported

from the non-zero vibration levels recorded at the base of the piers and the top of the side abutments during ambient measurements. Thus, soil-structure interaction effects cause the combined soil-foundation-superstructure system to appear as less stiff than the superstructure itself, resulting in lower values of the modal frequencies which is consistent with the results observed in Table 5.3.

Figure 5.29 compares the measured power spectral densities with the power spectral densities predicted by the identified optimal modal models for selected sensors for the Polymylos bridge (Figure 5.29a) and the Kavala bridge (Figure 5.29b) zoomed at the frequency range near the four closely-spaced and overlapping modes. As it is seen, the fit of the measured power spectral density is very good which validates the effectiveness of the proposed modal identification software based on ambient vibrations. Figure 5.30 compares the Fourier transform of the earthquake-induced accelerations and the FT of the accelerations predicted by the optimal modal model for selected sensors. A very good fit is also observed, validating the effectiveness of the proposed modal identification software based on earthquake recordings.

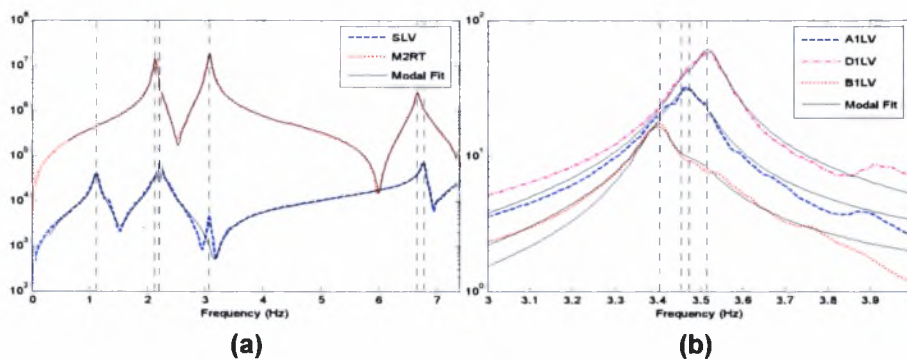


Figure 5.29: Comparison between measured and optimal modal model predicted power spectral densities for selected sensors (a) Polymylos bridge, and (b) Kavala bridge (zoomed at frequency range of four closely-spaced modes)

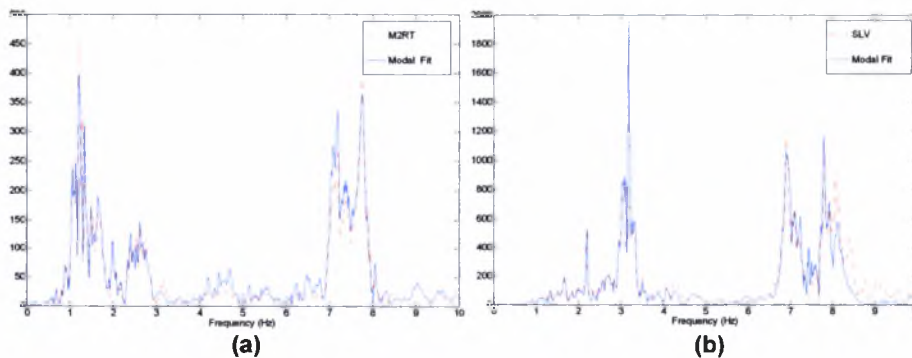


Figure 5.30: Comparison between measured and optimal modal model predicted Fourier transforms of the Polymylos earthquake accelerations recordings for selected sensors

Chapter 6

Modal Identification Toolbox (MIToolL)

6.1 Introduction

This chapter presents the software MIToolL (Modal Identification Toolbox) that has been developed for model identification of structures and it is in the form of a user's manual. This software has been developed in the System Dynamics Laboratory of the department of Mechanical and Industrial Engineering of University of Thessaly.

MIToolL software for modal identification was originally developed in MATLAB 7.0 (R14) environment. The software includes Graphical User Interface (GUI) so to be simple to use and most comprehensible even to unspecialized persons. It allows the full exploration and analysis of signals that are measured on specific points on a structure when it is excited for an Experimental Modal Analysis (EMA), Operational Modal Analysis (OMA) or for earthquake induced vibrations, and it is fully adaptable to satisfy the user's requirements by allowing the resetting of most of its operational parameters.

The modal identification software that has been developed comprises signal processing toolbox for analysing the response measurements of a structure, that are next processed using a variety of modal identification methodologies for the estimation of the modal characteristics. By the graphical interface the user first defines the signals which are time histories (usually accelerations and forces) measured on the structure using a sensor network and then, if a frequency relative methodology will be applied, he transforms them in the frequency domain setting also the frequency band for the identification. Next, the number of modes to be identified and their estimation of their modal frequencies and modal damping ratios are decided either by visual inspection of the response of the structure in the frequency domain, or using stabilization diagrams that can be computed. Lastly, after selecting the proper methodology that will be applied for the modal identification, the algorithm for processing the signals and estimating the values of the structure's modal frequencies, modal damping ratios, modeshape components and modal participation factors starts by pressing a single button. The modal identification results are presented on the GUI and also in Matlab command window and in output files.

MIToolL software was created in Matlab but its GUI is developed for users that do not possess any sophisticated knowledge of the Matlab environment. The only thing a MIToolL software user needs, apart from the experience in modal identification problems for ambient and earthquake loads, is to know how to create and manage the .mat files in Matlab that are used for the input and output of the software.

This chapter is divided in two parts. The first part presents in details the operations and prospects of the MIToolL software. In the first subsections the MIToolL GUI main window is presented with most of the operations that can be evaluated with the software and also some information about the form of the compatible with the MIToolL input files. The next subsections present all the menus of the software and all their operations are described. These operations can be divided in two categories, those concerning the pre-processing operations including all the configurations

for importing the measured data in the software and for fully defining the modal identification problem, and those concerning the post-processing operations that include operations for presenting and exporting the results. The second part is a step-by-step user guide for identifying the modal characteristics of the $\Gamma 9$ bridge at Polymylos (Greece) using real ambient vibration response measurements and for identifying the modal characteristics of the $\Gamma 2$ bridge at Kavala (Greece) using vibration response measurements due to simulated earthquake loads.

6.2 MITool Software

6.2.1 Installation notes for MITool software

MITool software is simply to install and use. It requires Matlab (version 7 or higher) installed in the computer with the folder “\MITool” added in the Matlab path. For example if Matlab is installed in folder `C:\MATLAB7\` the folder MITool can be copied in subfolder `C:\MATLAB7\work\`. Then in the Matlab file menu the selection *Set Path...* and by pressing *Add with Subfolders* pushbutton the folder `C:\MATLAB7\work\MITool` is selected. Finally, in Matlab Command Window the following command should be executed

```
>> MITool
```

This command opens the GUI window of the MITool software that will be described in details in the next section.

6.2.2 MITool Graphical User Interface (GUI)

MITool GUI main window (Figure 6.1) includes a number of menus on the upper part of the window that contain all the executable operations of the software. Also it contains many user defined input components (popup menus, radiobuttons i.e.) concerning the illustration, the definition of the modal identification program and the execution of the modal identification procedure. Some of these menus and the other components are not enabled at the beginning, preventing the user to execute illogical operations during the identification procedure. These software components are automatically enabled subsequently during the identification procedure. For example the pushbutton that will start the evaluation of the modal identification procedure is not enabled before the user completes all the necessary operations and configurations for fully defining the identification problem.

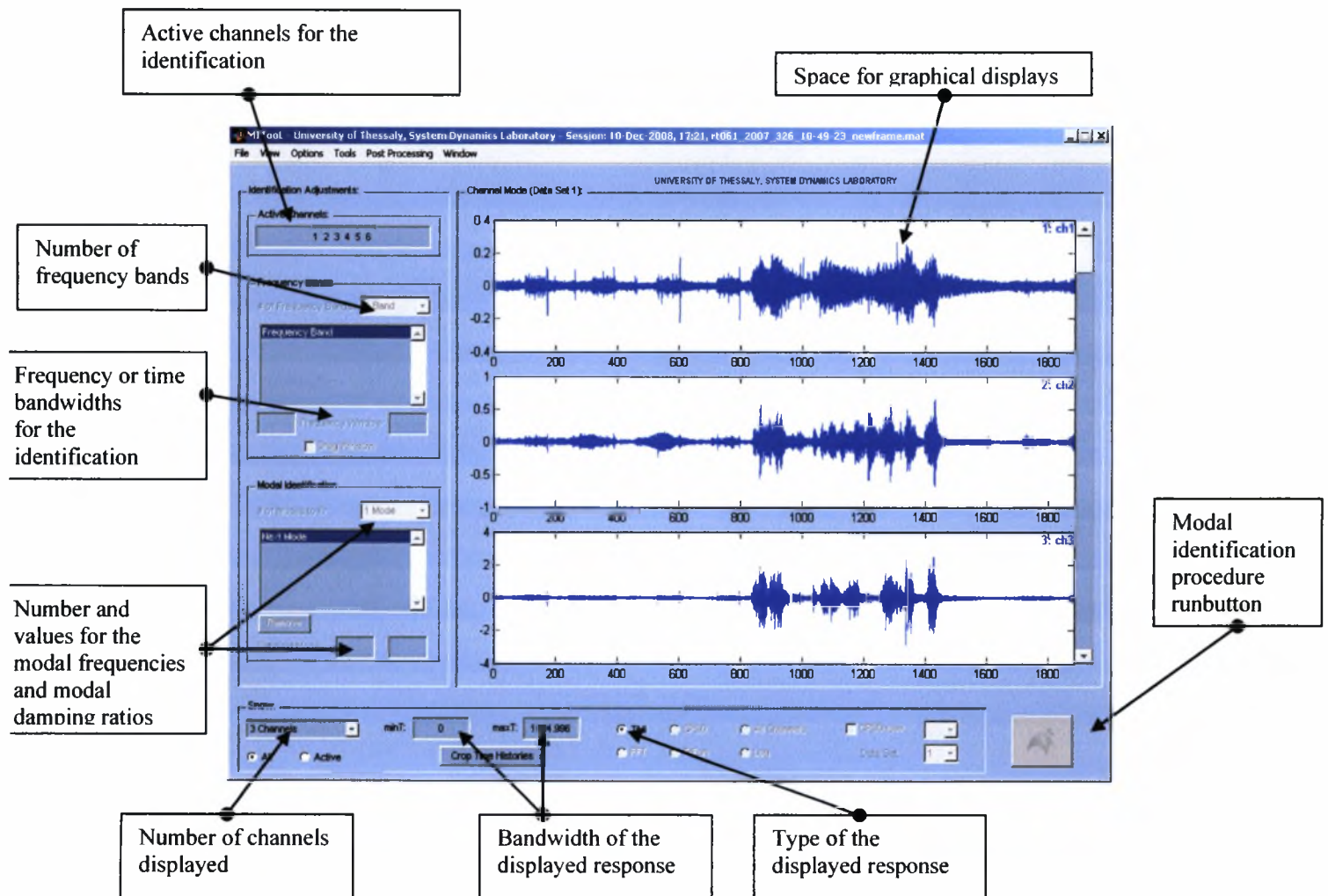


Figure 6.1: Graphical User Interface of MITool software

6.2.2.1 Input files for MITool

For executing the modal identification procedure of a structure with the MITool software the data from the measured responses (time histories) of the structure must be properly imported in the software. Also the software has the capability to graphically display the structure with the sensor locations on it, if all the information about the structure and sensor network is properly imported in the software. This geometrical information about the structure can be included in the same .mat files with the measured responses. The .mat input file that is loaded by the MITool software must contain arrays with specific names and format so that it should be compatible with the MITool software. The names and format of the arrays included in this .mat input file that has to be created for every measurement is next described.

- accel: Double array that contains the measured time histories (accelerations by default) of the structure. It has number of rows equal to the number of measurement samples and the number of columns equal to the number of sensors that are used for the measurement of the response and the base excitation (for the case of earthquake induced vibrations).
- Ft: Double array that contains the measured force excitations. This array is needed only for the case of experimental modal analysis where the artificial excitation force is measured. It is a column array number of rows equal to the number of measurement samples.
- dt: Double array (scalar) that contains the time discretization of the response time histories.
- channeltext: Cell array that contains the names of the sensors.
- ndim: Double array (scalar) that contains the number of dimensions for the graphical display of the structure.
- FENode: Double array that contains the number and location of nodes for the graphical illustration of the structure as a linear mesh. The first column is the number of the node, the second column is the coordinate of the node in the x axis, the third column is the coordinate of the node in the y axis and the fourth column is the coordinate of the node in the z axis.
- FEelt: Double array that contains connectivity between nodes. It contains the line element number and the nodes connected for the graphical display of the structure as a linear mesh. The first column is the number of the liner element, the second column is the number of node that the line element starts and the third column is the number of node that the line element ends.
- sensors: Double array that contains the number and the location of the sensors on the structure. The first column is the number of the sensor, the second column is the number of the node where the sensor is located, the third column is the direction which the sensor can measure (1 for measuring in the x axis, 2 for measuring in the y axis and 3 for measuring in the z axis) and the fourth column is an amplitude ratio (default value must be 1 for all sensors)

Remark: The names of the arrays that are compatible with the software (accel, dt, channeltext i.e.) can be defined to be different using the *Preferences* option in the *File* menu of the MITool software.

6.2.2.2 The File menu

The File menu (Figure 6.2) includes operations that allow the user to import data in the MITool software and export data to Matlab workspace and to .mat files. From the file menu the user can load the measured time histories and also the data for the graphical display of the structure and the sensor network (*Load Experimental Data & Structure*) that have been described in the previous section. Another important operation in the File menu is the *Load Session* and *Save Session* operations where the user can save his current application with all its configurations and afterwards restore it. These operations are very important to avoid the repetition of time consuming operations as for example the calculation of the cross power spectral density functions that can be done only once and the application can be saved and then loaded many times and used in the modal identification problem. The *Preferences* operation opens a dialog box where the user can configure the input and output parameters of the MITool software.

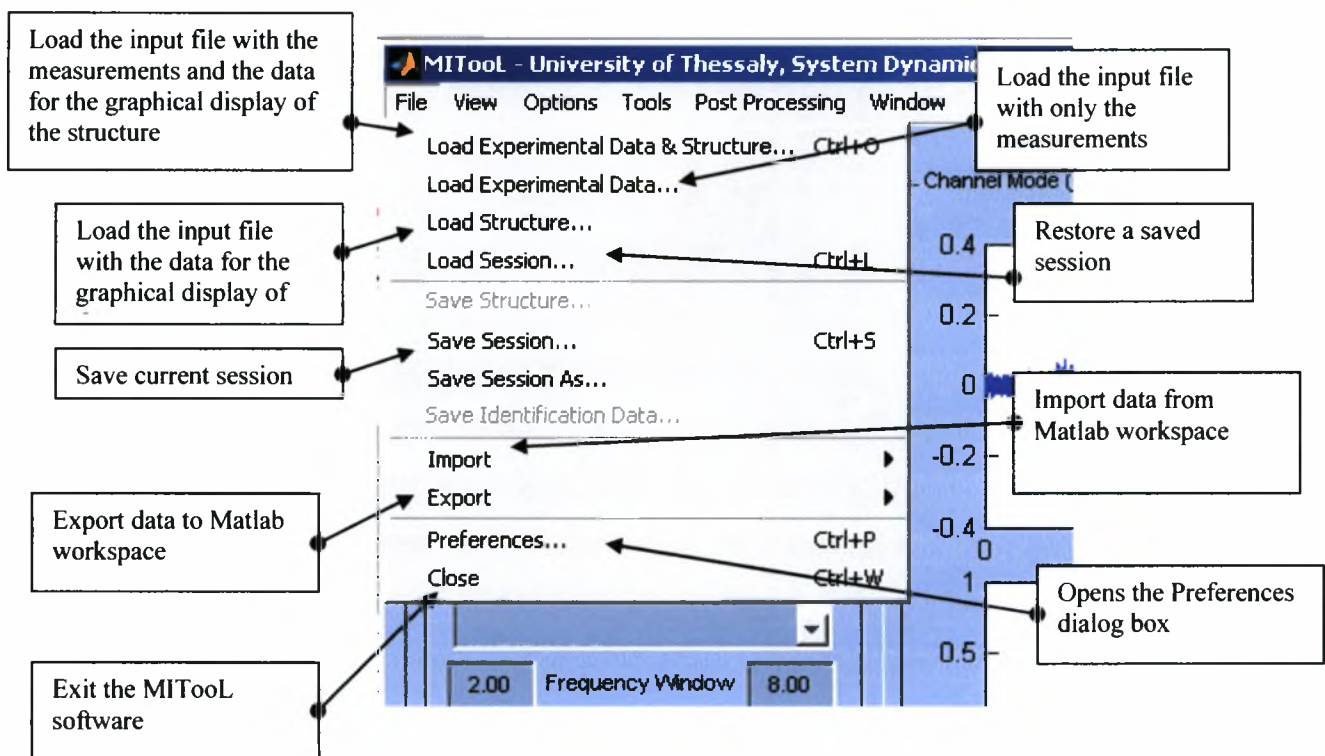


Figure 6.2: The File menu

6.2.2.3 The Preferences dialog box

The Preferences dialog box (Figure 6.3a) includes all the information the user can define so the input files that are loaded are compatible with MITool software. One of the most important configurations in this dialog box is the definition of the identification case (*Type of Identification*) that will be evaluated. For the case of Operational Modal Analysis (OMA) the user must choose the *Multi-Output Only* radiobutton, for the case of earthquake bases modal identification the user must choose the *Multi-Input Multi-Output* radiobutton and for the case of experimental modal

identification where one excitation force is applied and measured on the structure the user must choose the *Single-Input Multi-Output* radiobutton. All the other edit fields concern the names of the arrays included in the input files as they are described in Section 6.2.2.1.

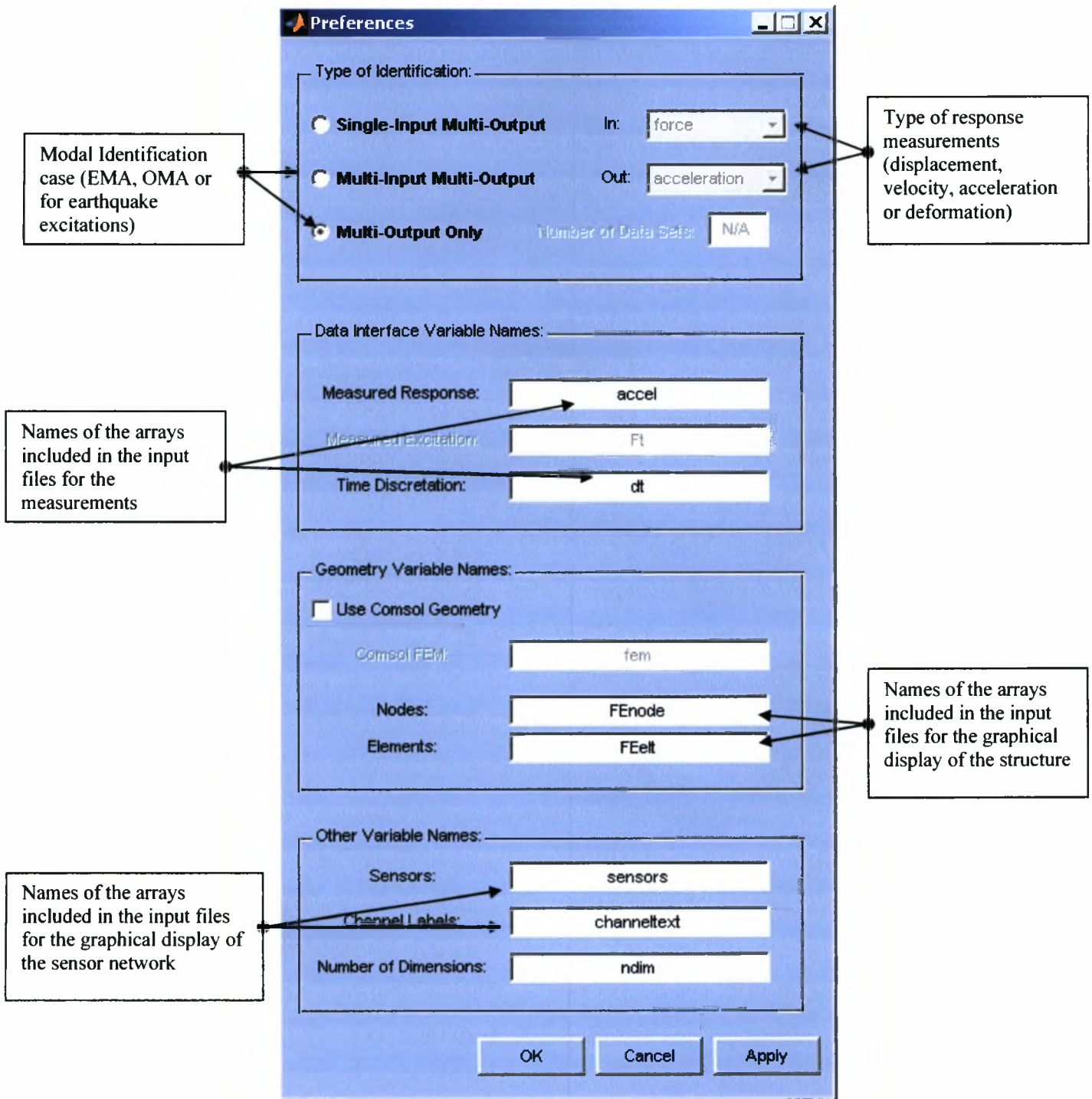


Figure 6.3a: The Preferences dialog box

In Figure 6.3b. the detail about the availability of the response measurements is presented for the case of modal identification based on ambient vibrations. The identification of the modal properties can be evaluated based on available measurements of

- a. acceleration
- b. velocity
- c. displacement
- d. deformation

depending on the instrumentation available.

The user can choose from the menu the type of measurements that are available for the modal identification. It should be noted that for the case of using deformations for the identification, the estimation of the modeshape components is not possible. Instead for this case the software computes the derivatives of the modeshape components.

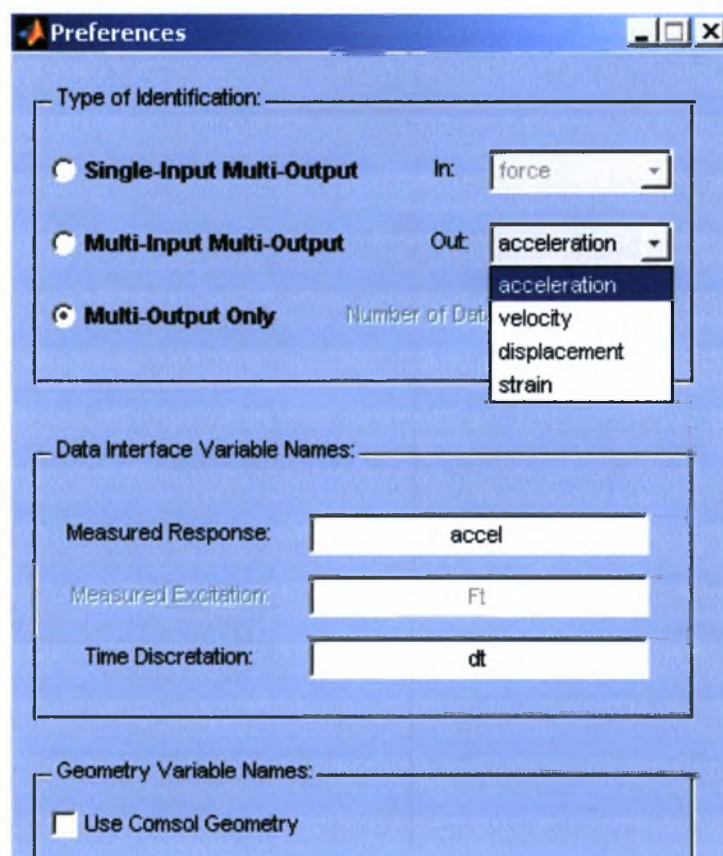


Figure 6.3b: The Preferences dialog box

6.2.2.4 The View menu

The View menu (Figure 6.4) allows the user to define the graphical display he wants to plot on the MITool software. So the graphical display of the measured signals and also the graphical display of the structure with the sensor network are available. From the *Show* panel on the lower part of the GUI window, the user can configure the different representations of the signals (Figures 6.5 and 6.6).

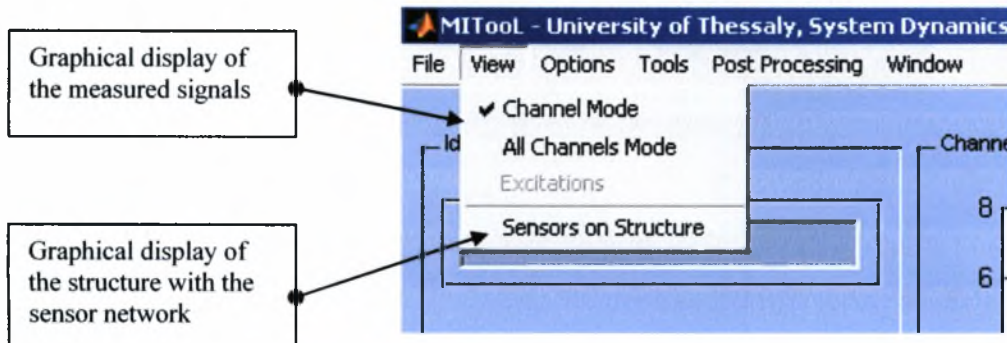


Figure 6.4: The View menu

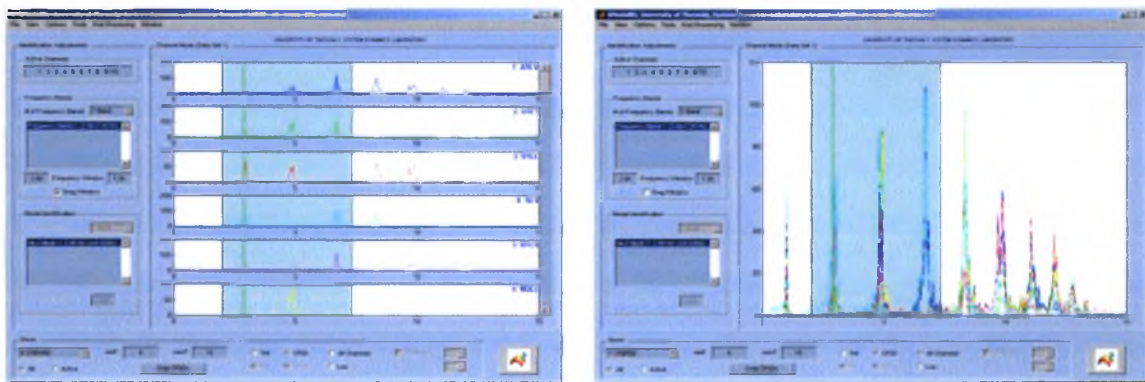


Figure 6.5: View Channel Mode and View All Channels Mode options

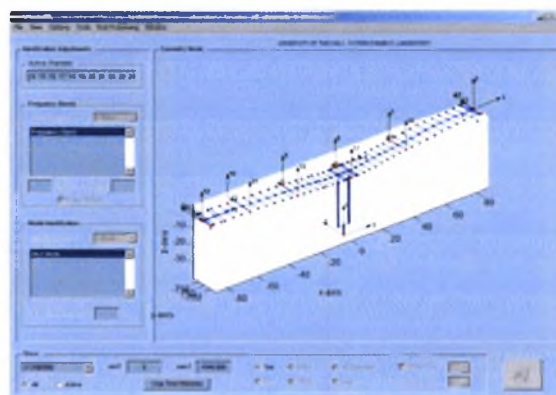


Figure 6.6: View Sensors on Structure option

6.2.2.5 The Options menu

The Options menu (Figure 6.7) gives the user the access to open all the dialog boxes that configure all the main properties of the modal identification algorithm. These dialog boxes, which will be presented in details in the next sections, concern configurations about the ambient vibration and the earthquake induced vibration identification algorithms, about the estimation of the Cross Power Spectral Density (CPSD) functions and also configurations about the gradient based (quasi-Newton) optimization algorithm that is used for the solution of the modal identification problem. For quicker access to all the dialog boxes there are keyboard shortcuts.

Many of the menus and the other components of the MITool software that are presented in the next subsections might not be enabled at the beginning, preventing the user to execute illogical operations during the identification procedure. These software components are automatically enabled continually during the identification procedure.

All the parameters of the MITool software algorithms have default values at startup. Modifying the values of many of these parameters is recommended only to specialized users in the modal identification problem. Any modifications in these software parameters made by a non-expert user may cause problems to the evaluation of the used algorithms and consequently failure to the modal identification procedure.

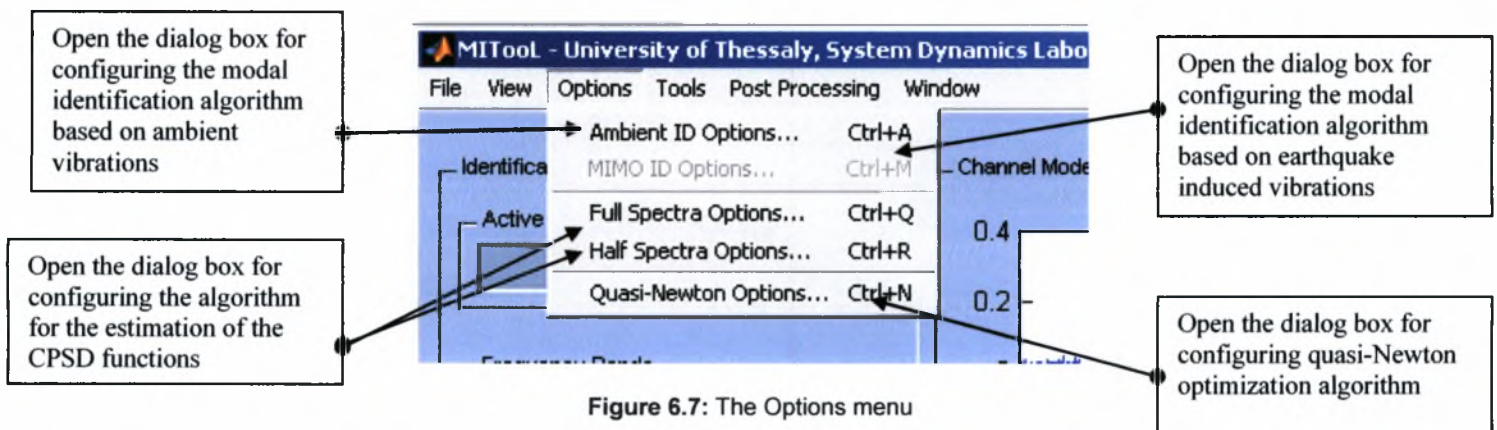


Figure 6.7: The Options menu

6.2.2.6 The Identification Options dialog box

The Identification Options dialog box (Figure 6.8) is the most important dialog box for configuring the parameters for solving the modal identification problem. The identification algorithms estimate the modal parameters (modal frequencies, modal damping ratios, modeshapes and modal participation factors) of a modal model, based on a least squares minimization of a measure of fit between the measured structural response and the response that is predicted by a modal model in a user defined frequency band. The methodologies implemented in the software for the identification of the modal parameters for the cases of classically and non-classically damped modal models and have been discussed in details in Chapter 4.

The modal identification algorithm with the MITool software is divided in three steps.

1. In the first step of the modal identification procedure only the modal frequencies and the damping ratios of the modal model of the structure are estimated in a specific, user defined, frequency band. By selecting the evaluation of the first step (*Run Step 1*) the values of the modal frequencies and the modal damping ratios can be chosen using the stabilization diagrams that are computed. Alternatively, by avoiding evaluating the first step, estimations of the values of the modal frequencies and the modal damping ratios can be decided by the user through visual inspection of the response of the structure in the frequency domain. In visual inspection, however, modal damping ratios are rough approximations of the estimated ones during the identification process.
2. In the second step of the modal identification procedure the modeshapes and the modal participation factors are computed given the values of the modal frequencies and the modal damping ratios estimated in the first step. In this step the user can decide between solving the problem of computing the modeshapes and the modal participation factors, which is a non-linear optimization problem, analytically (Step 2a, *Type of Analysis: SVD of $R(\omega, \zeta)$*), or using gradient based quasi-Newton computational methods for solving the nonlinear optimization problem (Step 2b, *Type of Analysis: $U(\omega, \zeta, g)$*). It should be noted that modal participation factors are not obtained when using the modal identification algorithm based on ambient (operational) vibrations.
3. In the third step of the modal identification procedure (*Run Step 3*) the values of all the modal parameters (modal frequencies, modal damping ratios, modeshapes and modal participation factors) are estimated by solving the whole non-linear optimization problem using gradient based quasi-Newton computational methods but applying very good initial estimations given in the first two steps of the algorithm.

It should be noted that for the solution of the modal identification problem using the steps 1 and 2a the evaluation of gradient based optimization methods is avoided. These methods are iterative and for the solution of problems with many response signals can be very highly time consuming. Instead, the estimates of the modal parameters are obtained by solving linear algebraic systems. The implementation of the third step in the identification algorithm is considered imperative for solving problems where is significant measurement noise in the signals and also for identifying closely spaced and overlapping modes. For fully comprehension of this three step algorithm for the modal identification problem based on ambient vibrations, a step by step example will be presented in the next section.

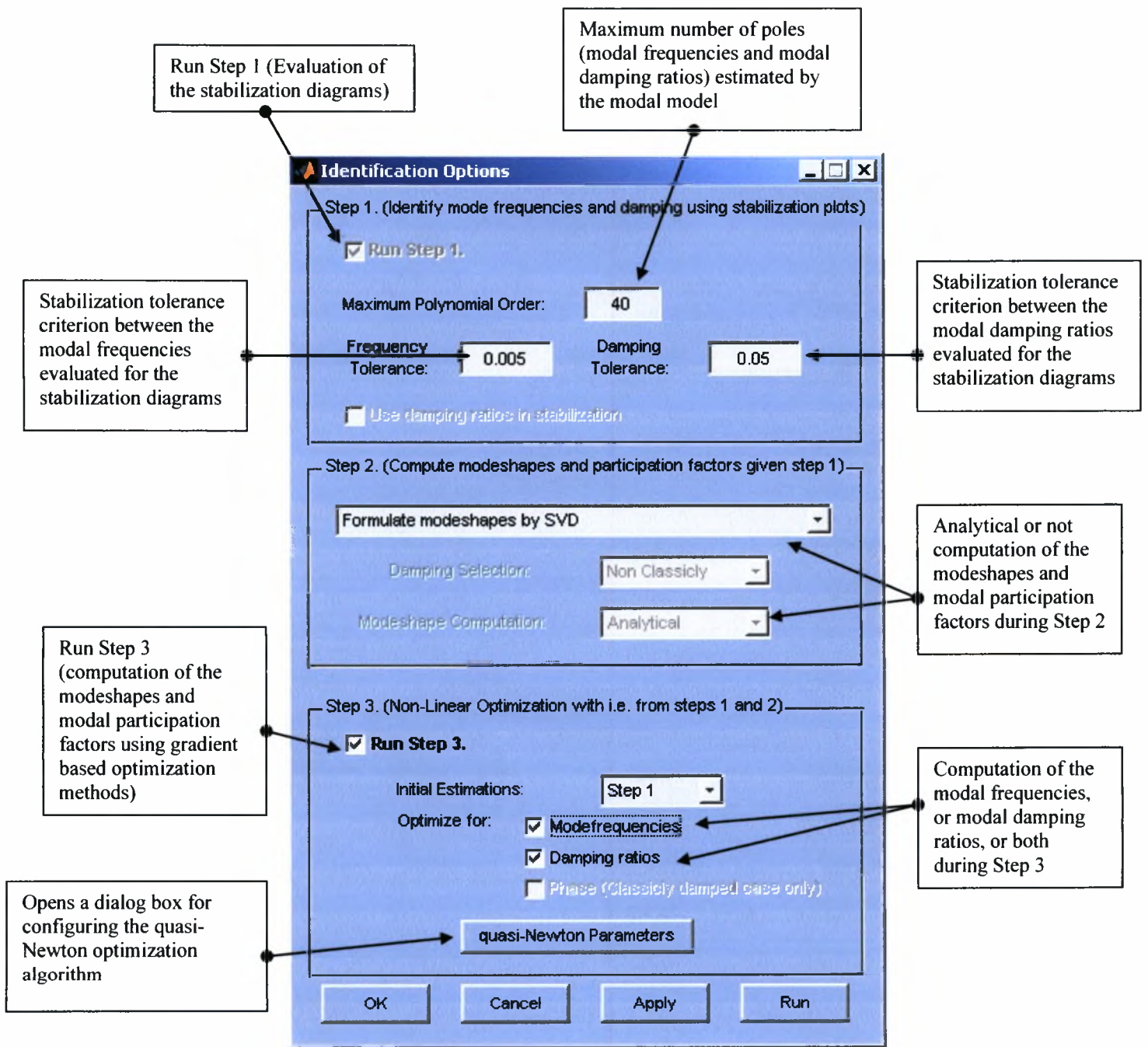


Figure 6.8: The Identification Options dialog box

6.2.2.7 The MIMO Options dialog box

The MIMO Options dialog box (Figure 6.9) includes the configurations of the modal identification algorithm for structures based on earthquake induced vibrations (measured base excitations). The evaluation of the modal identification algorithm estimate the modal parameters (modal frequencies, modal damping ratios, modeshapes and modal participation factors) of a modal model, based on a least squares minimization of a measure of fit between the measured structural response and the response that is predicted by a modal model in a user defined time sequent or frequency band. The MITool software includes two modal identification methodologies for the case of earthquake induced vibrations (Nikolaou 2008). The first methodology computes the modal parameters by minimizing an error function that quantifies the difference between the measured responses (time histories) of the structure and the responses that are predicted by the modal model in the time domain. The second methodology works respectively but in the frequency domain, minimizing an error function that quantifies the difference between the Fourier transform of the measured responses of the structure and the Fourier transform of the responses that are predicted by the modal model. The two methodologies are applied for the identification of the modal parameters for the cases of classically and non-classically damped modal models and have been discussed in details in Section 4.4.

For the evaluation of the MIMO identification algorithm, the user must first define which of the measured signals correspond to base excitations (*Excitation DOFs*) and which of the sensors are active response signals (*Active DOFs*). Only the active sensors will be used in the modal identification procedure. Next, the user must define the modal identification methodology that will be used depending on the analysis domain (time or frequency) and depending on the type of modal model (classically or non-classically). Finally, for the case where modal sweeps will be used, the maximum number of modal sweeps and the modal sweep tolerance, related to convergence criteria for the termination of the modal sweeping procedure, should be defined. The selection of the modal groups for sweeping is made in the *Modal Grouping* dialog box (Figure 6.10) which is opened by the *Advanced* pushbutton. The pushbutton *All Modes* groups all modes in one group avoiding modal sweeping.

It should be noted that for the solution of the MIMO modal identification problem for the case of earthquake induced vibrations with the frequency domain methodology, the three step algorithm is implemented in the software as well. The configurations of the three step algorithm are included in the MIMO Options dialog box and they are equivalent to the Identification Options configurations described in the previous subsection.

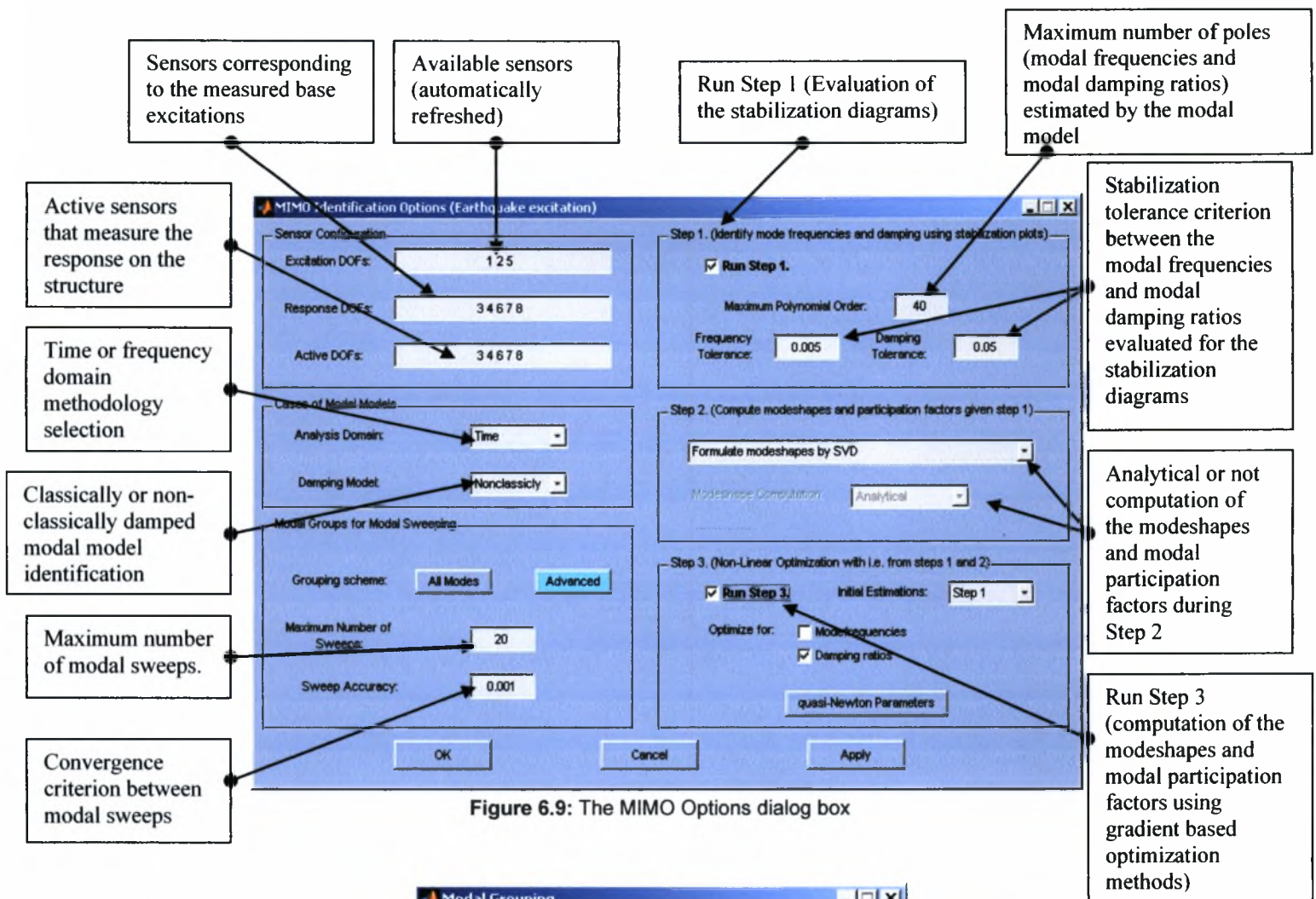


Figure 6.9: The MIMO Options dialog box

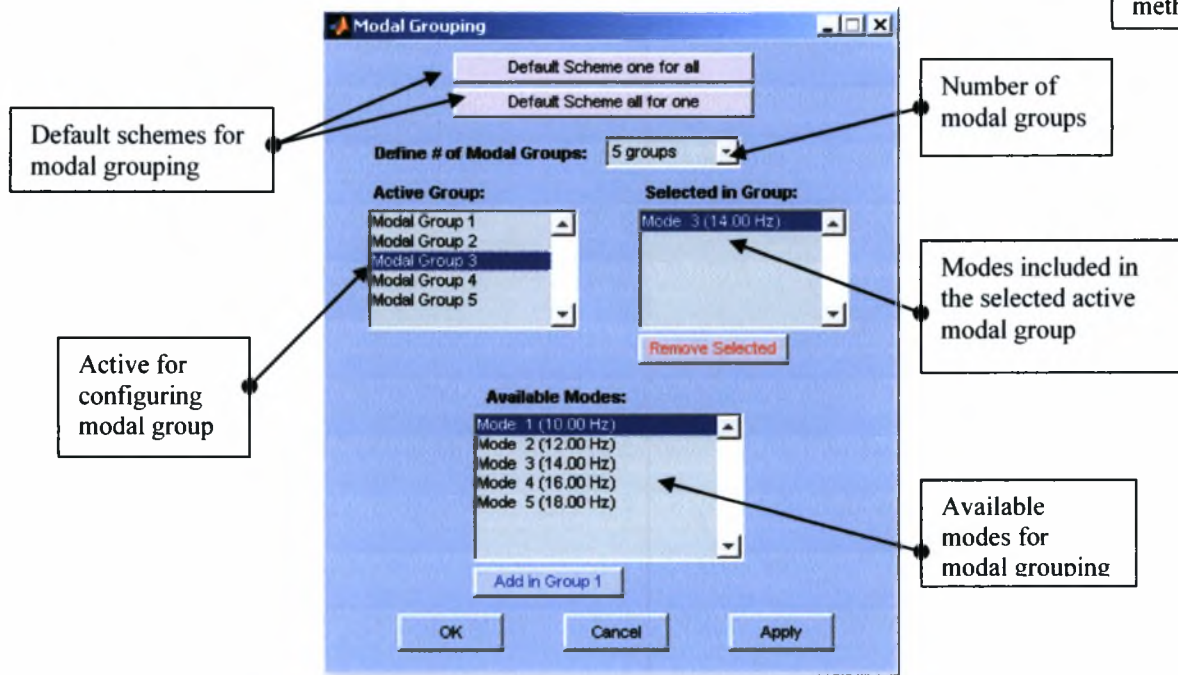


Figure 6.10: The Modal Grouping dialog box

6.2.2.8 The Full Spectra Options and the Half Spectra Options dialog boxes

The Full Spectra Options dialog box (Figure 6.11) includes the parameters of the algorithm for computing the cross power spectral density functions (CPSD) of the measured responses. The computation of the CPSD functions is required for the modal identification methodologies based on ambient vibrations. The efficiency of the modal identification methodologies depends highly on the efficiency of the evaluation of the CPSD functions. Two methodologies for the efficient computation of the CPSD functions are integrated in the MITool software. These two methodologies have already been discussed in details in Chapter 3. With the first methodology, known as the *correlogram approach*, the CPSD functions are estimated from the Fourier Transform of the correlation functions of the measured signals. The second methodology is known as the *periodogram approach* or Welch method. In both methodologies the user can apply a window in the signals (exponential, hanning i.e.) in order to reduce the effect of leakage. For the case of computing the *positive spectra* described in Chapter 3 (positive or half spectra approach) the same configurations can be applied as the correlogram approach for the full CPSD functions (full spectra).

When applying the Welch method the parameters for the efficient computation of the CPSD functions (Figure 6.12) must be selected properly so that the computed CPSD functions contain all the information for the modal characteristics to be identified without overestimating the response signal (adequate discretization) and avoiding the aliasing and leakage effects. The user must also define the number of segments that the signals will be divided and also the higher limit of the frequency bandwidth in which the CPSD functions will be estimated. For adequate discretization, an estimation for the lowest mode frequency that is expected must be applied and also an estimation of the magnitude of the modal damping ratios. Finally for distinguishing and identifying closely spaced modes, one of the most difficult issues in modal identification problems, the user must define an adequate frequency difference between the closely spaced modes expected. Many of the values of the parameters of the algorithm for computing the CPSD functions have default values and some others are estimated automatically by the software taking into account the measured signal that is to be analyzed. Any modifications to the default values of these parameters must be made with caution and are recommended only to users that are familiar with the problem of estimating the CPSD functions and signal processing techniques. Any modifications in these software parameters made by a non-expert user may cause problems to the evaluation of the used algorithms and consequently failure to the modal identification procedure.

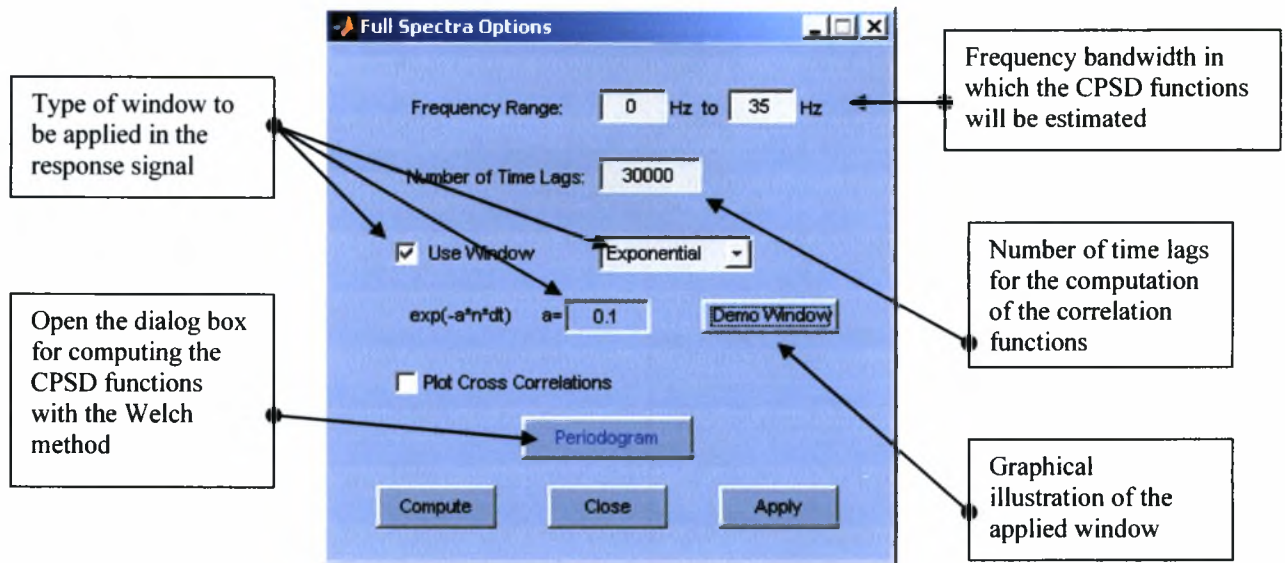


Figure 6.11: The Full Spectra Options dialog box

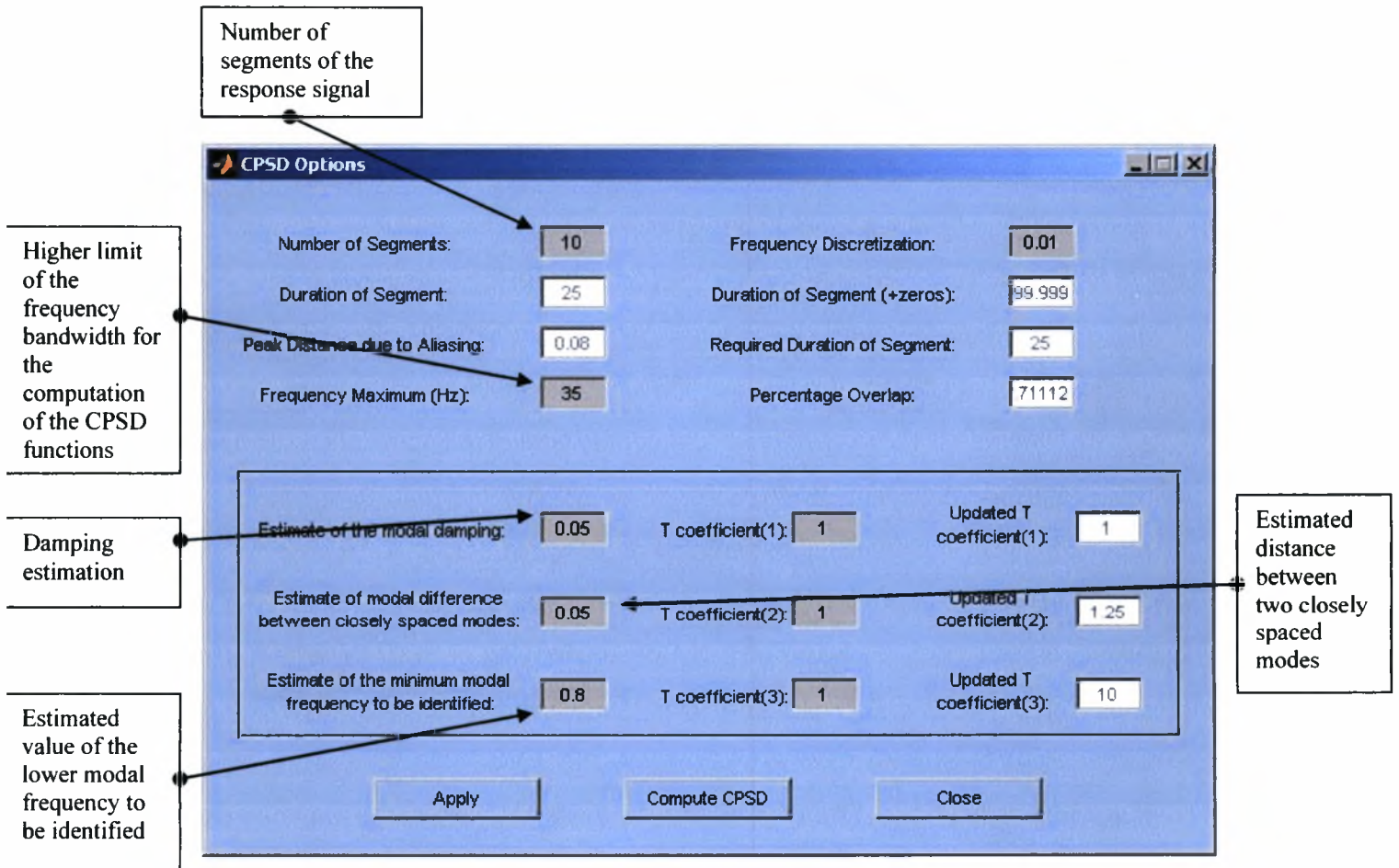


Figure 12: The CPSD Options dialog box

6.2.2.9 The Quasi-Newton Options dialog box

The Quasi-Newton Options dialog box (Figure 6.13) includes the parameters of the optimization algorithm that minimizes the error function that quantify the difference between the measured responses of the structure and the responses that are predicted by the modal model and is evaluated during the modal identification procedure for both ambient vibrations and earthquake induced vibrations. The minimization of the error function (objective function) with the MITool software is accomplished using the *fminunc* and *fmincon* function of Matlab Optimization Toolbox library.

The parameters of the minimization algorithm that are available to MITool software are those that define the gradient based methodology and also the convergence criteria that have to be accomplished for terminating the algorithm. During the evaluation of the minimization algorithm, the progress of the procedure can be displayed in the Matlab Command Window by selecting the *Display: iter* operation. Modifying properly the convergence parameters (*TolFun* and *TolX*) of the *fminunc* and *fmincon* minimization functions greater convergence can be achieved and consequently better results for the modal identification problem. The parameters available in the Quasi-Newton Options dialog box are briefly presented below. For more details about the minimization functions *fminunc* and *fmincon* the user should refer to Matlab Help Manual for the Optimization Toolbox.

GradObj	Defines if analytic expressions for the gradients of the objective function are used (on) or not (off).
Display	Defines the amount of information displayed in Matlab Command Window during the evaluation of the minimization algorithm. The selections, <i>off</i> displays no information, <i>iter</i> displays information for every iteration of the minimization algorithm and <i>final</i> displays information only about the termination and the convergence of the algorithm.
DerivativeCheck	Compares the values computed for the gradients of the objective function using the analytical expressions with the values computed using finite difference scheme.
MaxFunEvals	Defines the maximum number of function (objective) evaluations for the termination of the minimization algorithm.
MaxIter	Defines the maximum number of iterations for the termination of the minimization algorithm.
TolFun	Maximum value of the gradient of the objective function that satisfy the convergence criterion.
TolX	Minimum value of the parameter step that satisfy the convergence criterion.

The analytic expression for the gradients of the objective function that are implemented in the MITool software and can be used by the gradient based optimization algorithms (GradObj selection on) for the solution of the modal identification problem increase the number of calculations per function evaluation but the convergence is succeeded in less number of iterations, eventually reducing the total computational time especially for difficult identification cases.

Parameters of the minimization functions *fminunc* and *fmincon* of Matlab Optimization Toolbox

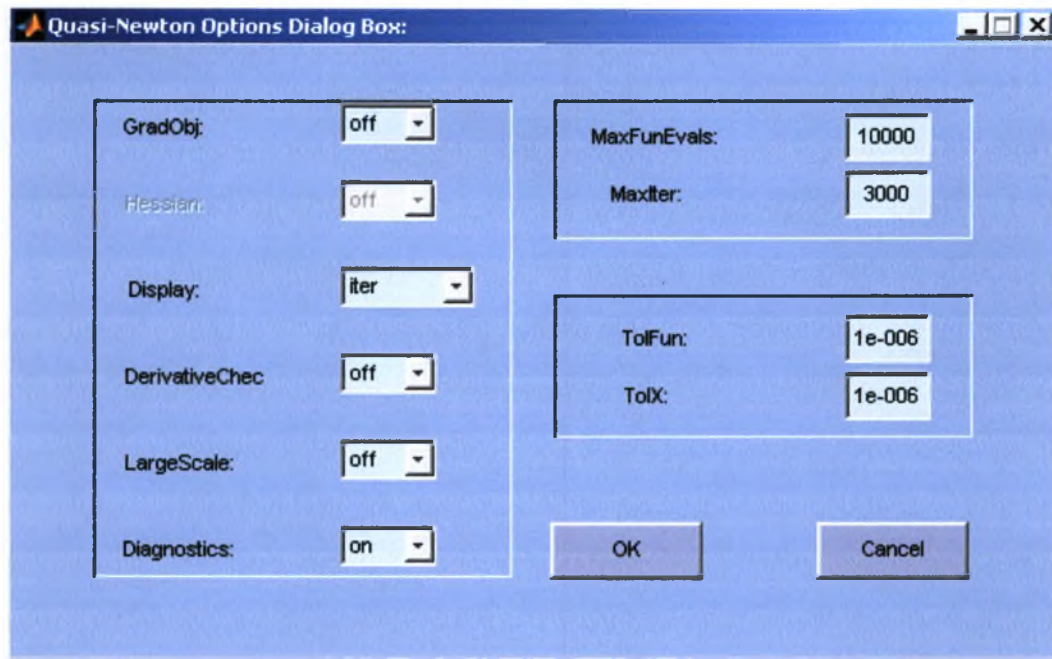


Figure 6.13: The Quasi-Newton Options dialog box

6.2.2.10 The Tools menu

The Tools menu (Figure 6.14) gives the user the access to the peripheral operations of the MITool software. From this menu the user can execute directly signal processing operations and convert the measured signals from the time domain to the frequency domain. These operations include Fourier Transform of the measured signals and computation of the CPSD functions. These operations are executed with the selected parameters from the Options menu dialog boxes and have already discussed in previous subsections.

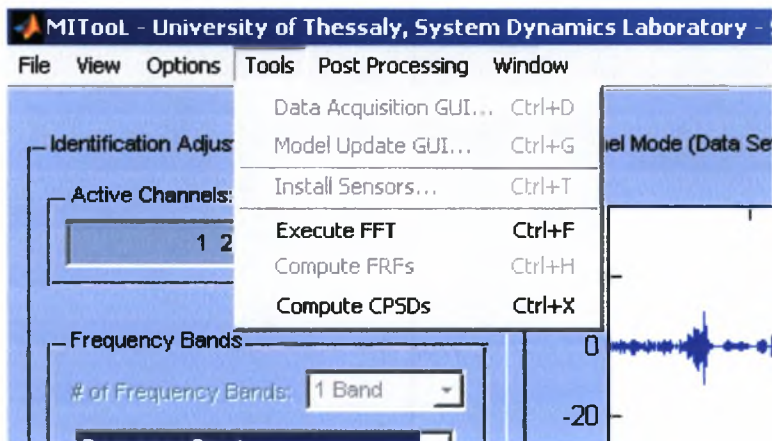


Figure 6.14: The Tools menu

6.2.2.11 The Post Processing menu

The Post Processing menu (Figure 6.15) is enabled automatically after the modal identification procedure is concluded for the first time and the modal model is estimated. From this menu the user can illustrate on the MITool software window the results of the modal identification procedure that is executed. In particular, the user can illustrate the response predicted by the modal model and compare it with the measured structural response (*Model Identification Fits*, Figure 6.16). Also the values of the modeshape components predicted by the modal model can be illustrated on the structure (*Plot Modeshapes on Structure*, Figure 6.17) and the values of the complex modeshape components for the case of non-classically damped modal model (*Plot Modeshapes Complex Projections*, Figure 6.18). Finally, an output text file can be created including the values for the modal frequencies, modal damping ratios, modeshape components and modal participation factors (*View Numerical Results*, Figure 6.19).

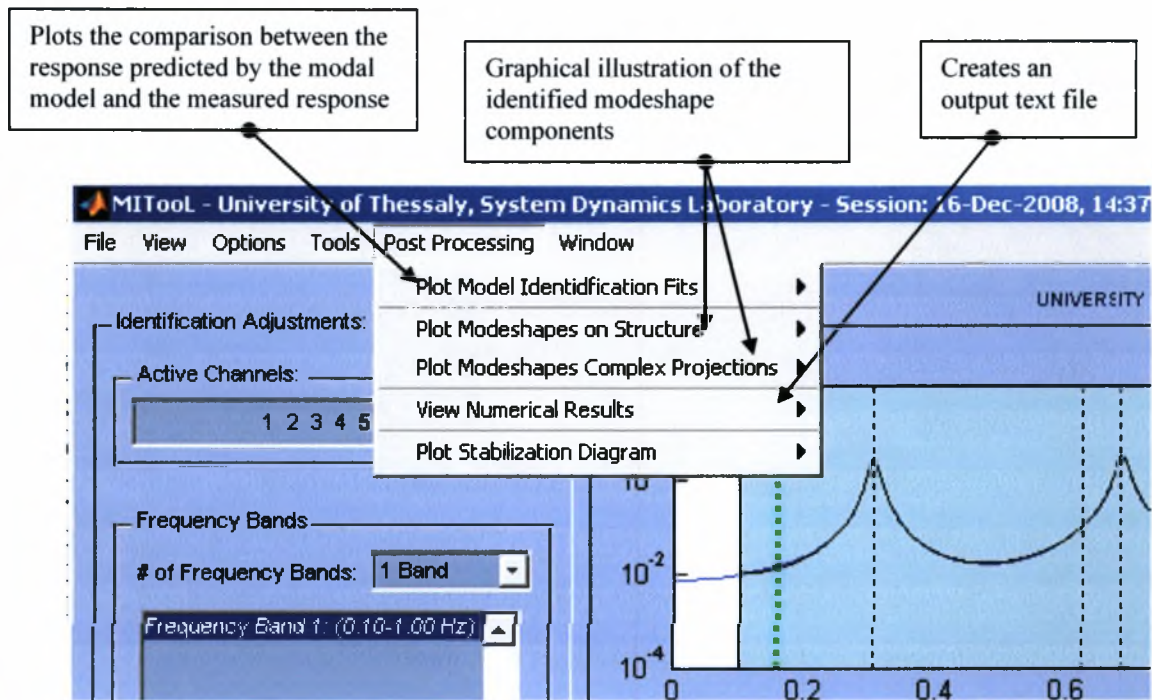


Figure 6.15: The Post Processing menu

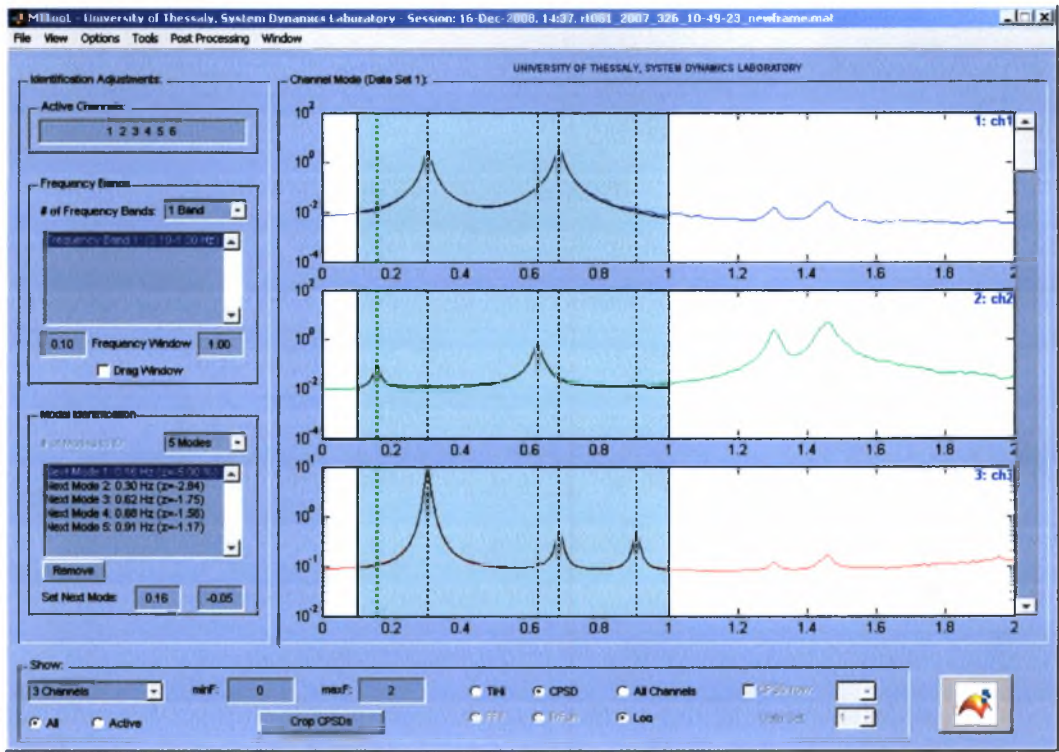


Figure 6.16: Comparison between the response predicted by the modal model and the measured response

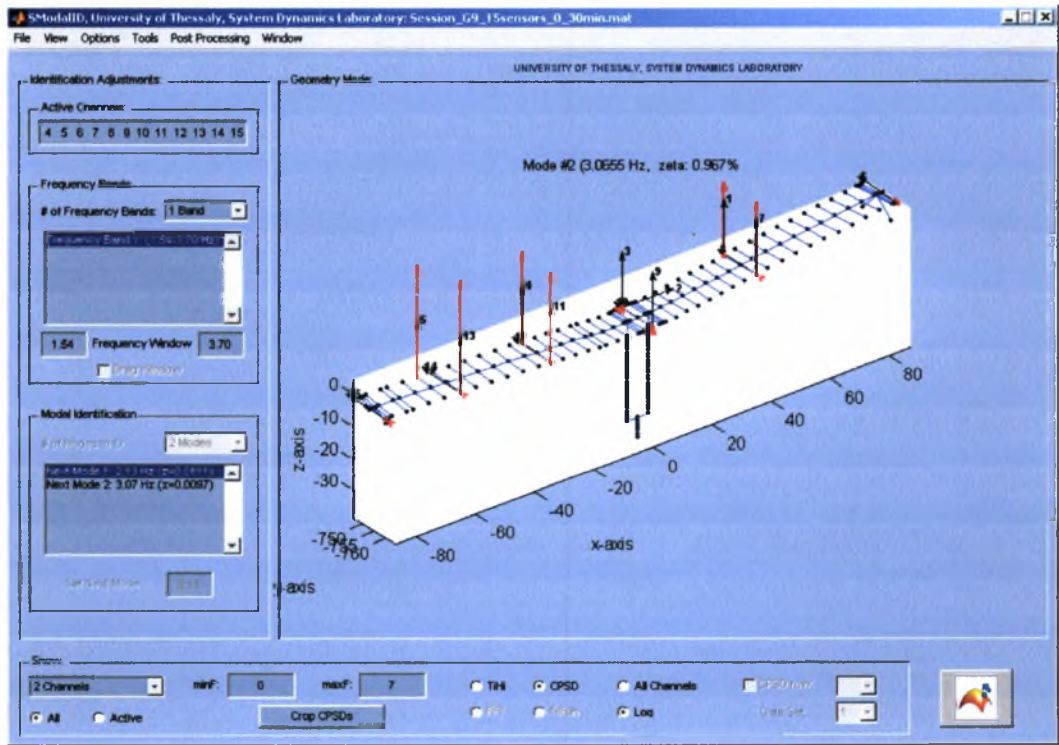


Figure 6.17: Graphical display of the identified modeshape components on the structure

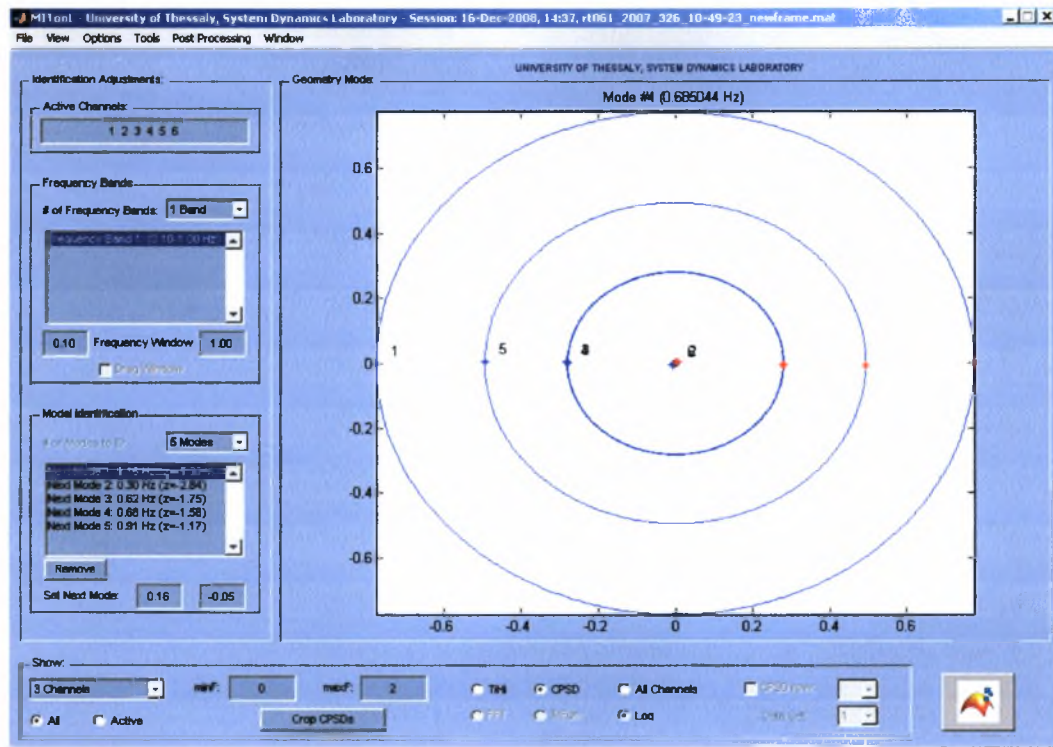


Figure 6.17: Graphical display of the identified complex modeshape components



Figure 6.19: Example of output text file

6.2.3 The Stabilization Diagrams

The stabilization diagrams (Figure 6.20) are evaluated during the structural modal identification procedure based on vibration measurements and contain information about the values of the modal parameters. In MITool software the evaluation of the stabilization diagrams depend on whether the user has selected to evaluate the first step of the three step modal identification algorithm, described in the previous section about the Identification Options dialog box, or not. The stabilization diagrams present possible values for the modal parameters as those are estimated analyzing the measured signals. The stabilization diagrams in MITool software are evaluated taking into account the values only for the modal frequencies and modal damping ratios. The user can choose which of those proposed values are corresponding to the physical poles of the structure and ignore the values that correspond to mathematical poles that arise from the environmental noise on the analyzed measured signals. These selected values are used for the continuation of the modal identification procedure and the estimation of all the modal parameters. The user is also able to repeat the stabilization procedure (Re-stabilize poles) modifying the stabilization tolerances for the modal frequencies and the modal damping ratios and resulting in different stable poles.

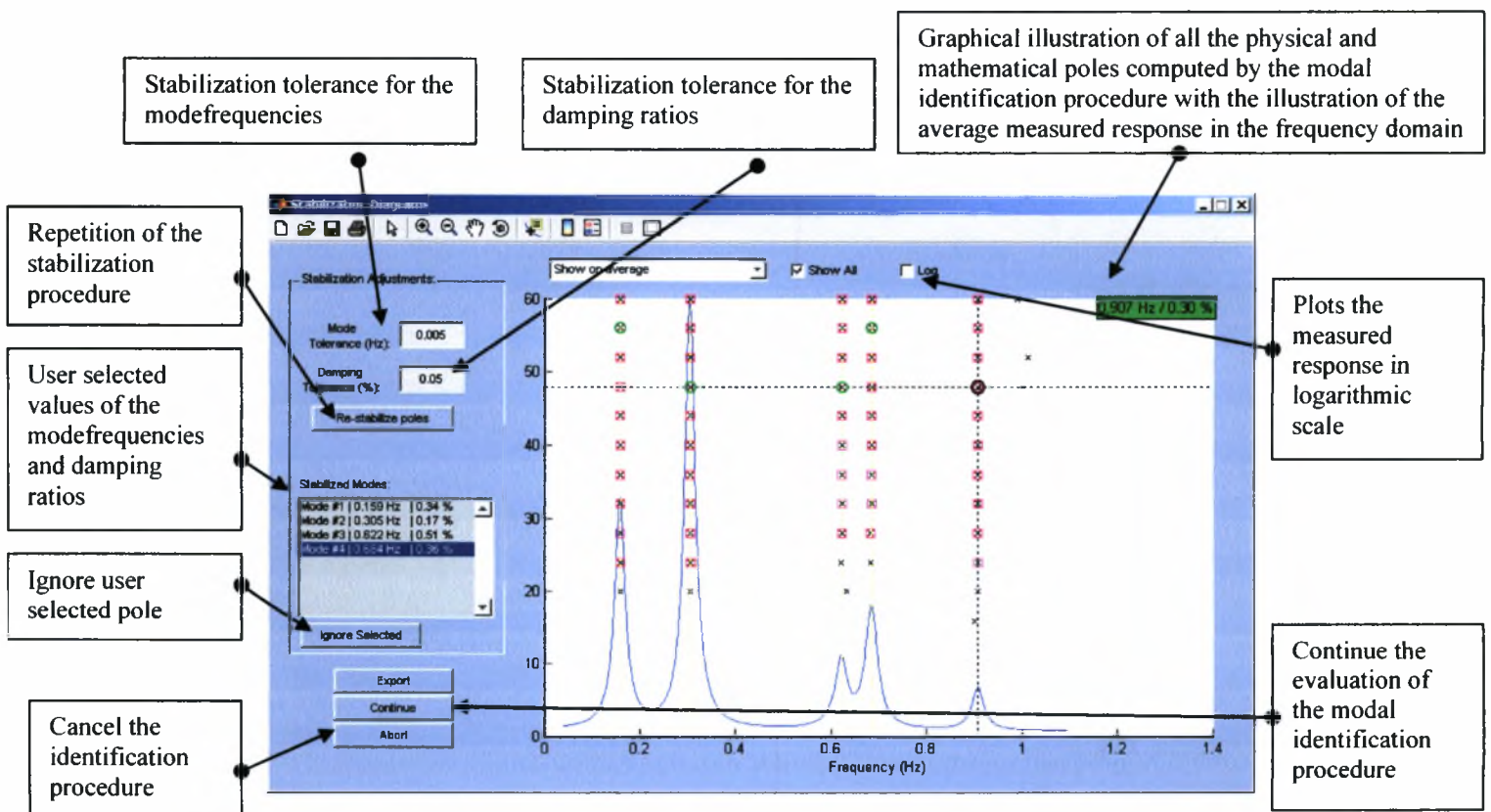


Figure 19: The stabilization diagram

6.3 Step-by-step user guide to modal identification with MITool software

This section presents a step-by-step guide for running the modal identification procedure using the MITool software for estimating the modal properties of structures. It includes two fully detailed examples of modal identification procedures of bridges, the first is an application with real ambient vibration measurements of the G9 bridge at Polymylos (Greece) and the second is an application with simulated earthquake induced vibration measurements of the G2 bridge at Kavala (Greece).

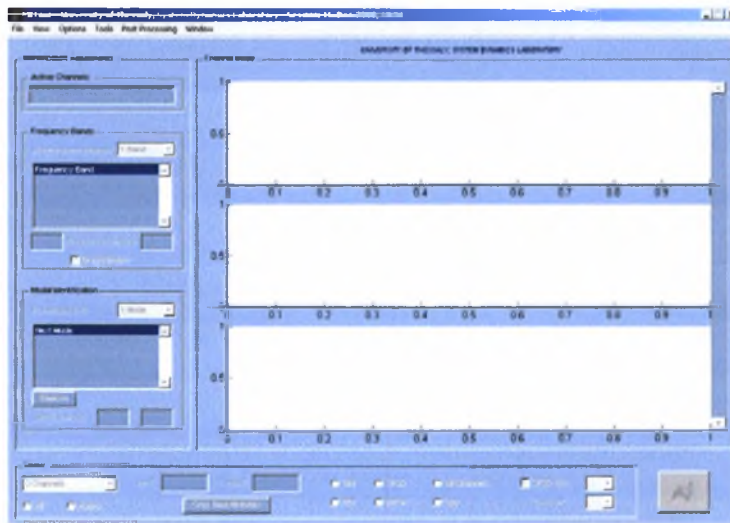
The two structures (G9-Polymylos and G2-Kavala) have been properly instrumented and the measured response data (time histories) along with data for a graphical display of the structure, containing information about the sensor locations, have been saved to compatible with the MITool software input files in the format described in previous subsection. The procedures that will be presented in the beginning concern the steps where the user imports (loads) in MITool software the measurement data and the graphical display data. In the next steps the measured signals (time histories) are converted in the frequency domain (Fourier transform, computation of the CPSD functions respectively). Next, the time or frequency bandwidth for the modal identification are defined as well as the number of modes that will be estimated applying the proper identification algorithm. Finally, the steps that concern the post processing and the illustration and exporting of the modal identification results with the MITool software will be presented.

6.3.1 Modal identification application on G9 bridge at Polymylos using ambient vibration measurements

Step 1: Launch MITool Software

1. MITool folder with its subfolders must be added to Matlab path.
2. Launch the MITool software by typing MITool in Matlab Command Window

Software response



Step 2: Multi Output Only Identification – Input File components

1. In the **File Menu** select **Preferences** (Ctrl-P).
2. In the Preferences dialog box select **Multi Output Only** (default) that defines that the modal identification procedure that will be evaluated concern multi output only measurements of ambient vibrations
3. All the other edit boxes concern the name of the arrays that are included in the input file that will be loaded and have been presented in details in subsection.

Software response

1. Preferences selection

2. Multi Output Only selection

3. Names of the arrays included in the input file

MITool - University of Thessaly, System Dynamics Laboratory

File View Options Tools Post Processing Window

- Load Experimental Data & Structure... Ctrl+O
- Load Experimental Data...
- Load Structure...
- Load Session... Ctrl+L
- Save Structure...
- Save Session... Ctrl+S
- Save Session As...
- Save Identification Data...
- Import
- Export
- Preferences... Ctrl+P
- Close Ctrl+W

Channel Mode

1
0.5
0
1

Preferences

Type of Identification:

- Single Input-Multi Output In: force
- Multi Input-Multi Output Out: acceleration
- Multi Output Only Number of Data Sets: N/A

Data Interface Variable Names:

Measured Response: accel

Measured Excitation: ft

Time Discretation: dt

Geometry Variable Names:

Use Consol Geometry

Consol FEM: fem

Nodes: FNode

Elements: FEel

Other Variable Names:

Sensors: sensors

Channel Labels: channeltext

Number of Dimensions: ndim

OK Cancel Apply

Step 3: Load Input file

1. From the **File Menu** select **Load Experimental Data & Structure** (Ctrl-O).
2. In the dialog box that popup select **Multi Output Only** radiobutton (already selected) and then **OK**.
3. In the dialog box *Load Experimental Data Set 1* select the input **.mat** file with the measured response data and the structural geometry and sensor data. For this example the file **G9_longitudinal_torsional_channels_0-30min.mat** is loaded. This file contains 30 minutes acceleration timehistory (200Hz sampling rate) measured by 6 sensors on the G9 Polymylos bridge.

Software response

1. Select Load Experimental Data & Structure

2. Select Multi Output Only

3. Input .mat file selection

MITool - University of Thessaly, System Dynamics Lab
File View Options Tools Post Processing Window
Load Experimental Data & Structure... Ctrl+O
Load Experimental Data...
Load Structure...
Load Session... Ctrl+L
Save Structure...
Save Session... Ctrl+S
Save Session As...
Save Identification Data...
Import
Export
Preferences... Ctrl+P
Close Ctrl+W

Channel Mod
1
0.5
0
1

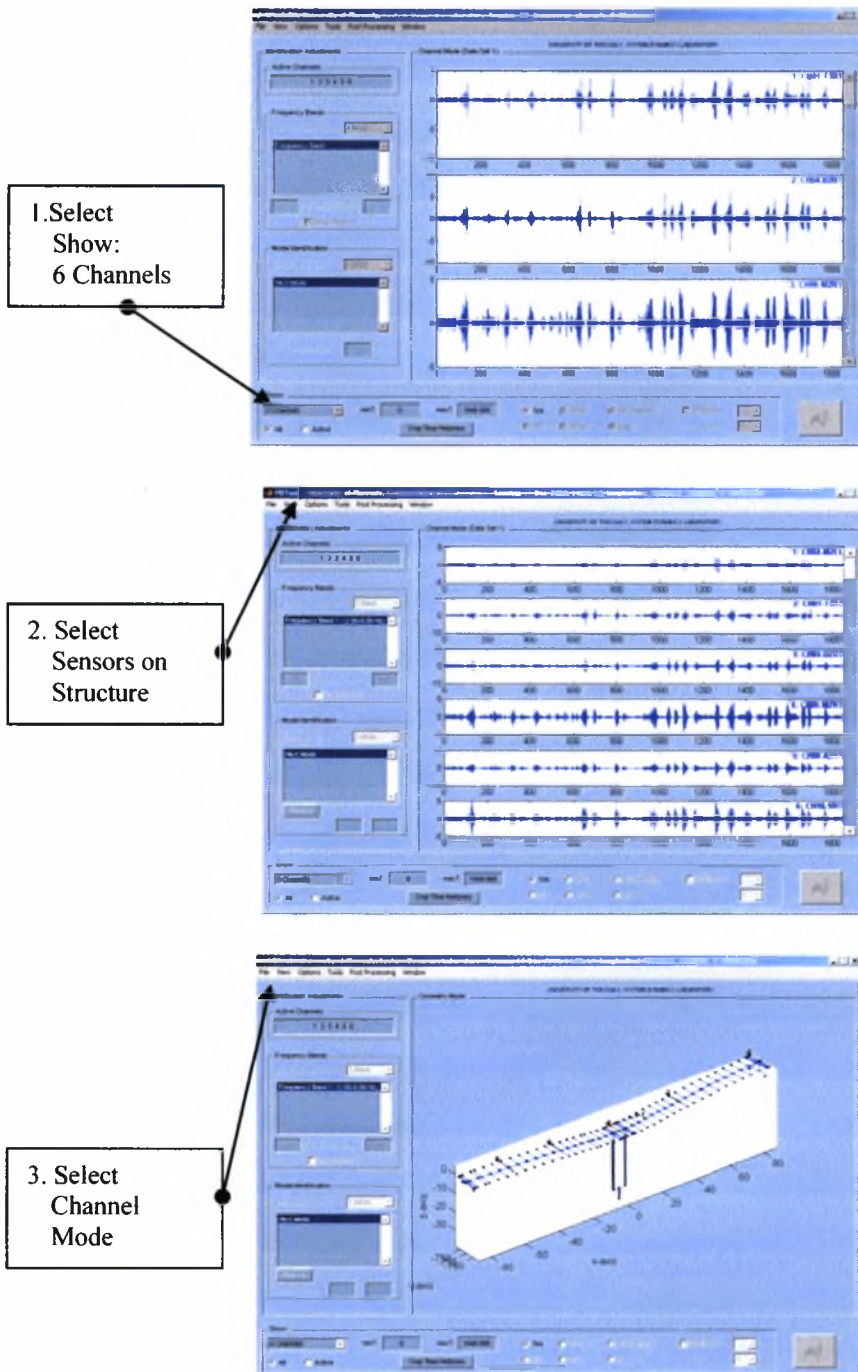
Experimental Modal Analysis
Select type of EMA:
 Single-Input Multi-Output
 Multi-Input Multi-Output (Earthquake)
 Multi-Output Only (Ambient) Advanced Options
OK Cancel Apply

Load Experimental Data Set 1
Look in: G9
0-30sec_8transverse_channels
0-30sec_10bending_channels
all_channels_0-30min
G2_20sensors_EQevent_21_2_07
G9_longitudinal_torsional_channels_0-30min
longitudinal_channels_0-30min
matlab
torsional_channels_0-30min
vertical_channels_0-30min
Type: MATLAB MAT-file
Date Modified: 08/08/2005 11:18
Size: 11.2 MB
File name: G9_longitudinal_torsional_channels_0-30min
Files of type: MAT-files (*.mat)
Open
Cancel

Step 4: Graphical display of measured signals and sensor network

1. In MITool software main window select *Show: 6 Channels*
2. For illustrating the structure geometry and the sensor network select from the **View menu** the **Sensors on Structure** option.
3. For illustrating the measured signals again from the **View menu** select **Channel Mode**.

Software response

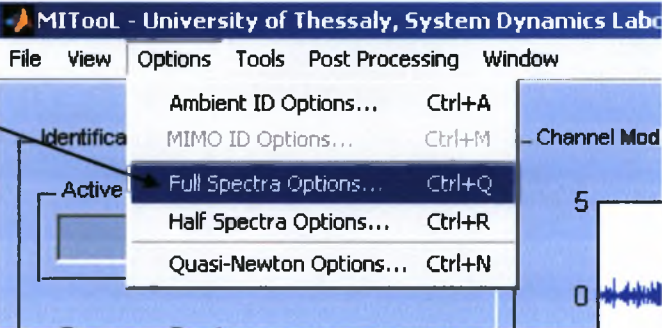


Step 5: Computation of CPSD functions

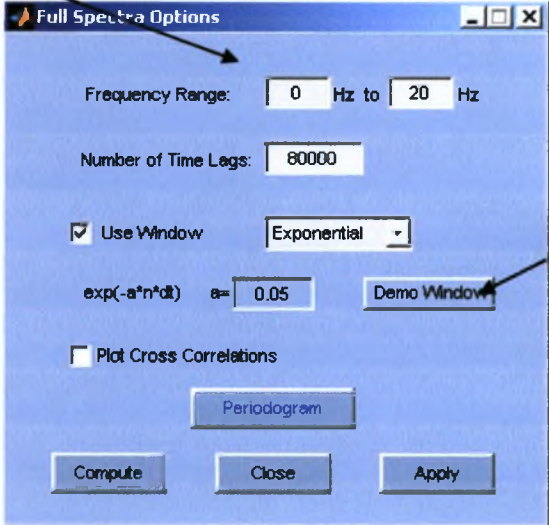
1. From the **Options Menu** select **Full Spectra Options** (Ctrl-Q).
2. In the **Full Spectra Options** dialog box enter the proper values for the parameters of the algorithm that computes the CPSD functions as they have been described in subsection 6.2.2.8.
3. The **Compute** starts the evaluation of the algorithm for the computation of the CPSD functions.
4. When the algorithm has finished the CPSD function are plotted on the main window. With the component *Log* in the *Show* panel the CPSD function are plotted in logarithmic scale.
5. From the **View menu** and the selection **All Channel Mode** or with the component *All Channels* in the *Show* panel all CPSD functions are plotted in the same axes.

Software response

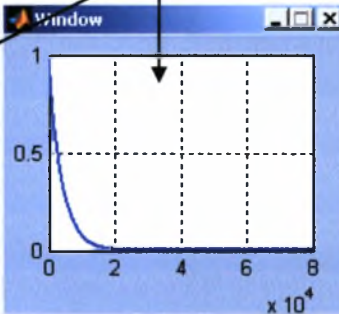
1. Select Options menu: Full Spectra Options

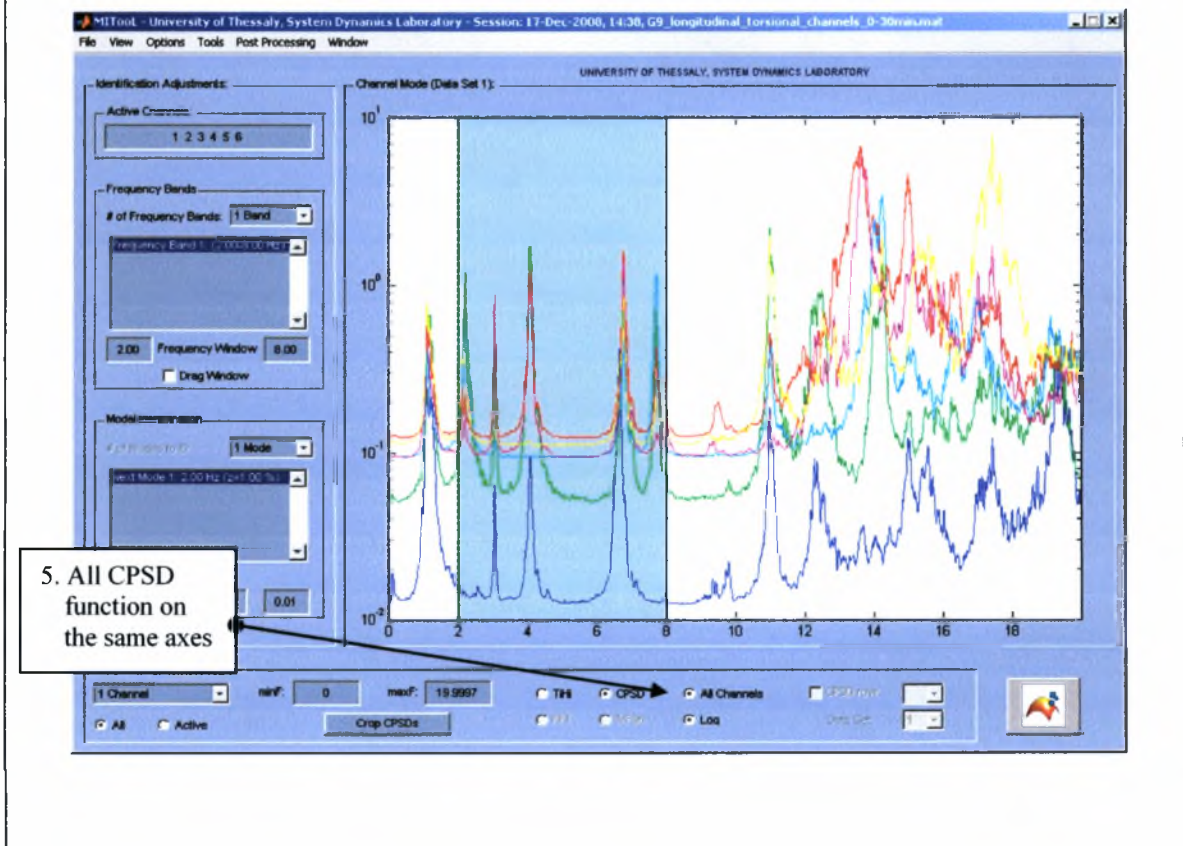
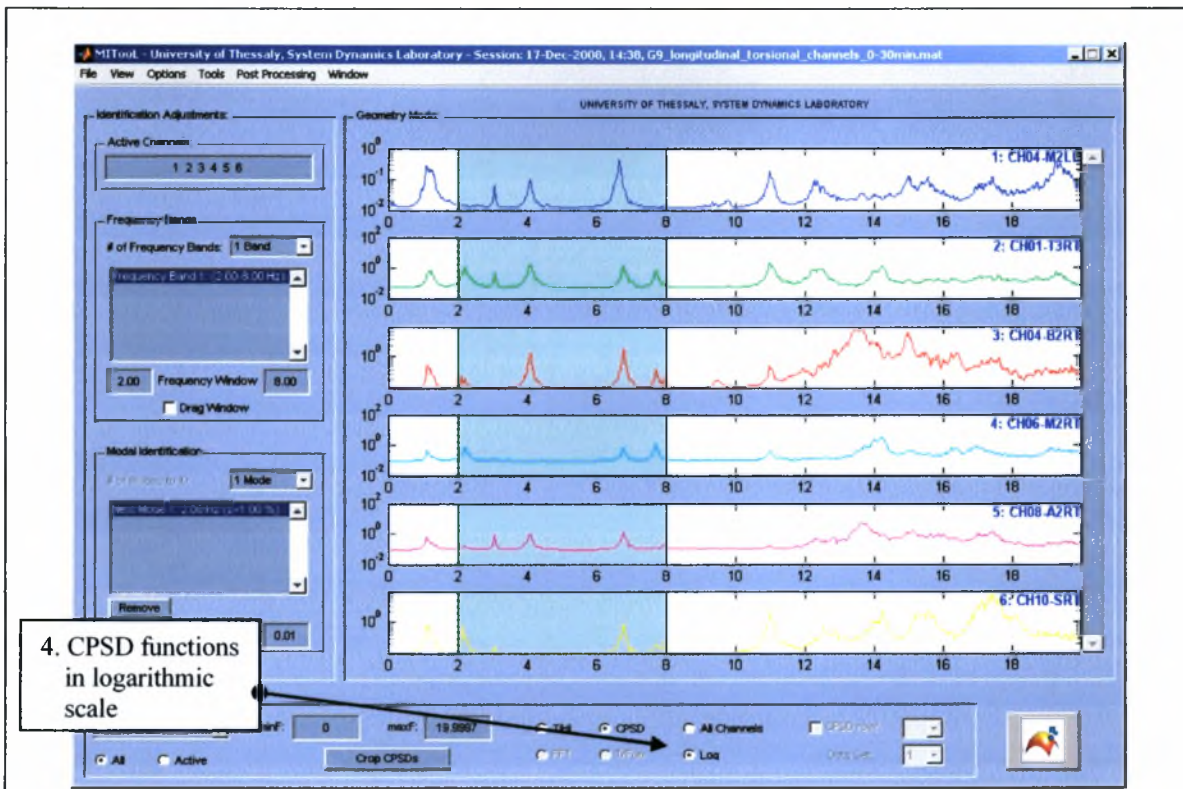


2. Full Spectra Options dialog box configurations



3. Graphical display of the exponential window that will be applied

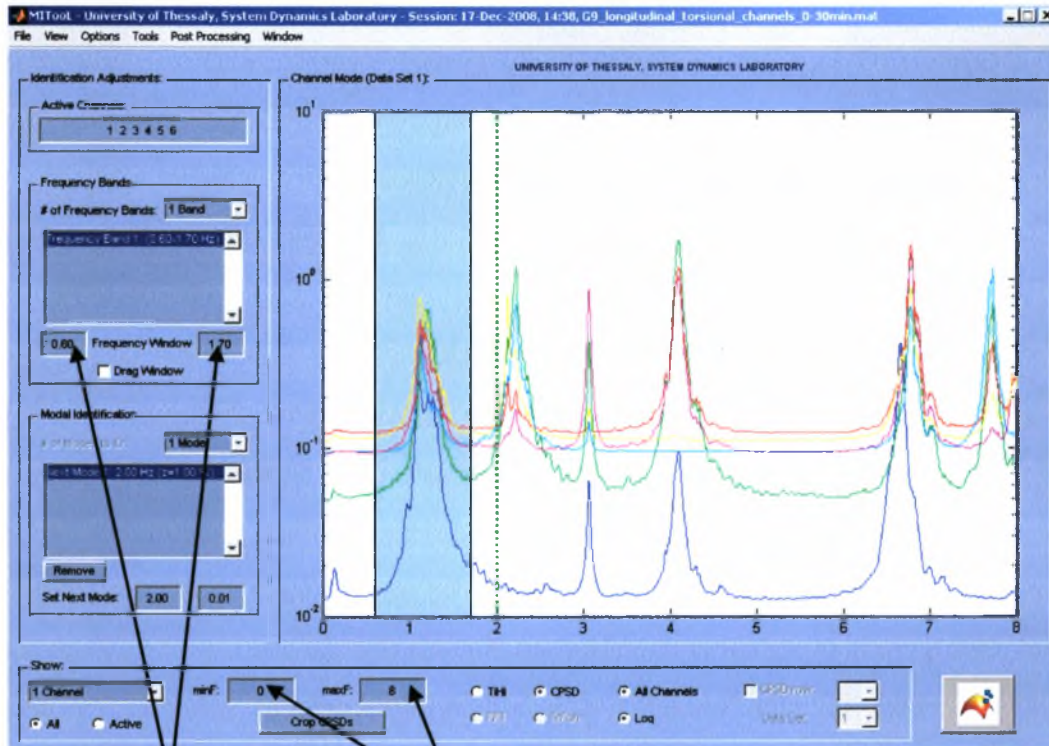




Step 6: Identification Frequency band

1. In *Show* panel in MITool main window define 0 to 8 Hz to be the frequency axes bandwidth by entering in the edit fields *minF: 0* and *maxF: 8*
2. The frequency band in which the modal identification procedure will be evaluated is defined in the *Frequency Window* edit fields enter 0.6 and 1.7 Hz
3. This procedure can be done also on the window of the MITool software by enabling the *Drag Window* button and dragging the displayed frequency band limits using the mouse cursor.

Software response



2. Identification frequency band
Frequency Window :
0.6 έως 1.7 Hz

1. The frequency axes bandwidth
minF: 0 maxF: 8

Step 7: Define Modal Identification algorithm

1. From the **Options Menu** select **Ambient ID Options** (Ctrl-A).
2. In the *Identification Options* dialog box select the configurations of the modal identification options as they were described in subsection 6.2.2.6.

Software response

The image shows two screenshots from the MITool software. The top screenshot shows the 'Options' menu with 'Ambient ID Options...' selected. A callout box points to this menu item with the text '1. Select Options menu: Identification Options'. The bottom screenshot shows the 'Identification Options (Amient Excitation)' dialog box. A callout box points to the dialog with the text '2. Modal identification algorithm configuration'. The dialog is divided into three steps:

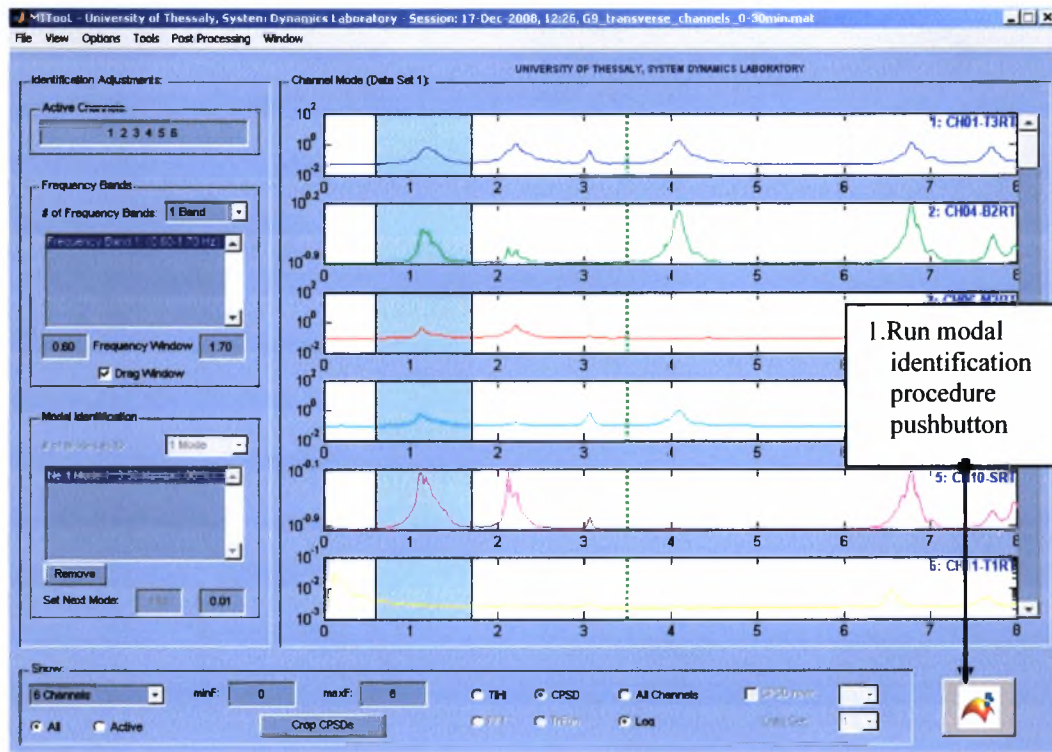
- Step 1. (Identify mode frequencies and damping using stabilization plots)**
 - Run Step 1.
 - Maximum Polynomial Order: 60
 - Frequency Tolerance: 0.005
 - Damping Tolerance: 0.05
 - Use damping ratios in stabilization.
- Step 2. (Compute modeshapes and participation factors given step 1)**
 - Formulate modeshapes by SVD
 - Damping Selection: Non Classicy
 - Modeshape Computation: Analytical
- Step 3. (Non-Linear Optimization with i.e. from steps 1 and 2)**
 - Run Step 3.
 - Initial Estimations: Step 1
 - Optimize for:
 - Mode frequencies
 - Damping ratios
 - Phase (Classicy damped case only)
 - quasi-Newton Parameters

Buttons at the bottom: OK, Cancel, Apply, Run.

Step 8: Modal identification procedure evaluation

1. Modal identification procedure starts with the *Run Modal Identification* pushbutton.
2. During the modal identification procedure evaluation the progress is displayed in Matlab Command Window.

Software response



The screenshot shows the Matlab Command Window displaying the progress of the modal identification procedure. The window shows a table with the following columns: Iteration, Func-count, F(x), Step-size, and Gradient-norm. The table shows the iterative process of the algorithm, with values for each parameter over 38 iterations.

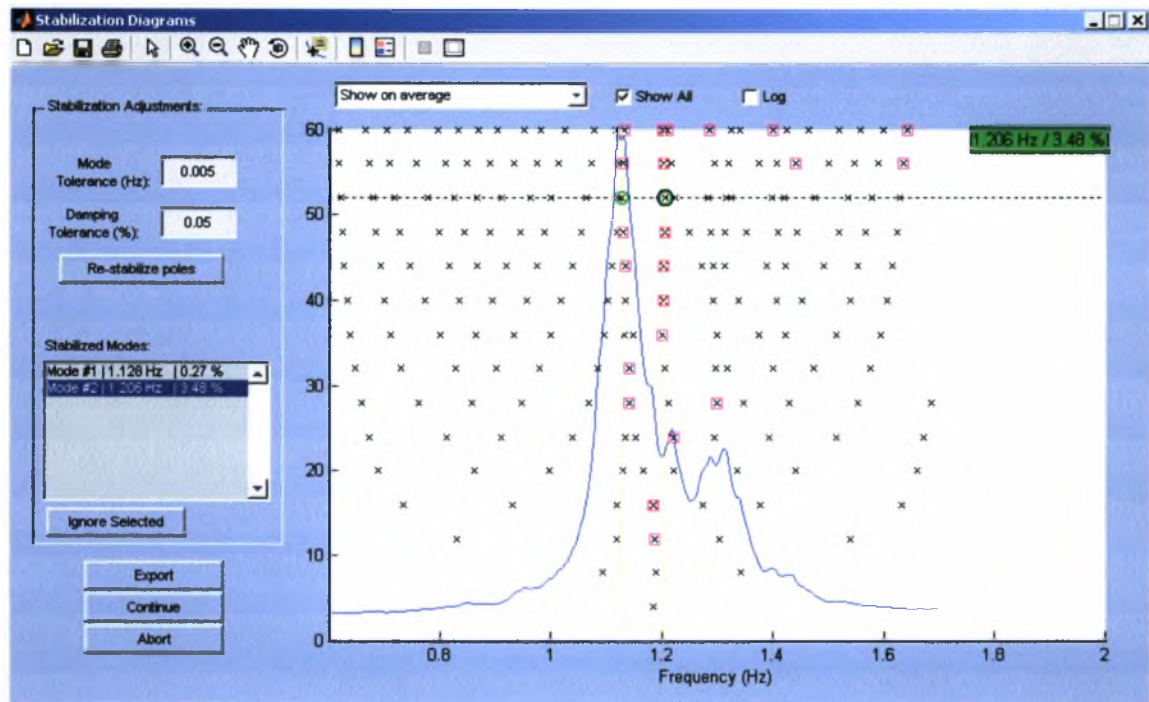
Iteration	Func-count	F(x)	Step-size	Gradient-norm
0	145	1375.56		10.2
1	280	246.035	0.0188192	10.1
2	435	35.1808	1	3.04
3	580	2.33142	1	3.22
4	725	1.02677	1	2.82
5	1015	0.78044	0.155826	1.93
6	1140	0.66652	1	1.65
7	1450	0.63324	0.29046	0.481
8	1585	0.59755	1	0.491
9	1885	0.561876	0.416606	2.1
10	2175	0.440208	0.5	1.04
11	2465	0.44661	0.62637	2.16
12	2760	0.42627	0.79	1.82
13	3190	0.404679	0.1	0.507
14	3480	0.388423	0.1	1.44
15	3935	0.270002	0.05	5.3
16	4350	0.374214	0.01	4.03
17	4920	0.354924	0.271	1.19
18	5385	0.352447	0.08	0.44
19	5945	0.345777	0.039	2.98
20	6380	0.342739	0.05	19.4
21	4470	0.34144	0.1	13.1
22	4940	0.320071	0.280019	2.87
23	7105	0.316858	1	1.08
24	7250	0.316888	1	1.1
25	7540	0.315272	0.392560	0.376
26	7810	0.314932	0.55132	0.451
27	7975	0.314622	1	0.303
28	8120	0.314373	1	0.345
29	8145	0.313897	1	0.376
30	8410	0.313247	1	0.383
31	8655	0.312493	1	0.389
32	8700	0.3128	1	0.0474
33	8845	0.312745	1	0.308
34	8990	0.312725	1	0.147
35	9135	0.312709	1	0.0465
36	9480	0.312702	1	0.0389
37	9425	0.312498	1	0.032
38	9570	0.312488	1	0.0313

2. Progress of the modal identification procedure in Matlab Command window

Step 9: Stabilization diagram

1. In the stabilization diagram that is evaluated during the modal identification procedure the physical poles should be selected avoiding to select the mathematical poles.
2. To continue the modal identification procedures using the selected poles press the *Continue* button.

Software response



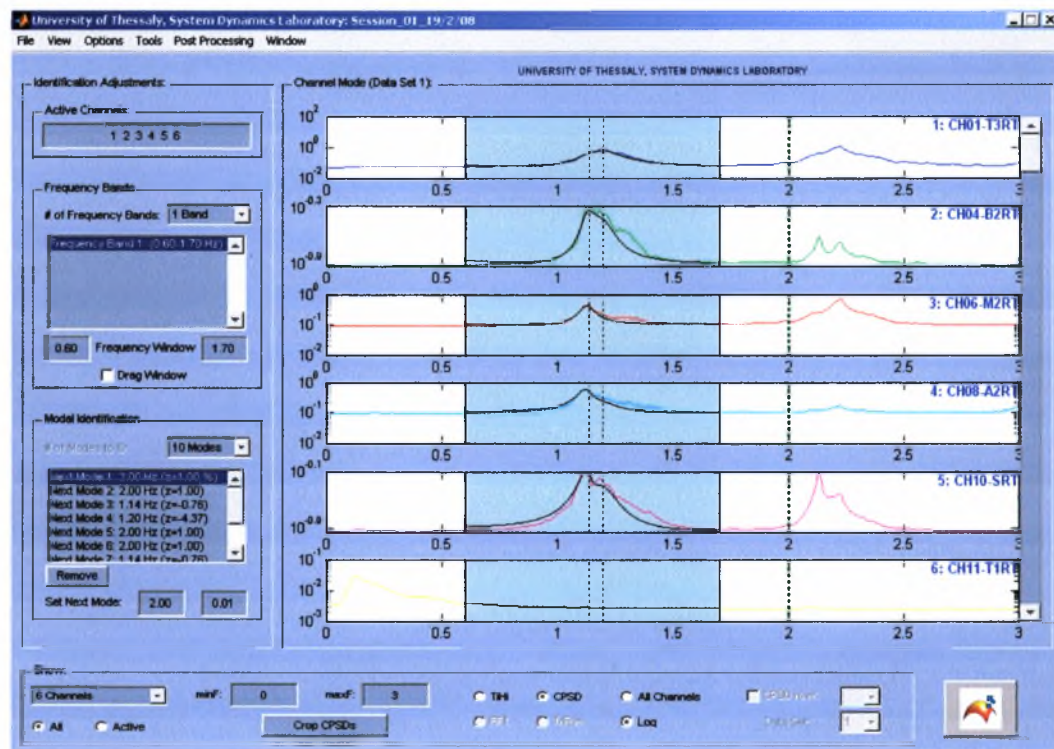
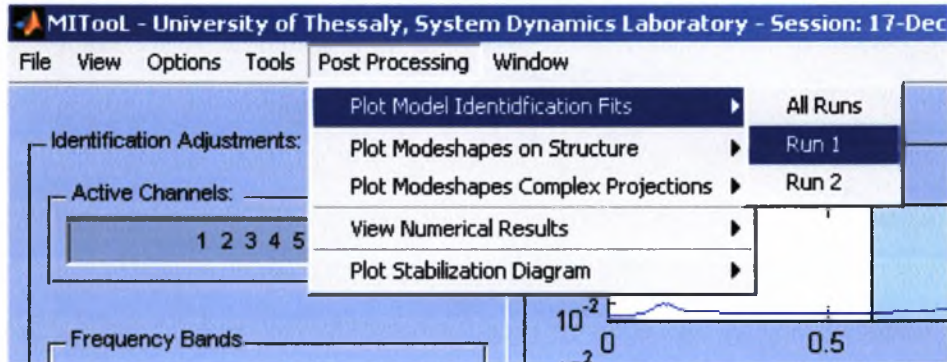
Remarks:

1. All poles are represented with an \times .
2. Represented with \square are the poles that are "stable" with respect to the modal frequency
3. Represented with \circ are the poles that are "stable" with respect to the modal damping ratio
4. The poles selection is user defined using the mouse cursor.

Βήμα 10° Post processing modal identification results

1. From the **Post Processing** menu select **Plot Model Identification Fits** to plot the response (CPSD function) predicted by the identified modal model.

Software response

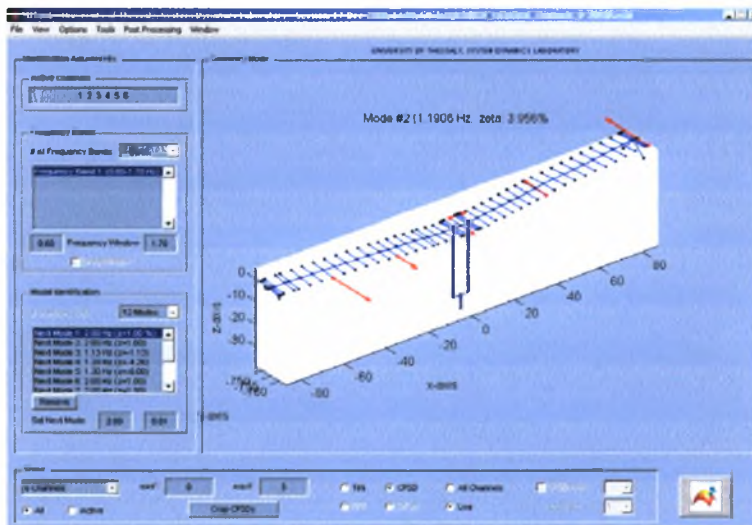
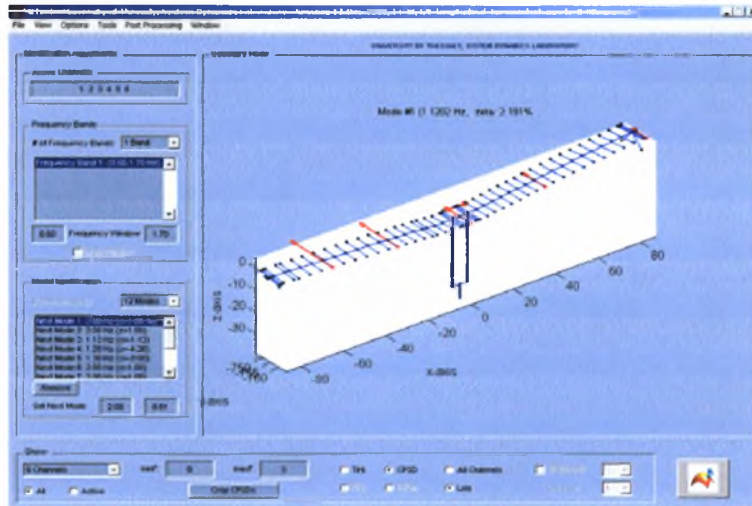
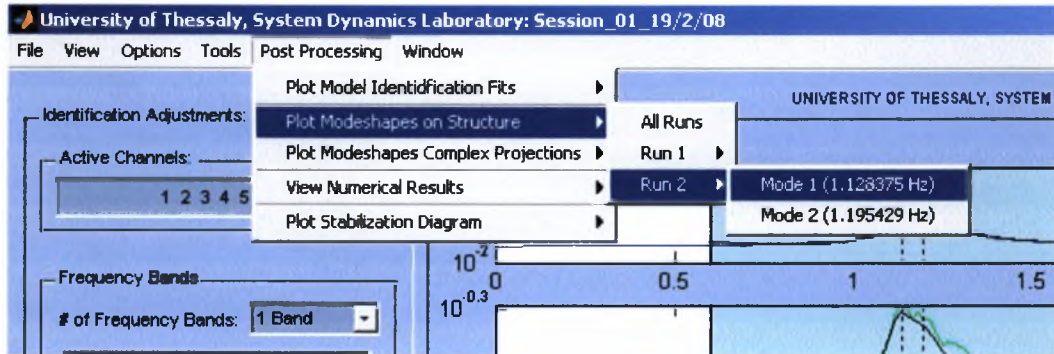


The black line represents the response (CPSD function) predicted by the identified modal model.

Step 10: Post processing modal identification results

2. To display the identified modeshape components on the structure select from the **Post Processing** menu the **Plot Modeshape on Structure** selection.

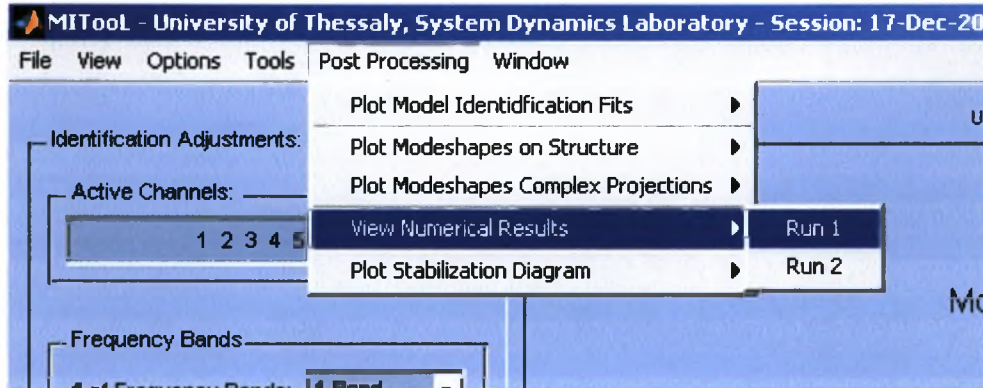
Software response



Step 10: Post processing modal identification results

3. To create and view an output file containing all the modal identification results from the **Post Processing** menu select **View Numerical Results**.

Software response



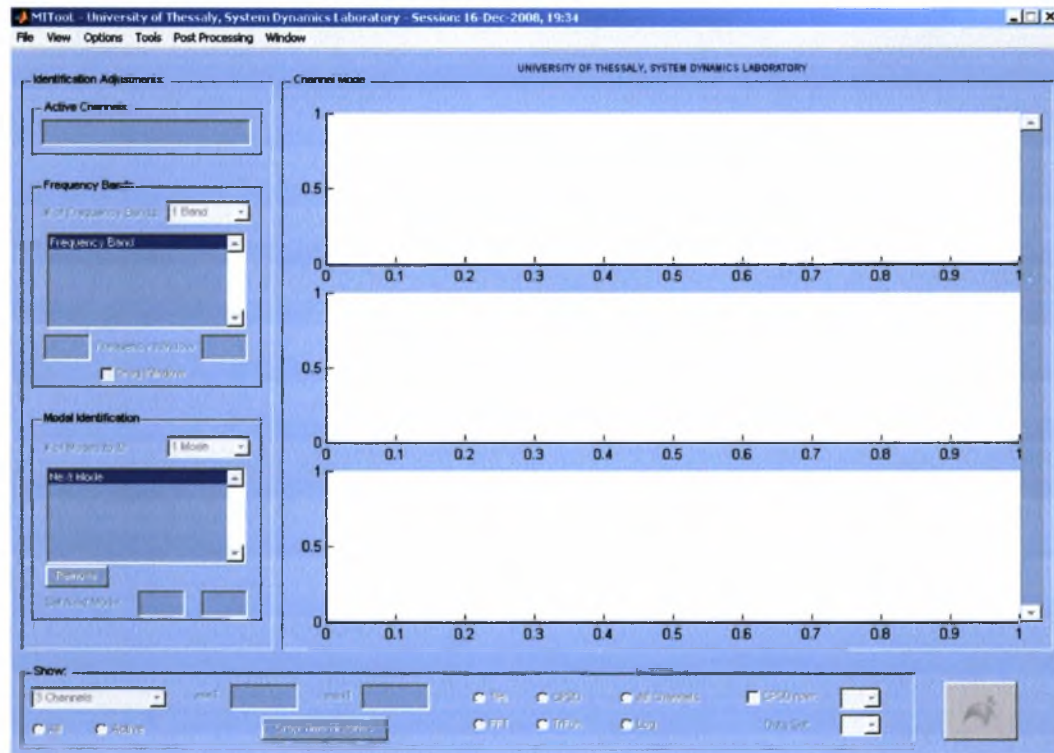
```
Editor - D:\entotsio\Modal Identification\outputfile1.txt
File Edit Text Cell Tools Debug Desktop Window Help
-----
1  -----
2  MODAL IDENTIFICATION RESULTS
3  -----
4  ModalTool Session : 2
5  -----
6  Measure of fit      : 0.05874
7  -----
8  MODE : 1
9  -----
10 Mode Frequency     : 1.12834 Hz
11 Damping Ratio     : 0.02534
12 Modeshape         :
13                   : 0.46658
14                   : 0.64713
15                   : 0.71223
16                   : 0.92684
17                   : 1.00000
18                   : 0.00995
19
20 Participation Factors :
21                   : -0.04135
22                   : -0.16530
23
24 -----
25 MODE : 2
26 -----
27 Mode Frequency     : 1.19558 Hz
28 Damping Ratio     : 0.04811
29 Modeshape         :
30                   : 1.00000
31                   : 0.58088
32                   : -0.06197
33                   : -0.40790
34                   : -0.80756
35                   : -0.00689
36
-----
plain text file Ln 9 Col 12 OVR
```

6.3.2 Modal identification application on G2 bridge at Kavala using simulated earthquake induced vibration measurements

Step 1: Launch MITool Software

1. MITool folder with its subfolders must be added to Matlab path.
2. Launch the MITool software by typing MITool in Matlab Command Window

Software response



Step 2: MIMO Identification – Input File components

1. In the **File Menu** select **Preferences** (Ctrl-P).
2. In the *Preferences* dialog box select **Multi Input Multi Output** radiobutton that defines that the modal identification procedure that will be evaluated concerns multi-input multi-output measurements of earthquake induced vibrations
3. All the other edit boxes concern the name of the arrays that are included in the input file that will be loaded and have been presented in details in subsection.

Software response

MITool - University of Thessaly, System Dynamics Labora

File View Options Tools Post Processing Window

Load Experimental Data & Structure... Ctrl+O
Load Experimental Data...
Load Structure...
Load Session... Ctrl+L
Save Structure...
Save Session... Ctrl+S
Save Session As...
Save Identification Data...
Import
Export
Preferences... Ctrl+P
Close Ctrl+W

Channel Mode
1
0.5
0
1

1. Preferences selection

2. Multi Input Multi Output radiobutton selection

3. Names of the arrays included in the input file

Preferences

Type of Identification:

Single-Input Multi-Output In: acceleration
 Multi-Input Multi-Output Out: acceleration
 Multi-Output Only Number of Data Sets: N/A

Data Interface Variable Names:

Measured Response: accel
Measured Excitation: Ft
Time Discretation: dt

Geometry Variable Names:

Use Consol Geometry
Consol FEM: fem
Nodes: FNode
Elements: FEel

Other Variable Names:

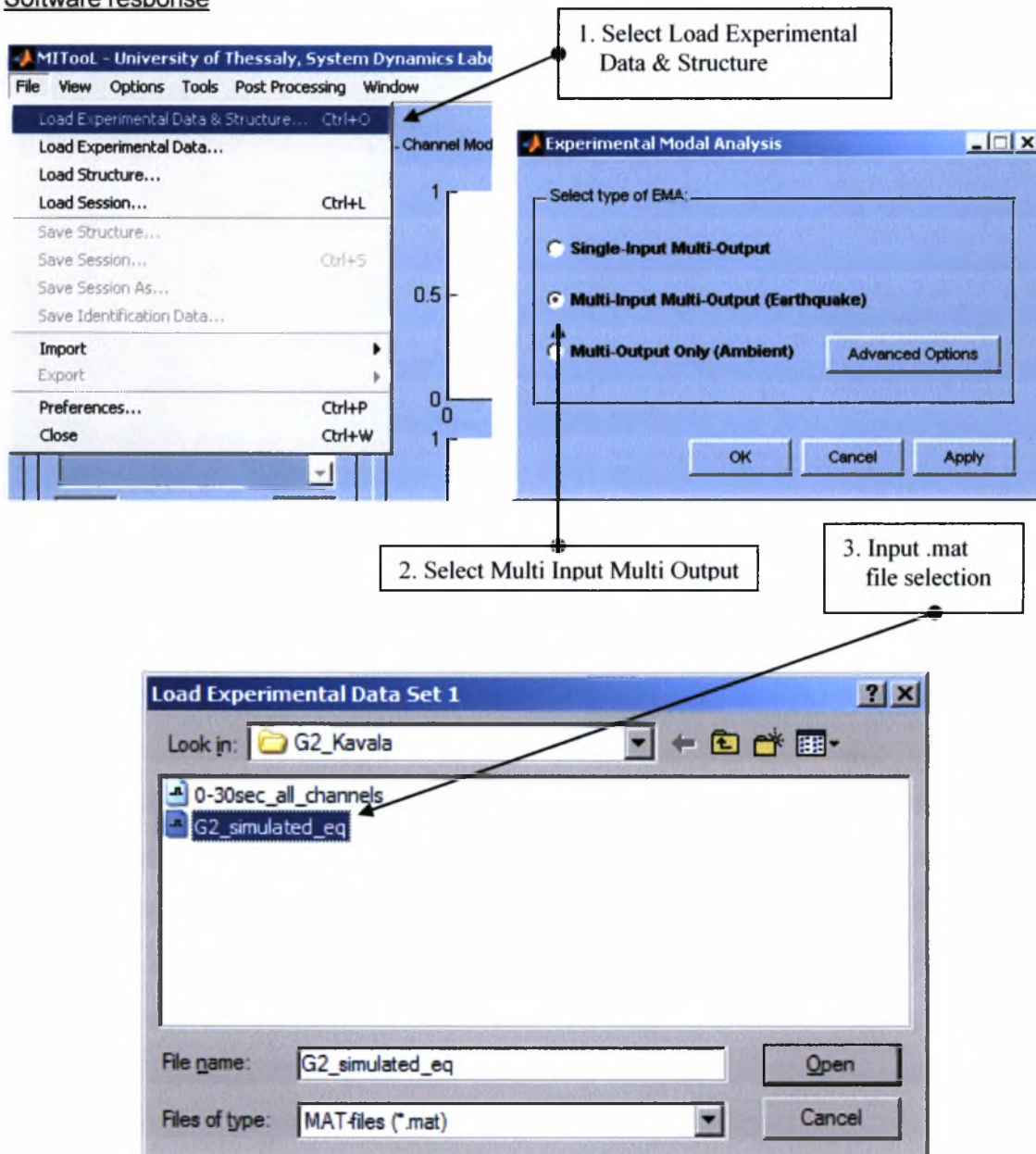
Sensors: sensors
Channel Labels: channeltext
Number of Dimensions: ndim

OK Cancel Apply

Step 3: Load Input file

1. From the **File Menu** select **Load Experimental Data & Structure** (Ctrl-O).
2. In the dialog box that popup select **Multi Input Multi Output** radiobutton (already selected) and then **OK**.
3. In the dialog box *Load Experimental Data Set 1* select the input **.mat** file with the measured response data and the structural geometry and sensor data. For this example the file **G2_simulated_eq.mat** is loaded. This file contains 46 seconds earthquake induced simulated acceleration time histories (200Hz sampling rate) by 6 sensors on the G2 Kavala bridge.

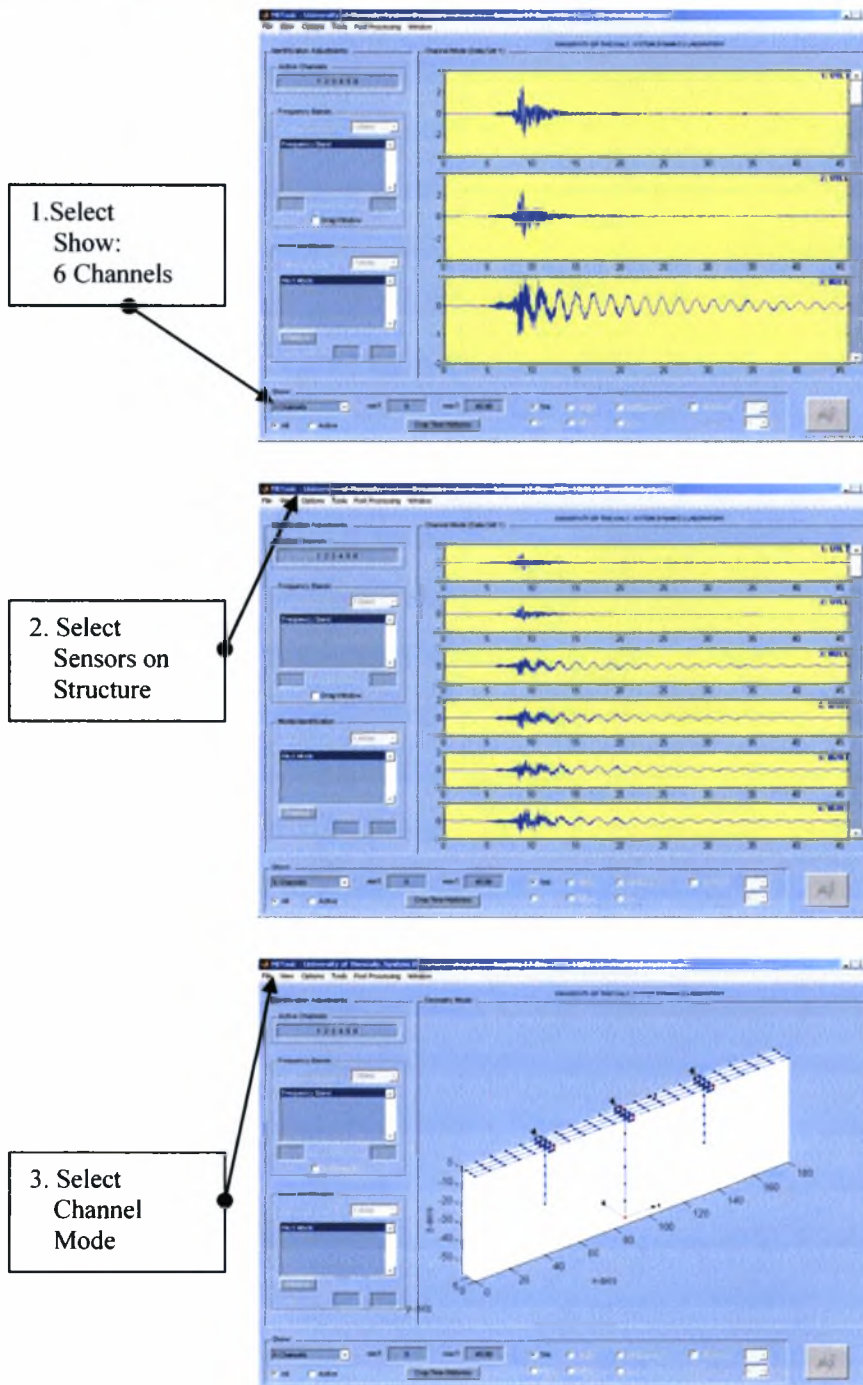
Software response



Step 4: Graphical display of measured signals and sensor network

1. In MITool software main window select *Show: 6 Channels*
2. For displaying the structure geometry and the sensor network select from the **View menu** the **Sensors on Structure** option.
3. For displaying the measured signals again from the **View menu** select **Channel Mode**.

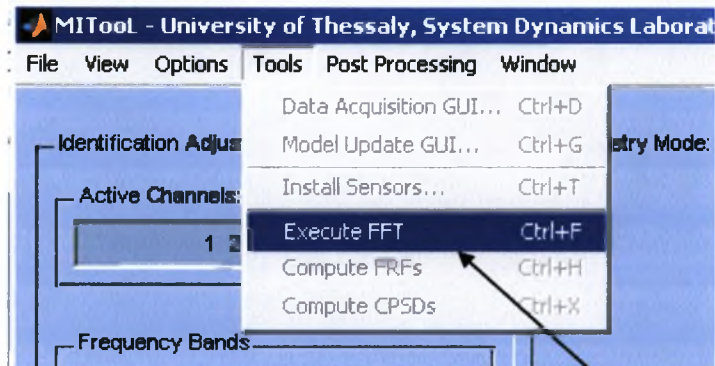
Software response



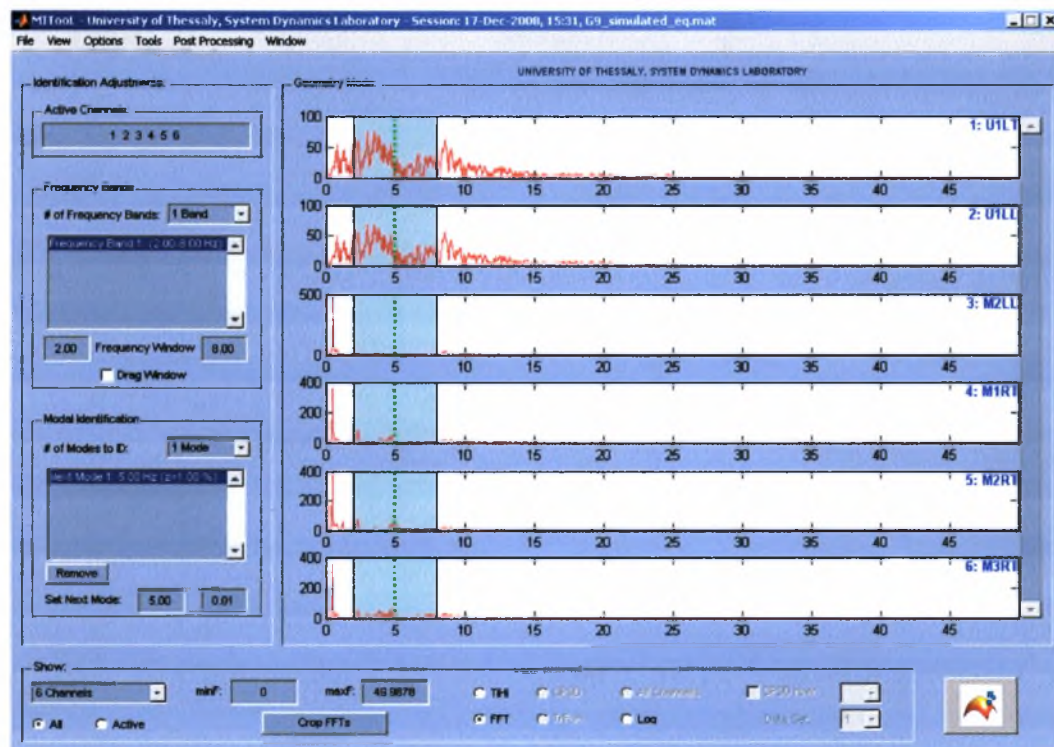
Step 5: Computing of Fourier Transform – Frequency domain

1. From the **Tools Menu** select **Execute FFT (Ctrl-F)**.
2. When the Fourier transform of the signal is completed the measured responses are plotted in the frequency domain. With the **Log** radiobutton from the **Show:** panel the response can be plotted in logarithmic scale.

Software response



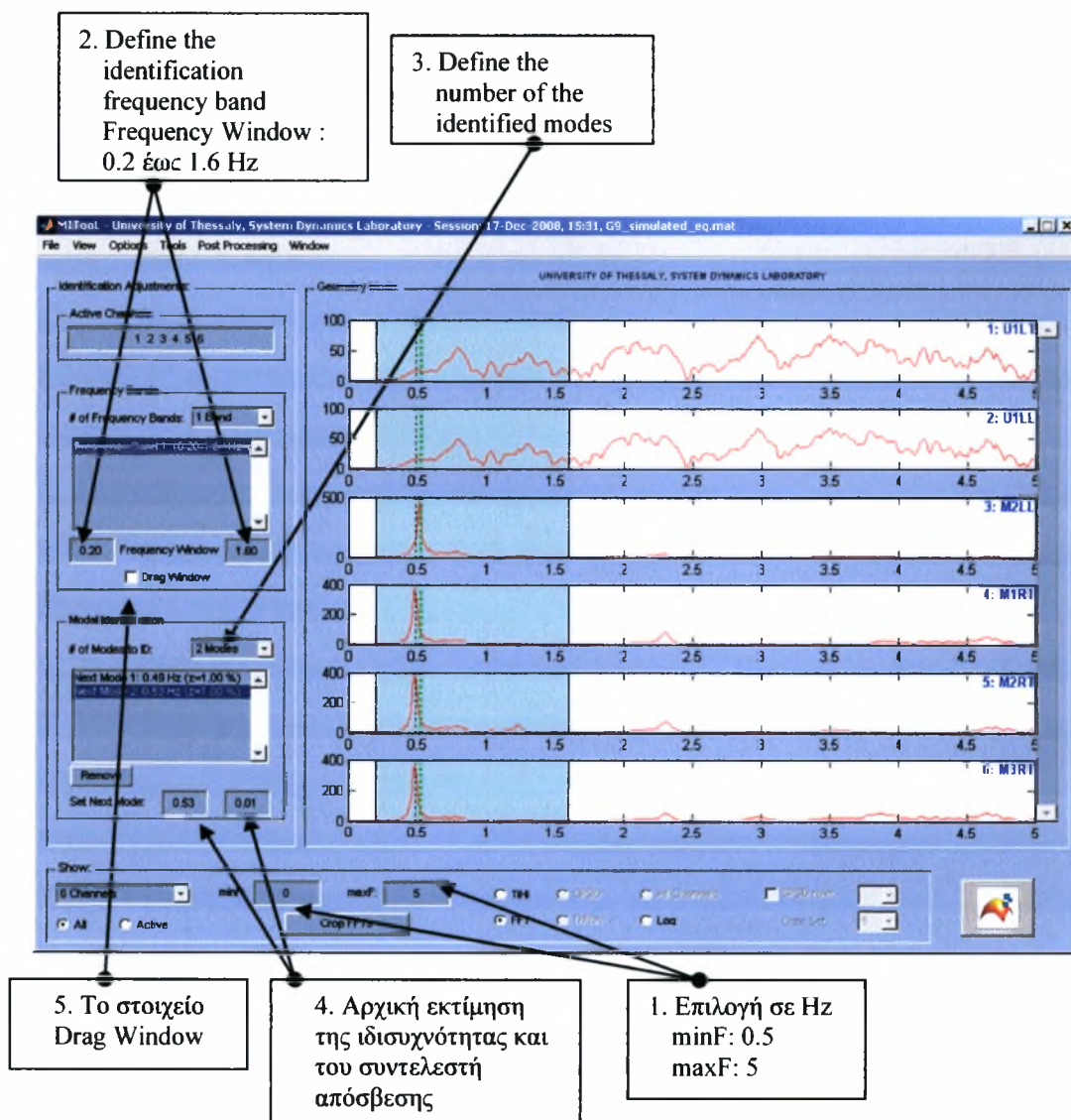
1. Evaluation of
Fourier Transform



Step 6: Initial estimate of the modal parameters

1. In *Show* panel in MITool main window define 0 to 5 Hz is the frequency axes bandwidth by entering in the edit fields *minF*: 0 and *maxF*: 5
2. The frequency band in which the modal identification procedure will be evaluated is defined in the *Frequency Window* edit fields enter 0.2 and 1.6 Hz
3. Select the number of modes to be identified to be 2 modes (# of Modes to ID: 2 Modes).
4. Insert for the two modes initial estimates for the mode frequencies to be 0.49 Hz for the first mode and 0.53 Hz for the second mode.
5. Operations 2, 3 and can be made interactively on the MITool software main window by selecting the *Drag Window* component.
6. Insert for the two modes initial estimates for the damping ratios to be 0.01 (1%) for both modes

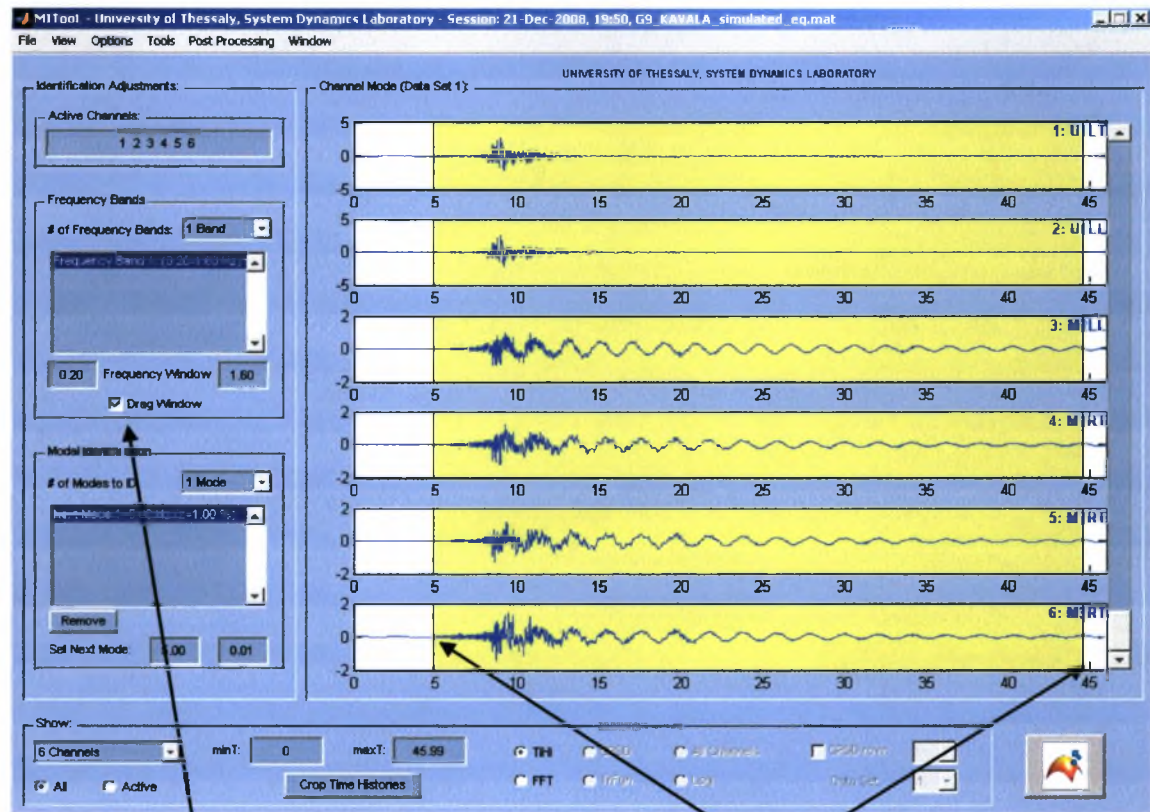
Software response



Step 7: Define the time window

1. In MITool main window select to show the time histories by selecting *TiHi* from the *Show* panel.
2. The time window in which the identification will be evaluated can be modified by enabling the *Drag Window* component and dragging the limits of the shaded time bandwidth using the cursor.

Software response



1. The Drag Window component

2. The time limits

Step 8: Define the MIMO identification parameters and methodology

1. From the **Options Menu** select **MIMO ID Options** (Ctrl-M).
2. In the MIMO Identification Options dialog box enter the sensors that measure the response (acceleration) at the base of the structure (*Excitation DOFs: 1 2*).
3. Select the methodology that works in the time domain from the *Analysis Domain* popup menu and to estimate the non-classically damped model from the *Type of Modal Model* popup menu.

Software response

The screenshot shows the 'MIMO Identification Options (Earthquake excitation)' dialog box. The 'Sensor Configuration' section has 'Excitation DOFs' set to '1 2', 'Response DOFs' to '3 4 5 6', and 'Active DOFs' to '3 4 5 6'. The 'Cases of Modal Models' section has 'Analysis Domain' set to 'Time' and 'Type of Modal Model' set to 'Nonclassically Damped'. The 'Model Groups for Modal Sweeping' section has 'Grouping scheme' set to 'All Modes', 'Maximum Number of Sweeps' set to '20', and 'Sweep Accuracy' set to '0.001'. The 'Advanced' button is highlighted. The 'Step 1' section has 'Run Step 1' checked, 'Maximum Polynomial Order' set to '40', 'Frequency Tolerance' set to '0.005', and 'Damping Tolerance' set to '0.05'. The 'Step 2' section has 'Formulate modeshapes by SVD' selected and 'Modeshape Computation' set to 'Analytical'. The 'Step 3' section has 'Run Step 3' unchecked and 'Field Estimators' set to 'Step 1'. The 'OK', 'Cancel', and 'Apply' buttons are at the bottom.

1. Select Identification Options from the Options menu:

2. Enter the base excitation sensors

3. Select the identification methodology

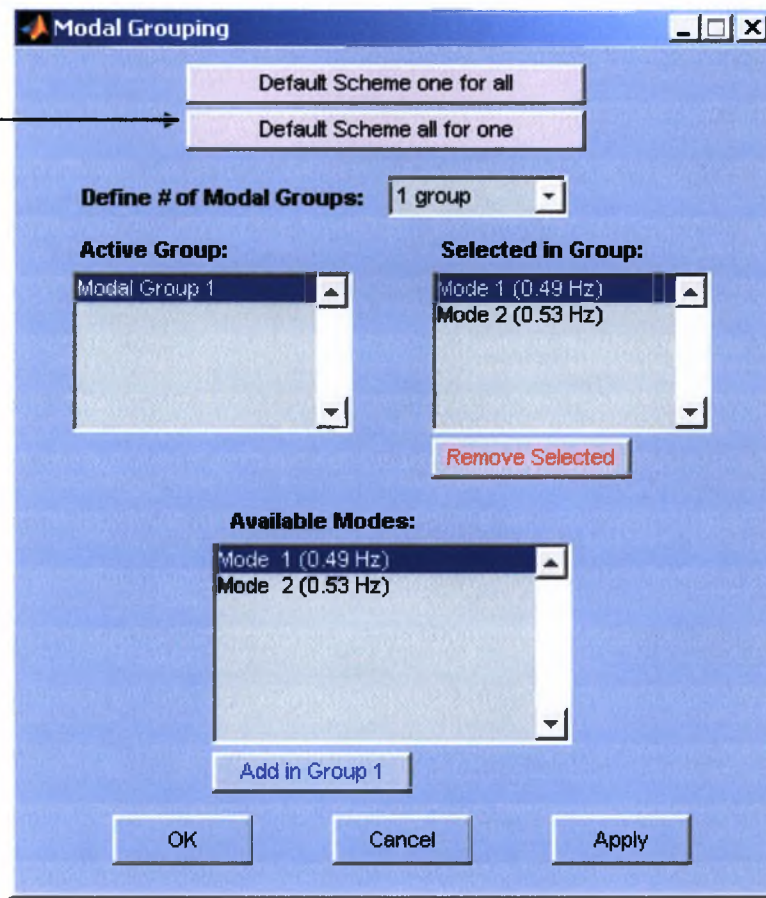
4. Advanced pushbutton that opens the Modal Grouping dialog box

Step 8: Define the MIMO identification parameters and methodology

1. From the *Modal Grouping* dialog box (*Advanced* pushbutton) select the default scheme for modal grouping (*Default Scheme all for one* pushbutton).

Software response

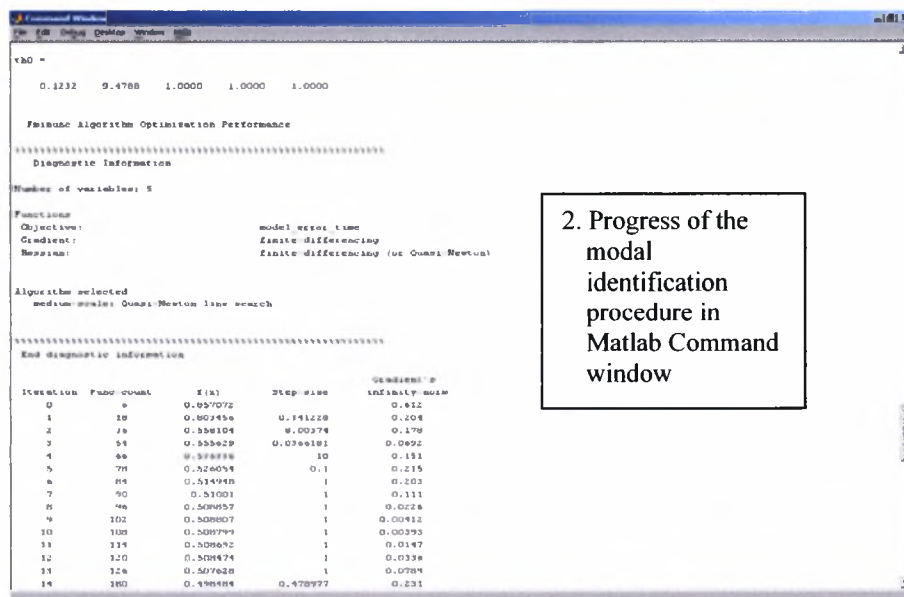
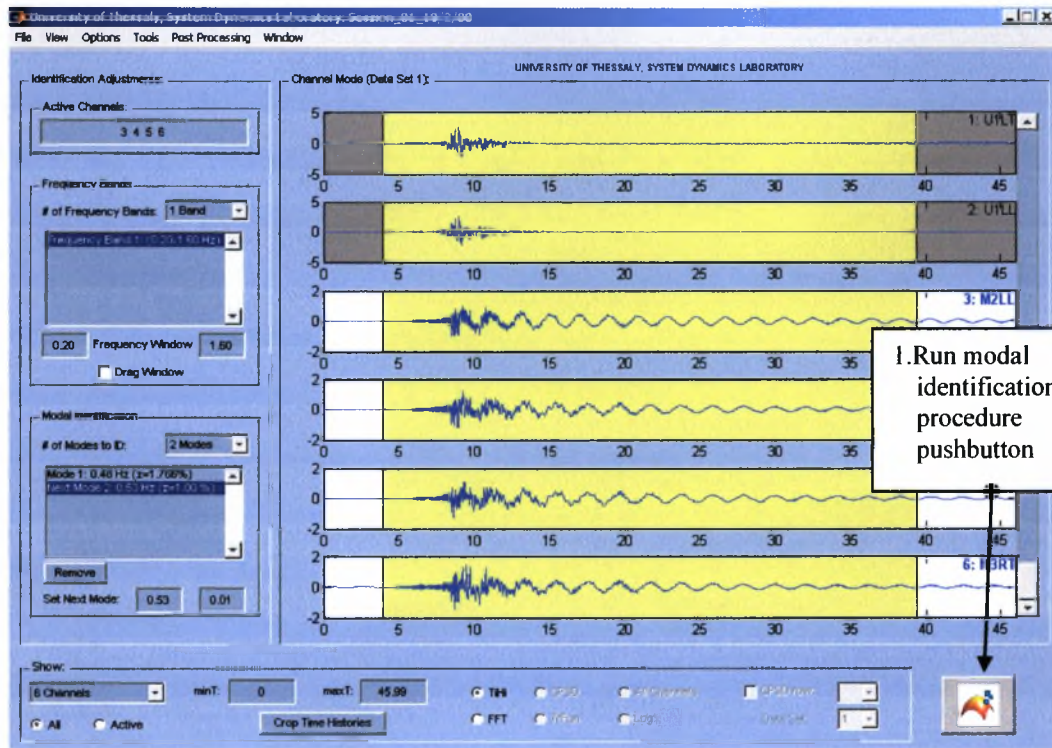
4. Select the default modal grouping all for one



Step 9: Modal identification procedure evaluation

1. Modal identification procedure starts with the *Run Modal Identification* pushbutton.
2. During the modal identification procedure evaluation the progress is displayed in Matlab Command Window.

Software response

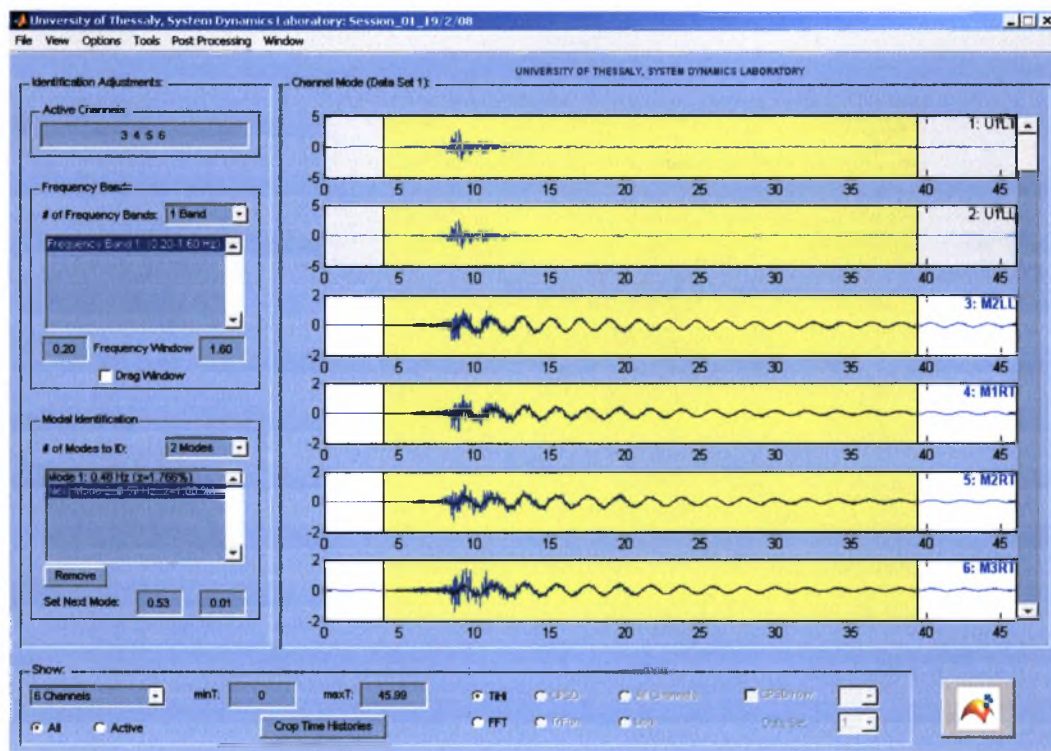
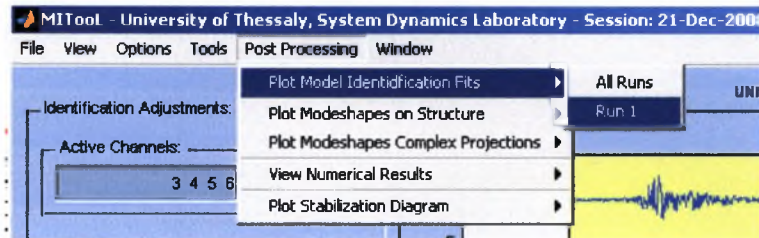


2. Progress of the modal identification procedure in Matlab Command window

Step 10: Post processing modal identification results

1. From the **Post Processing** menu select **Plot Model Identification Fits** to plot the response (time histories) predicted by the identified modal model.

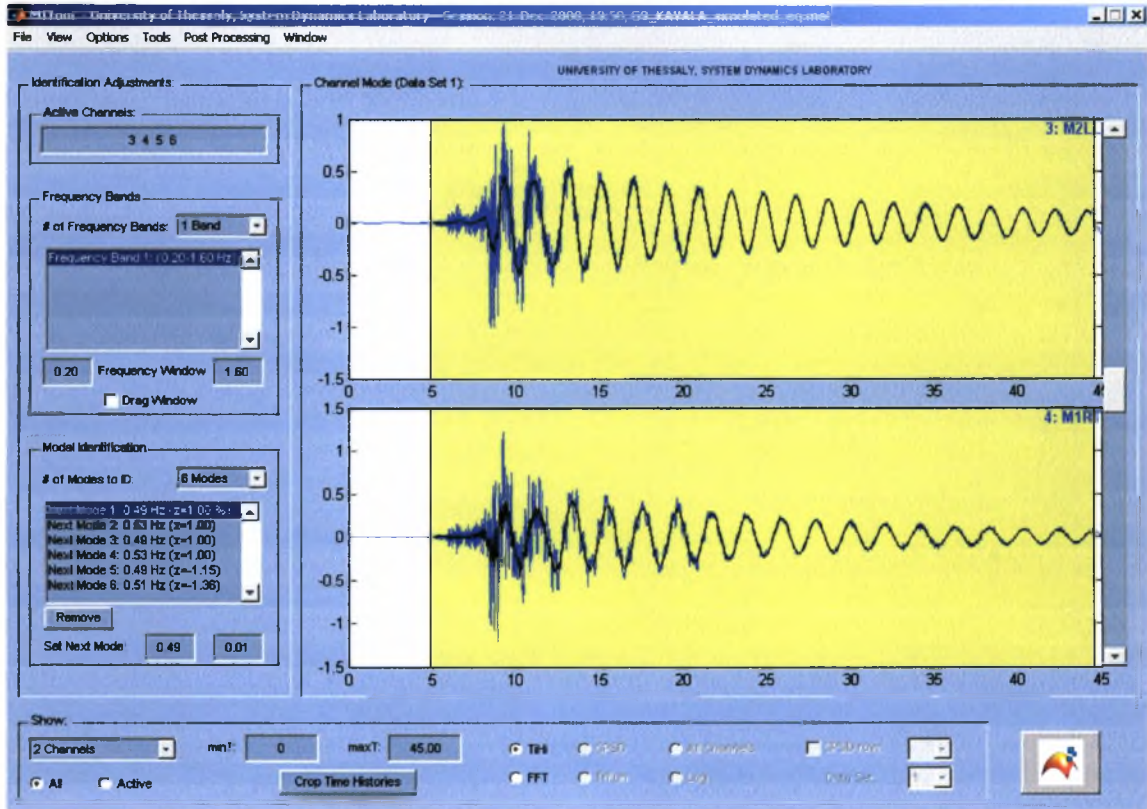
Software response



Step 10: Post processing modal identification results

- The number of signals displayed in the MITool main window is defined in the Show panel.

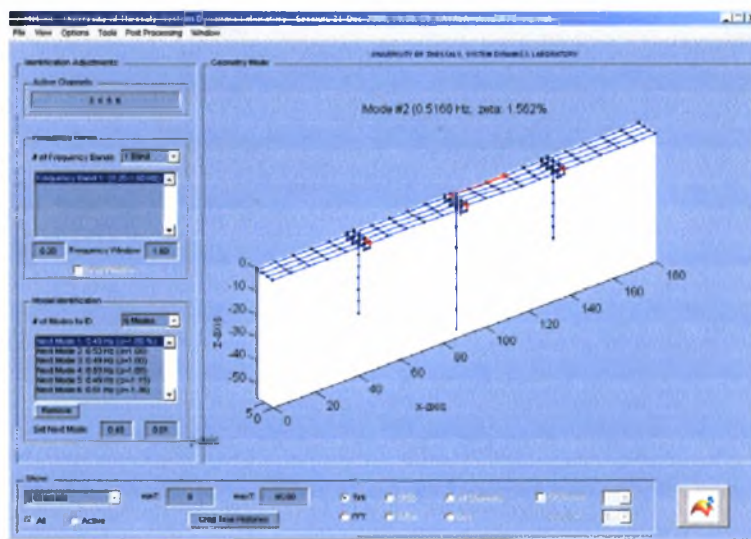
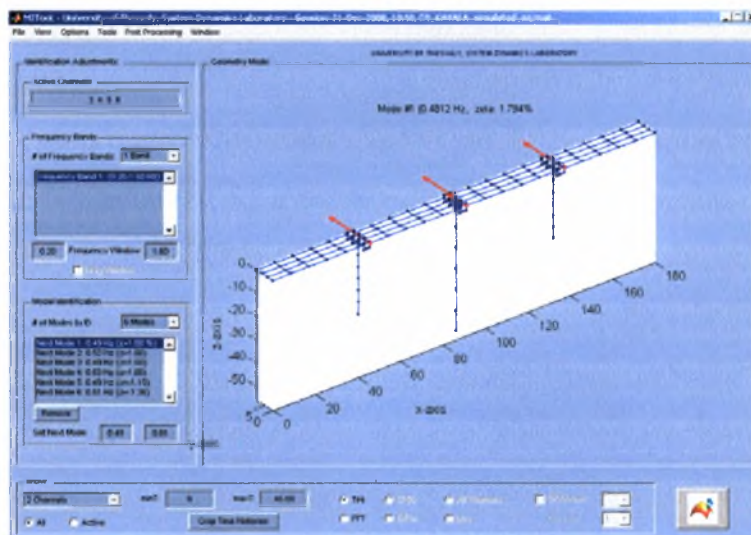
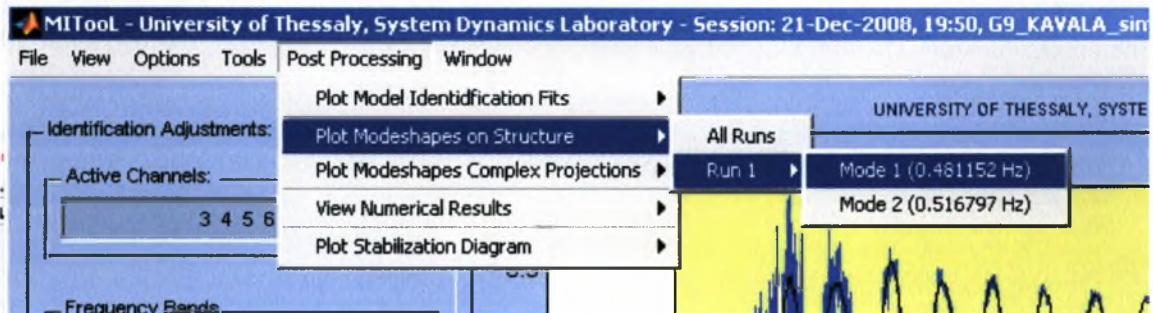
Software response



Step 10: Post processing modal identification results

4. To display the identified modeshape components on the structure select from the **Post Processing** menu the **Plot Modeshape on Structure** selection.

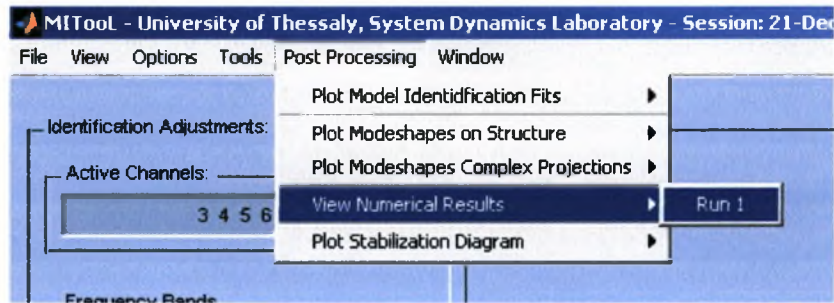
Software response



Step 10: Post processing modal identification results

5. To create and view an output file containing all the modal identification results from the **Post Processing** menu select **View Numerical Results**.

Software response



The screenshot shows a text editor window with the following content:

```
1
2 -----
3          MODAL IDENTIFICATION RESULTS
4 -----
5          ModelTool Session : 2
6 -----
7          MODE : 1
8 -----
9
10 Mode Frequency      : 0.48453 Hz
11 Damping Ratio       : 0.79529 %
12 Modeshape           :
13                     0.04250
14                     0.91849
15                     1.00000
16                     0.90361
17
18 Participation Factors :
19                     0.00011
20                     -0.06818
21
22 -----
23          MODE : 2
24 -----
25
26 Mode Frequency      : 0.51486 Hz
27 Damping Ratio       : 0.63811 %
28 Modeshape           :
29                     1.00000
30                     -0.07646
31                     -0.10092
32                     -0.10638
33
34 Participation Factors :
35                     0.00011
36                     -1.00000
37 -----
```

The text editor window has a menu bar (File, Edit, Text, Cell, Tools, Debug, Desktop, Window, Help) and a toolbar. The status bar at the bottom indicates "plain text file" and "Ln 28 Col 34".

Conclusions

In this thesis, the applicability of frequency and time domain identification methods in the field of modal analysis has been improved and generalized. The techniques developed in this thesis are applicable for an Experimental Modal Analysis (EMA), Operational Modal Analysis (OMA) and identification based on earthquake induced vibration measurements. The main objective of this work has been to determine the modal and other parameters of non-classically damped modal models used to describe the response of linear structures subjected to artificial, ambient and earthquake loads. The methodologies developed have been tested and implemented in a user friendly software.

Specifically, linear system theory is used to formulate the equations of motion that govern the response (displacement, velocity and acceleration) of structures. Modal analysis is used to describe the response at the measured (observable) degrees of freedom of the structure in terms of the eigenproperties (eigenvalues and eigenvectors) and the excitation. Several mathematical models are used to describe the vibrational behaviour of a structure with a limited number of parameters. These models are highly non-linear in their parameters and most identification algorithms do not directly identify the model parameters. Instead, the modal parameter estimation methods proposed identify scalar matrix fraction models, also known as common denominator models, left and right matrix fraction description models and state space models from the experimental measurements. The relation between these models and the modal parameters were discussed. Furthermore a distinction between continuous-time and discrete-time models was made.

The estimation of the power spectra between the outputs and the reference outputs is also discussed. The auto and cross power spectral density functions are the primary data for model parameter identification based on output-only (ambient) measurements. Basically, two classical approaches exist for the estimation of auto and cross power spectral density functions. The periodogram estimator operates directly on the spectra of different time blocks resulting from a division of the time sequences. The correlogram approach first estimates the correlation functions in the time-domain and next the power spectra are obtained by transferring the correlations to the frequency-domain. Finally, the estimation of the half (or positive) power spectra is also discussed.

The modal identification methodologies introduced are based on the minimization of an error function using a least squares minimization approach. The formulation was presented for the general case of non-classically damped modal model. It is shown how this model can be used to identify model parameters from both input-output measurement and from output-only measurements in absence of the input measurements.

For the cases of EMA and OMA the identification has been performed by analysis in the frequency domain. The optimal values of the modal parameters, such as modal frequencies, modal damping ratios, modeshapes and modal participation factors are obtained by the implementation of an output error methodology. In particular, estimates of the modal frequencies

and modal damping ratios are provided by solving a system of linear algebraic equations using the right-matrix fraction model or the common denominator model. Stabilization diagrams are used to distinguish between physical and mathematical modes. This method is an extension of the PolyMAX or polyreference least-squares complex frequency domain method, developed by Peeters et al. (2004), in order to treat non-classically damped modal models describing a system's response characteristics based on artificial or ambient vibration data. The estimates of the modeshapes and the participation factors are provided by solving a system of linear algebraic equations. Two different approaches have been developed for the computation of the modeshapes and participation factors. In the first approach the modal properties are derived directly by Singular Value Decomposition (SVD) of the resulting numerator matrix. In the second approach the advantage that the error function is quadratic with respect to the modeshapes is used, so the modeshapes are computed by taking stationary conditions in order to develop a linear system of equations from which the modeshapes are derived.

For earthquake induced vibrations, the identification has been performed by analysis in the time domain and in the frequency domain. The methods developed by McVerry (1980) in the frequency domain and Beck and Jennings (1980) in the time domain, have been extended in this work to treat non-classically damped modal models. Additionally, a time domain methodology for identifying the modal and other parameters of classically damped modal models has been also developed as a special case. The optimal values of the modal parameters, such as modal frequencies, modal damping ratios and modeshapes, were obtained by the implementation of an output error methodology. In time domain analysis, the optimal values were obtained by minimizing a measure of fit between the output measured acceleration time histories and the acceleration time histories predicted by a modal model. A modal sweep approach was proposed for which each mode was optimized separately while the contribution from the rest of the modes was held constant. In frequency domain analysis, the optimal values were obtained by minimizing a measure of fit between the theoretical Fourier transform of the model responses predicted by a modal model and the Fourier transform of the measured response accelerations.

A three step approach was proposed for solving the error optimization problem implemented by all modal identification methodologies. In the first step, the modal frequencies and modal damping ratios were efficiently estimated by solving a system of linear algebraic equations. Stabilization diagrams are used to distinguish between physical and mathematical modes. In the second step, the resulted values of modal frequencies and modal damping ratios from the first step were used for the time and the frequency domain methodologies, in order to efficiently compute the modeshape components and the modal participation factors by solving linear algebraic systems of equations. Finally, in the third step, the solution of a nonlinear optimization problem using as starting values for the modal properties the values that were obtained from the previous steps were shown to improve the modal estimates for the identification of closely spaced and overlapped modes. A novel aspect of this thesis is the use of the three step approach to identify the modes of a structure under earthquake induced vibrations.

The applicability and effectiveness the modal identification methodologies and software were demonstrated by applying them to a small scale laboratory structure using artificially (impulse hammer) excited vibration measurements and an under construction Egnatia Odos bridge at Metsovo (Greece) using ambient vibration measurements. For the case of the laboratory structure, several modes were identified and it was observed that an accurate fit resulted between the Frequency Response Functions predicted from the optimal modal model and the

Frequency Response Functions computed by the measured acceleration time histories. For the case of Metsovo bridge fifteen modes were effectively identified but not all the types of the modes were confidently identified due to the small number of sensors used. An accurate fit was observed from the convergence of the Cross Power Spectral Density functions predicted from the optimal modal model to the Cross Power Spectral Density functions estimated by the measured accelerations. It was also observed that the estimated modal frequencies and damping ratios resulted from the Stabilization Diagrams were accurately identified (no major discrepancies between the modal frequencies and damping ratios resulted from the Stabilization Diagrams and the modal identification algorithm), thus validating their effectiveness.

The modal model identification methods were also applied to two representative R/C bridges of the Egnatia Odos at Polymylos (Greece) and at Kavala (Greece) to identify their modal properties for ambient and earthquake-induced vibrations. The lower transverse, longitudinal and vertical modes of the two bridges were identified, including four-closely spaced and overlapping bending modes for the Kavala bridge. The damping values of the bending modes are of the order of 0.4% to 0.7% which is significantly lower than the damping values of the lower transverse and longitudinal modes. This is attributed to the higher damping provided mostly by the elastomeric bearings and the soil for the latter modes. The modal frequencies due to earthquake-induced vibrations are found to be 4% to 15% higher than the modal frequencies due to ambient vibrations. This is attributed mainly to the soil-structure interaction effects contributing to the dynamics of the bridge systems during excitation from wind and traffic loads. These effects are not present in the identified dynamics of the system based on the earthquake induced vibrations due to the use of the input acceleration measurements at the base of the piers and the abutments.

The modal model identification methods were implemented in a Graphical User Interface software termed Modal Identification Tool (MITool). The software was developed in Matlab and has been presented in this thesis in the form of a user's manual. All the operations and pre- and post-processing prospects of the MITool software were presented in details. Also, a step-by-step user guide was provided in this thesis in order to demonstrate the use of the MITool software. The user guide was demonstrated by identifying the modal characteristics of the $\Gamma 9$ bridge at Polymylos (Greece) using real ambient vibration response measurements and by identifying the modal characteristics of the $\Gamma 2$ bridge at Kavala (Greece) using vibration response measurements due to simulated earthquake loads.

The MITool developed in this thesis is useful for identifying the non-classically damped modal models of a variety of structures, including civil engineering structures (buildings, bridges, offshore structures), ground vehicle, aircrafts and various machine parts, operating under various load conditions. Such loading conditions include known loads that are generated by exciters and measured in controlled laboratory experiments, unknown ambient loads involved during the operation of the structure, and earthquake-induced loads that are measured using appropriately installed acceleration sensor network installed in the base of the civil infrastructure.

An important direction for future work is to develop modal identification software to estimate the modal properties of fixed base structures using ambient vibration measurements and including the ambient measurements at the base as input measurements in the software. This is a challenging problem that remains unresolved. Such theoretical development along with the corresponding software will allow one to identify, in the expense of adding more sensors at the

multiple bases of a structure, the modal properties of the fixed base buildings and bridges using ambient vibration measurements, while ignoring the effects of soil structure interaction.

References

- [1] Basseville M., Benveniste A., Goursat M., Hermans L., Mevel L., Van der Auweraer H. (2001), "Output-only subspace-based structural identification: from theory to industrial testing practice", *ASME Journal of Dynamic Systems Measurement and Control*, Vol. 123 (4), pp. 668-676.
- [2] Beck J.L. (1978), "Determining models of structures from earthquake records", Report No. EELRL 78-01, Earthquake Engineering Research Laboratory, California Institute of Technology, Pasadena, CA.
- [3] Beck J.L. and Jennings P.C. (1980), "Structural identification using linear models and earthquake records", *Earthquake Engineering and Structural Dynamics*, Vol. 8, pp. 145-160.
- [4] Beck J.L., May B.S., Polidori D.C. (1994), "Determination of modal parameters from ambient vibration data for structural health monitoring", *Proceedings of the 1st World Conference on Structural Control*, Los Angeles, USA, pp. 1395-1402.
- [5] Blackman R.B. and Tukey J.W. (1958), *The measurement of power spectra from the point of view of communication engineering*, Dover Publications, Inc., New York.
- [6] Bohle K., Fritzen C.P. (2003), "Results obtained by minimizing natural frequencies and MAC-value errors of a plate model", *Mechanical Systems and Signal Processing*, Vol. 17 (1), pp. 55-64.
- [7] Boswald M. and Govers Y. (2008), "Taxi vibration testing - An alternative method to ground vibration testing of large aircraft", *International Conference on Noise and Vibration Engineering (ISMA2008)*, Katholieke Universiteit Leuven, Leuven, Belgium, 15-17 September, 2008.
- [8] Brincker R., Zhang L., Andersen P. (2001), "Modal identification of output-only systems using frequency domain decomposition", *Smart Materials and Structures*, Vol. 10, pp. 441-445.
- [9] Cauberghe B. (2004), "Applied frequency-domain system identification in the field of experimental and operational modal analysis", PhD Thesis, Department of Mechanical Engineering, Vrije Universiteit Brussel, Belgium.
- [10] Chaudhary M.T.A., Abe M., Fujino Y. (2002), "Investigation of atypical seismic response of a base-isolated bridge", *Engineering Structures*, Vol. 24, pp. 945-953.
- [11] Christodoulou K., Papadimitriou C. (2007), "Structural identification based on optimally weighted modal residuals", *Mechanical Systems and Signal Processing*, Vol. 21, pp. 4-23.
- [12] Christodoulou K., Ntotsios E., Papadimitriou C., Panetsos, P. (2008), "Structural Model Updating and Prediction Variability using Pareto Optimal Models." *Computer Methods in Applied Mechanics and Engineering*, Vol. 198 (1), pp.138-149
- [13] Doebling S.W., Farrar C.R. , Prime M.B. (1998), "A summary review of vibration-based damage identification methods", *The Shock and Vibration Digest*, Vol. 30 (2), pp. 91-105

- [14] Farrar C., Baker W., Bell T., Cone K., Darling T., Duffey, T., Eklund A., Migliori A., (1994), "Dynamic Characterization and Damage Detection in the I-40 Bridge over the Rio Grande", Technical Report LA-12767-MS, Los Alamos National Laboratory.
- [15] Felber A.J. (1993), "Development of a hybrid bridge evaluation system", PhD Thesis, University of British Columbia, Vancouver, Canada.
- [16] Fritzen C.P., Jennewein D., Kiefer T. (1998), "Damage detection based on model updating methods", *Mechanical Systems and Signal Processing*, Vol. 12 (1), pp. 163-186.
- [17] Giagopoulos D. and Natsiavas S. (2007), "Hybrid (numerical-experimental) modeling of complex structures with linear and nonlinear components", *Nonlinear Dynamics*, Vol. 47 (1-3), pp. 193-217.
- [18] Guillaume P., Hermans L., Van der Auweraer H. (1999), "Maximum Likelihood Identification of Modal Parameters from Operational Data", *Proceedings of the 17th International Modal Analysis Conference (IMAC17)*, pp. 1887-1893.
- [19] Hermans L., Van der Auweraer H., Guillaume P. (1998), "A frequency-domain maximum likelihood approach for the extraction of modal parameters from output-only data", *Proceedings of the 23rd International Seminar on Modal Analysis (ISMA23)*, pp. 367-376.
- [20] Hermans L. and Van der Auweraer H. (1999), "Modal testing and analysis of structures under operational conditions: Industrial applications", *Mechanical Systems and Signal Processing*, Vol 13 (2), pp. 193-216.
- [21] Heylen, W., Lammens, S., Sas, P. (1997), *Modal Analysis Theory and Testing*, Katholieke Universiteit Leuven, Department of Mechanical Engineering.
- [22] Katafygiotis L.S. and Yuen K.V. (2001), "Bayesian spectral density approach for modal updating using ambient data", *Earthquake Engineering and Structural Dynamics* Vol. 30 (8), pp. 1103-1123.
- [23] Klepka A. and Tadeusz U. (2008), "Hardware and software tools for in-flight flutter testing", *International Conference on Noise and Vibration Engineering (ISMA2008)*, Katholieke Universiteit Leuven, Leuven, Belgium, 15-17 September, 2008.
- [24] Kim C., Kim N., Jung D., Yoon J. (2001), "Effect of vehicle mass on the measured dynamic characteristics of bridges from traffic-induced vibration test", *Proceedings of the 19th International Modal Analysis Conference (IMAC19)*, pp. 1106-1111.
- [25] Lam H.F., Katafygiotis L.S., Mickleborough N.C. (2004), "Application of a statistical model updating approach on phase I of the IASC-ASCE structural health monitoring benchmark study", *Journal of Engineering Mechanics (ASCE)*, Vol. 130 (1), pp. 34-48.
- [26] Ljung L. (1999), *System Identification: Theory for the User*. Prentice-Hall, New York, USA.
- [27] Mahmoudabadi M., Ghafory-Ashtiany M., Hosseini M. (2007), "Identification of modal parameters of non-classically damped linear structures under multi-component earthquake loading", *Earthquake Engineering and Structural Dynamics*, Vol. 36, pp. 765-782.
- [28] Maia, N. and Silva, J. (1997), *Theoretical and Experimental Modal Analysis*, John Wiley & Sons.

- [29] Marple S.L. (1987), *Digital spectral analysis*, Prentice-Hall, New York, USA.
- [30] McVerry G.H. (1980), "Structural identification in the frequency domain from earthquake records", *Earthquake Engineering and Structural Dynamics*, Vol. 8, pp. 161-180.
- [31] Mottershead J.E., Friswell M.I. (1993), "Model updating in structural dynamics: A survey", *Journal of Sound and Vibration*, Vol. 167, pp. 347-375.
- [32] Nikolaou I. (2008), "Structural modal identification methods based on earthquake-induced vibrations", MS Thesis Report No. SDL-08-2, Department of Mechanical and Industrial Engineering, University of Thessaly, Volos, Greece.
- [33] Ntotsios E., Christodoulou K., Papadimitriou C. (2006), "Optimal Experimental Design in Structural Dynamics." *5th International Conference on Computational Stochastic Mechanics*, Rhodes, Greece
- [34] Ntotsios E., Papadimitriou C., Panetsos P., Karaiskos G., Perros K., Perdikaris Ph. (2008), "Bridge health monitoring system based on vibration measurements", *Bulletin of Earthquake Engineering*, doi: 10.1007/s10518-008-9067-4.
- [35] Parloo E., Verboven P., Guillaume P., Van Overmeire M. (2003), "Force identification by means of in-operation modal models", *Journal of Sound and Vibration*, Vol. 262 (1), pp. 161-173.
- [36] Parloo E. (2003), "Application of Frequency-domain System Identification in the Field of Operational Modal Analysis", Ph.D. Thesis, Department of Mechanical Engineering, Vrije Universiteit Brussel, Belgium.
- [37] Papadimitriou C., Beck J. L., Au, S. K. (2000), "Entropy-Based Optimal Sensor Location for Structural Model Updating", *Journal of Vibration and Control*, Vol. 6 (5), pp. 781-800.
- [38] Papadimitriou C., Beck J.L., Katafygiotis L.S. (2001), "Updating robust reliability using structural test data", *Probabilistic Engineering Mechanics*, Vol. 16, pp. 103-113.
- [39] Papadimitriou C. (2005), "Pareto Optimal Sensor Locations for Structural Identification", *Computer Methods in Applied Mechanics and Engineering*, Vol. 194 (12-16), pp. 1655-1673.
- [40] Peeters B. and De Roeck G. (1999), "Reference-based stochastic subspace identification for output-only modal analysis", *Mechanical Systems and Signal Processing*, Vol. 13 (6), pp. 855-878.
- [41] Peeters B. (2000), "System Identification and Damage Detection in Civil Engineering", PhD thesis, Dept. of Civil Engineering, Katholieke Universiteit Leuven, Belgium.
- [42] Peeters B. and De Roeck G. (2001), "One-year monitoring of the z24-bridge: environmental effects versus damage events", *Earthquake Engineering and Structural Dynamics*, Vol. 30 (2), pp. 149-171.
- [43] Peeters B., Van der Auweraer H., Guillaume P., Leuridan J. (2004), "The PolyMAX frequency-domain method: A new standard for modal parameter estimation?", *Shock and Vibration*, Vol. 11 (2-4), pp. 395-409.

- [44] Peeters B., Van der Auweraer H. (2005), "Recent developments in operational modal analysis", *EURODYN 2005*, C. Soize & G.I Schueller (eds), Millpress, Rotterdam, pp. 149-154.
- [45] Peeters B., Hendricx W., Debille J. (2009), "Modern solutions for ground vibration testing of large aircraft", *Sound and Vibration*, Vol. 43 (1), pp. 8-15..
- [46] Roberts S. (2001), "Identification of the modal parameters affecting automotive ride characteristics", *Proceedings of the 19th International Modal Analysis Conference (IMAC19)*, pp. 270-274.
- [47] Safak E. (1995), "Detection and identification of soil-structure interaction in buildings from vibration recordings", *Journal of Structural Engineering (ASCE)*, Vol. 121 (5), pp. 899-906.
- [48] Tan R.Y. and Cheng W.M. (1993), "System identification of a non-classically damped linear system", *Computers and Structures*, Vol. 46, pp. 67–75.
- [49] Teughels A., De Roeck G., Suykens J.A.K. (2003), "Global optimization by coupled local minimizers and its application to FE model updating", *Computers and Structures*, Vol. 81 (24-25), pp. 2337-2351.
- [50] Teughels A. and De Roeck G. (2005), "Damage detection and parameter identification by finite element model updating", *Archives of Computational Methods in Engineering*, Vol. 12 (2), pp. 123-164.
- [51] Van Overschee P. and De Moor B. (1996), *Subspace Identification for Linear Systems: Theory-Implementation-Applications*, Kluwer Academic Publishers.
- [52] Vanik M.W., Beck J.L., Au S.K. (2000), "Bayesian probabilistic approach to structural health monitoring", *Journal of Engineering Mechanics (ASCE)*, Vol. 126, pp. 738-745.
- [53] Verboven P. (2002), "Frequency domain system identification for modal analysis", PhD Thesis, Department of Mechanical Engineering, Vrije Universiteit Brussel, Belgium.
- [54] Welch P.D. (1967), "The use of fast Fourier transform for the estimation of power spectra: A method based on time averaging over short modified periodograms", *IEEE Transactions on Audio and Electroacoustics*, Vol. 15, pp. 70-73.
- [55] Werner S.D., Beck J.L., Levine M.B. (1987), "Seismic response evaluations of Meloland road overpass using 1979 Imperial Valley earthquake records", *Earthquake Engineering and Structural Dynamics*, Vol. 15, pp. 249-274.

ΣΥΓΓΡΑΦΕΑΣ

ΤΙΤΛΟΣ

ΔΗΞΗ

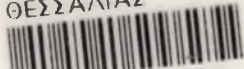
ΟΝΟΜΑΤΕΠΩΝΥΜΟ ΔΑΝΕΙΖΟΜΕΝΟΥ

ΠΑΝΕΠΙΣΤΗΜΙΟ ΘΕΣΣΑΛΙΑΣ
ΒΙΒΛΙΟΘΗΚΗ

Τηλ.: 24210 06300-1



ΠΑΝΕΠΙΣΤΗΜΙΟ
ΘΕΣΣΑΛΙΑΣ



004000091983

